Reciprocal patterning of spontaneous activity and the developing visual cortex

Leighton, Alexandra Helen

2021

document version
Publisher's PDF, also known as Version of record

Reciprocal patterning of spontaneous activity and the developing visual cortex

Alexandra Helen Leighton

Design by Alexandra Leighton
Typset by Guido Meijer and Alexandra Leighton

VRIJE UNIVERSITEIT

RECIPROCAL PATTERNING OF SPONTANEOUS ACTIVITY AND THE DEVELOPING VISUAL CORTEX

ACADEMISCH PROEFSCHRIFT

ter verkrijging van de graad Doctor aan
de Vrije Universiteit Amsterdam,
op gezag van de rector magnificus
prof.dr. V. Subramaniam,
in het openbaar te verdedigen
ten overstaan van de promotiecommissie
van de Faculteit der Bètawetenschappen
op dinsdag 7 september 2021 om 11.45 uur
in de aula van de universiteit,
De Boelelaan 1105

door

Alexandra Helen Leighton

geboren te London, Verenigd Koninkrijk

promotoren: prof.dr. P.R. Roelfsema
prof.dr. C.N. Levelt

promotiecommissie:

prof.dr. H.A. Verhoef (Voorzitter)
dr. J. Gjorgjieva
prof.dr. H.D. Mansvelder
dr. N.L.M. Cappaert
prof.dr. J.G G. Borst
prof.dr. S. Spijker

#MeToo

Tarana Burke

Win or lose,
sink or swim,
one thing is certain,
we'll never give in.

Side by side,
hand in hand,
we all stand,
together.

Paul McCartney
& the Frog Chorus

CONTENTS

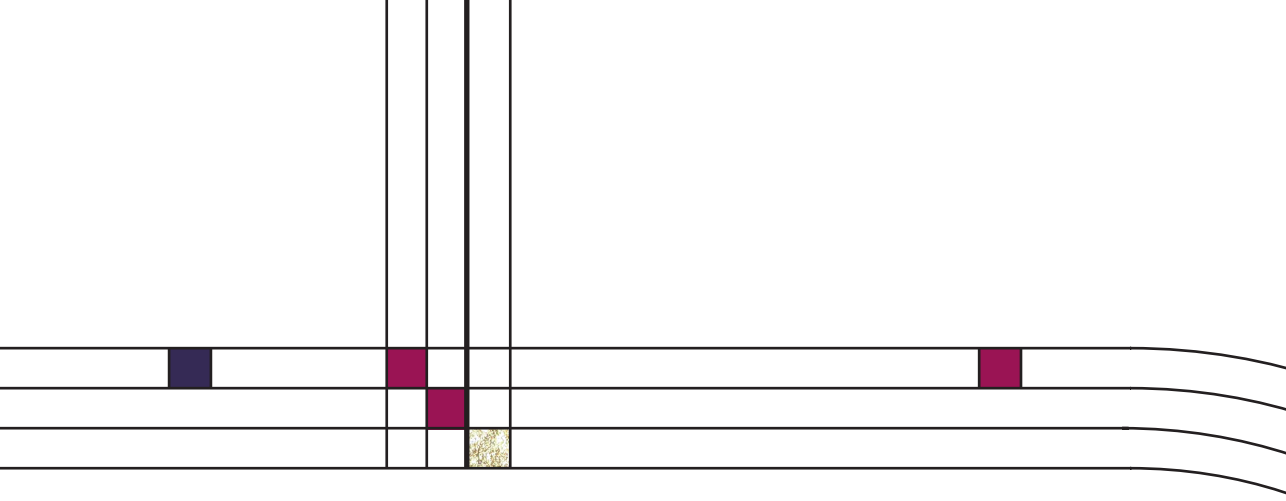

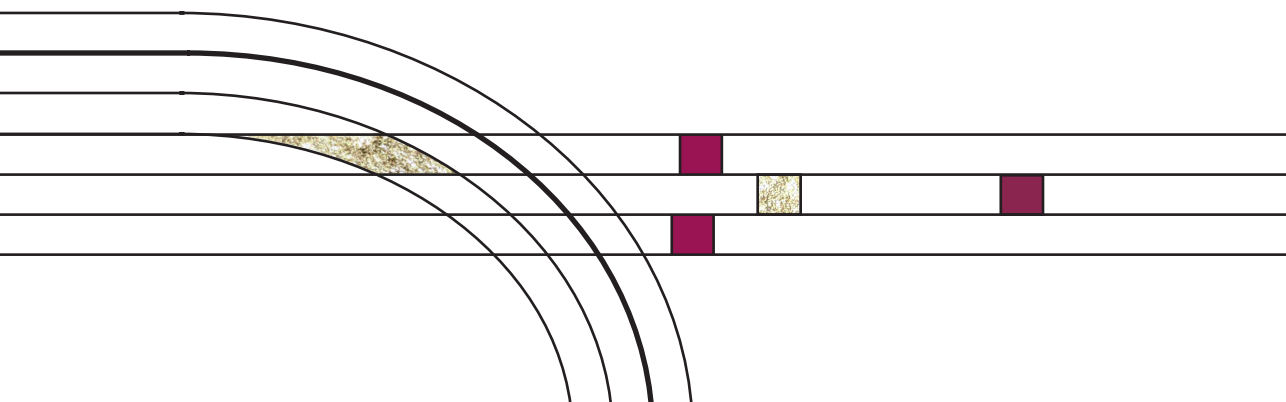

CHAPTER 1

Introduction

Partly adapted from Leighton and Lohmann, 2016

One of the strangest aspects of neuroscience is using a system to study itself. Admittedly, the brain of an adult human and that of a developing mouse are not exactly the same, but in many ways the similarities outweigh the differences. This recurrent loop of examiner and examinee is part of the appeal of the field, as any progress we make brings us closer to understanding ourselves. Massive international effort has led to great advances in our knowledge of how the brain works, but we remain quite far removed from being able to build a functioning brain. This perspective makes it all the more remarkable that each of our own brains managed to build itself from scratch. With just a little external guidance, we produced a system capable of consciousness, forward planning, empathy- and, for some, the ability to build embarrassingly large libraries of Taylor Swift lyrics.

Understanding how the brain develops is important for many reasons, which can be split into two main camps. First and most pragmatically, many diseases and disorders have their roots in neural development, and early treatment of neurodevelopmental disorders can reduce suffering for the patient. In some cases, there may only be certain developmental windows in which interventions are effective (Meredith, 2015).

Secondly, watching a brain build itself can help us understand how it is organised. What does a neuron take into account when deciding whether or not to stabilize an input? Which features are so important to develop that they include built-in levels of redundancy? By understanding how the system is initially created, we can outline some of the constraints and priorities that shape the adult brain.

Developing neurons become wired into functional networks in three phases

One of the most fundamental tasks that must be performed by the brain is to process incoming sensory stimuli. Eventually, we are able to build up a map of our world, interacting with objects and recognizing people. To begin with, we need to answer more basic questions- is this bright light on the ceiling or on the floor? Is my mother to my left or on my right? To perform these tasks, the brain contains many maps that represent the sensory environment. In the visual system, retinal ganglion cells representing adjacent parts of the visual field project to neighbouring cells in higher order areas. Inputs from the left and right eyes are separated in

monocular regions for precise localization, and combined in binocular regions to integrate information from both eyes and allow for depth perception. This precise wiring between neurons occurs during early brain development and relies on three successive mechanisms.

Initial, rough organization is instructed by genetically encoded molecular guidance cues, which unfold independently of activity (Benjumeda et al., 2013). For instance, the first connections from retinal ganglion cells to upstream targets are instructed by ephrins- the ligands of the Eph receptor tyrosine kinases, which guide projections from the lateral geniculate nucleus (LGN) to primary visual cortex (V1) (Cang et al., 2005a). These cues appear in a gradient across the target area, giving some directional information that results in a coarse retinotopic organization.

For accurate sensory processing, this framework needs to be refined, through both pruning of excessive connections and increased arborisation within the correct termination zones (Simon and O'Leary, 1992). To perform this refinement, sensory areas become active, even before the senses have become operational. Spontaneous waves of depolarisations sweep across the nervous system, strengthening correct connections and suppressing incorrect ones, shaping synapses into a useful network. This refinement can be measured either functionally, by determining the size of the regions within the higher visual areas that are activated by given stimuli, or anatomically, by labelling projections and determining the size of the area in which they terminate.

Finally, the senses will start picking up patterned, incoming stimuli. These signals contain valuable information about the environment and are used to further fine-tune the brain, allowing animals to adapt to their surroundings.

This thesis focuses on the role of spontaneous activity in the visual system during development, when initial connections are refined even before the opening of the eyes. A large body of work now supports the idea that, rather than being a mere side-effect of the system, spontaneous activity actually contains information which readies the nervous system, so that sensory information can be used by the animal as soon as possible. We will use the neonatal mouse as our model. Mouse

pups can process visual information as soon as the eyes open, before they having experience with such precisely patterned sensory input (Cang et al., 2005b; Ko et al., 2013; Rochefort et al., 2011; Zhang et al., 2012a).

In vivo imaging techniques allow the observation of the natural neural activity in the brain of the living animal, even at the level of the individual synapse. Advanced (opto)genetic methods make it possible to subtly modulate the spatio-temporal properties of activity and measure the consequences, aiding our understanding of how these characteristics relate to the function of spontaneous activity. Such experiments have had a huge impact on our knowledge by permitting direct testing of ideas about plasticity mechanisms at play in the intact system, opening up a provocative range of fresh questions.

Spontaneous activity patterns in the visual system

In rodents, the eyelids do not open until P14. Throughout these first two postnatal weeks, cells in the retina depolarise spontaneously, creating waves of correlated activity that travel across the retina (as reviewed in Torborg and Feller, 2005). Activity from the retina can propagate to the LGN, the superior colliculus (SC) (Ackman et al., 2012), and the visual cortex, as demonstrated by a drop in spontaneous activity frequency in V1 when the eye is removed (Siegel et al., 2012). In vivo simultaneous calcium imaging of SC and V1 has demonstrated that the location of origin and direction of travel of waves is matched between these areas, confirming that waves of spontaneous activity can indeed convey information about the spatial properties of the retina to the visual cortex (Ackman et al., 2012). These retinally-driven 'L-events' can be identified as those in which only a subset of cells (20-80%) are active. In contrast, events in which more than 80% of cells are active ('H-events') are unaffected by retinal enucleation, indicating a different source of initiation (Siegel et al., 2012). During the second postnatal week, activity 'desynchronises' as events becomes more frequent, activity becomes less correlated between cells, and calcium amplitudes decrease (Rochefort et al., 2009), (Fig 1).

In accordance with the imminent onset of visual input, the visual system becomes responsive flashes of flashes from P8. Colonnese et al., (2010) defined an early 'bursting phase' in rats before eye-opening, between P8 and P11, where a bright light flash evokes a bursting pattern through the closed eyelid. During this phase,

the cortex will respond to a light stimulus, but these responses vary greatly in terms of features such as response amplitude, the time of onset after the stimulus or the number of spikes fired, even when in response to identical stimuli. This variation in response pattern does not depend on whether the animal is awake or sleeping. From P12, two days before eye opening, the next phase begins- from then, cortical responses to a stimulus become consistent and these responses are modulated by the vigilance state of the animal (Colonnese et al., 2010).

Spontaneous activity shapes the developing visual system

That spontaneous activity has an active role in shaping the developing brain was initially demonstrated by experiments which blocked spontaneous activity entirely, causing severe disruptions of the organization of sensory areas (Cang et al., 2005a; Chandrasekaran et al., 2005). Since these early experiments, our grasp on the rules which underlie the patterning of the neonatal brain has greatly increased. This is mainly due to technical improvements which have allowed subtle and specific manipulations of spontaneous activity, rather than overall elimination. These

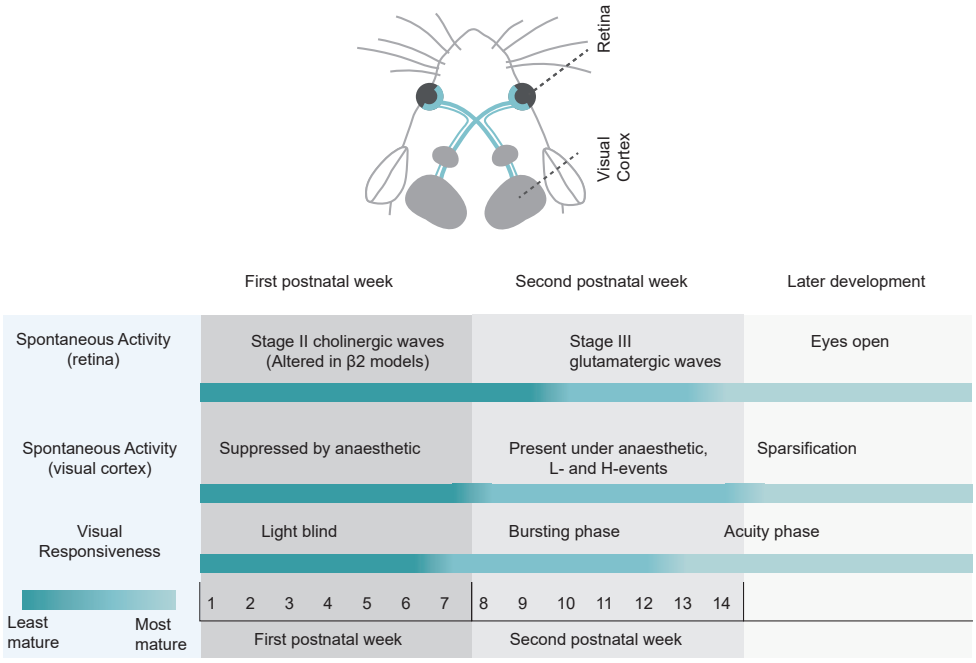

Figure 1. Spontaneous and evoked activity during early postnatal development.

experiments focused primarily on retinotopy as well as eye-specific segregation of projections to the SC and the LGN. The main aim was to clarify the information content of these waves- which characteristics (for instance their timing, spatial properties, frequencies or wave amplitudes) are important for their function? Thanks to this recent work, we can begin to sketch out the role of spontaneous activity, more clearly delineating which processes do and which do not rely on intrinsically generated activity (Fig 2A).

As described above, one major source of spontaneous activity in the visual system is the retina. The wave characteristic of spontaneous activity in the developing retina provides spatiotemporal information- as the wave travels, neighbouring retinal ganglion cells will fire in turn, passing on information about their spatial relationship in the temporal properties of the wave. When a mouse opens its eyes at around P14, neurons in the primary visual cortex have already been thoroughly organized according to the spatial structure of the retina, as V1 shows retinotopic maps, eye-specific segregation, and orientation tuning of individual neurons (Godecke et al., 1997; Ko et al., 2013; Rochefort et al., 2011; Smith and Trachtenberg, 2007).

A common model of disrupted retinal activity is the β2 global knock-out mouse. These mice lack the β2 subunit of the nicotinic acetylcholine receptor, which leads to altered retinal activity during the first postnatal week. In wild-type mice, a clear wave-front travels over the retina in a successive activation of ganglionic cells. In contrast, the β2 global knock-out shows almost simultaneous activation of much larger groups of neurons (Fig 2A, B). These activations are gap-junction dependent and of lower frequency and amplitude when compared to controls. When dye injections are used to visualize geniculocortical projections, the termination areas are larger, (Cang et al., 2005b), and this corresponds to less fine-tuned functional retinotopy in the SC (Mrsic-Flogel et al., 2005), LGN and V1 (Cang et al., 2005b; Grubb et al., 2003; McLaughlin et al., 2003) of β2 KO mice. Besides retinotopy, the segregation of terminals from the ipsilateral and contralateral eyes (eye-specific segregation) is disrupted.

One major limitation of the β2 KO mouse is that both the frequency and the spatial properties of retinal activity are different to wild type mice. Several variations of

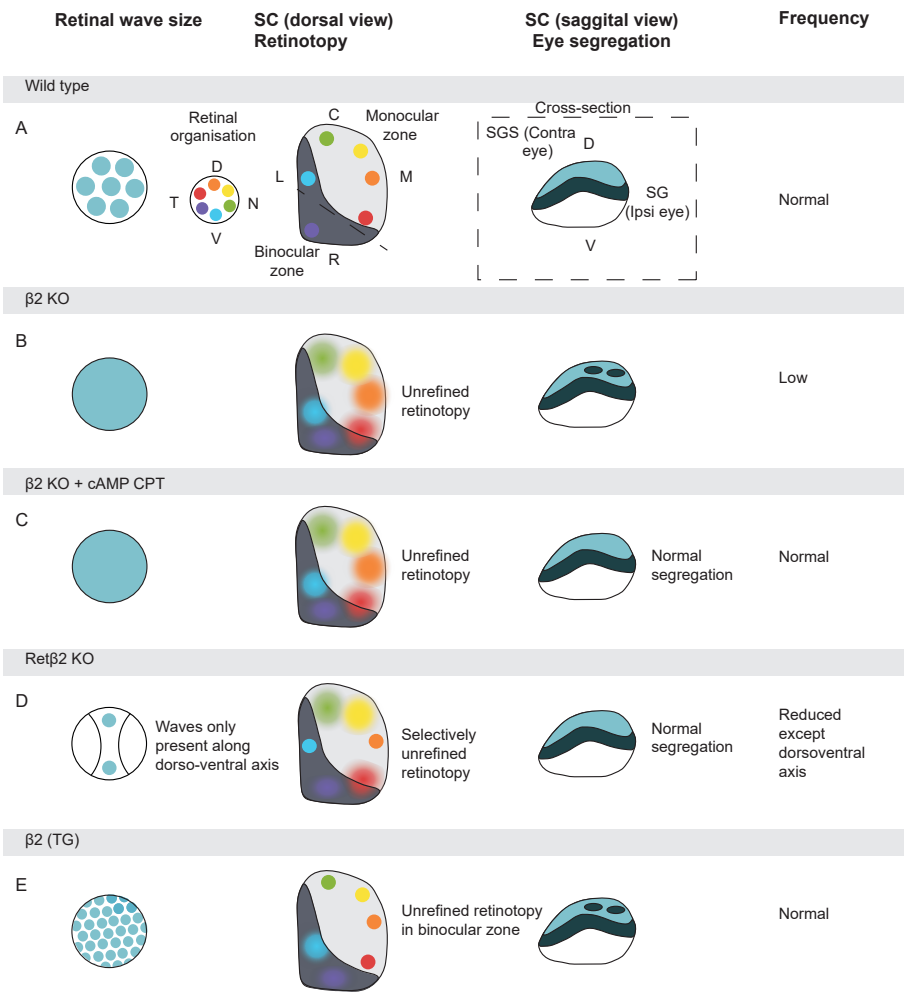

Figure 2. Manipulations of spontaneous activity frequency and wave size and the consequences for retinotopy and eye-specific segregation in the superior colliculus.

A. Wild type waves lead to refined retinotopy and segregation of ipsi- and contralateral projections.

B. The whole body β2 knockout has low frequency activity over large areas of the retina and unrefined retinotopy and eye-specific segregation.

C. Applying cAMP-CPT to the β2 knockout increases frequency to wild type levels (Burbridge et al., 2014).

D. Partially disrupting wave activity also has spatially selective consequences for retinotopy (Burbridge et al., 2014).

E. Truncated, small waves disturb segregation (Xu et al., 2011).

the β2 mouse have been used to more specifically manipulate activity patterns by varying either the frequency or the spatial spread of waves. These experiments have allowed us to link specific properties of spontaneous activity to higher area patterning.

The first conclusion we can draw is that the refinement of retinotopy depends on local correlations within retinal waves. Genetic models in which local correlations are maintained have accurate retinotopy, whereas retinotopy is disrupted by large activations (Burbridge et al., 2014; Xu et al., 2011, 2015). In contrast, retinotopy is fairly resistant to changes in the overall firing rate of retinal activity- the frequency of spontaneous activity can be greatly reduced with no negative impact on retinotopy (Burbridge et al., 2014). Also, pharmacologically restoring the firing rate of retinal waves in the β2 KO to wild-type levels does not save the retinotopic map (Fig 2C). Burbridge et al., (2014) used a Ret β2-cKO mouse (Fig 2D) as an elegant demonstration of the link between retinal waves and higher area retinotopy. In this mouse, the β2 subunit is knocked out selectively in temporal and nasal areas of the retina, locally altering wave activity. The rest of the retina, along the dorso-ventral axis, showed clearly propagating waves. The effect of this is noticeably reflected in the SC, where terminations from the altered, peripheral retina spread over a larger area than those from the non-expressing areas. Overall, it seems that retinal waves contain local spatial information about the retina essential for normal retinotopy, indicating an instructive role for spontaneous activity. It is fairly intuitive that the precise mapping of retinotopy relies on local spatial information- if activity is correlated over a larger area, downstream neurons will not be able to distinguish as carefully between inputs coming from different locations.

In contrast, eye specific segregation appears depend on overall firing rate. In both the LGN and SC, projections from both eyes initially terminate in partially overlapping areas. During the first two postnatal weeks these terminations are refined, clearly dividing where inputs from each eye are segregated and where they are combined to produce binocular vision. In contrast to retinotopy, restoring the firing rate of the retina in whole body β2 knockout mice using CPT-cAMP improves segregation. Results from the Rx-β2cKO mouse confirm this, as their lower frequency results in selective disruption of eye-specific segregation (Xu et al., 2015). Overall firing rate cannot be the only important factor, as mice with wild-type frequency but spatially

smaller waves (β2 (TG)) have disrupted eye-specific segregation (Xu et al., 2011), Fig 2E. It therefore seems that spatial information is important, but at a different scale than for retinotopy; rather than small local correlations, the overall area activated by each wave may be essential in eye-specific segregation. There may be an activity threshold for segregation, which can either be reached by frequent or by large-scale activity.

Zhang et al., (2012) used optogenetic activation of retinal ganglion cells to test the role of spontaneous activity in eye-specific segregation of the SC and LGN. The more the stimuli overlapped between the eyes, the more the disruption in eye-specific segregation worsened. Asynchronous stimulation of the eyes (with more than 100 ms difference) did not disrupt segregation, suggesting a sub-second resolution for this competition. Synchronous stimulation could also disrupt segregation even after eye-specific segregation, indicating an important role for retinal waves not only in creating but also in maintaining segregation, as has been previously reported (Demas et al., 2006).

The difference between retinotopy and eye-specific segregation is not a complete opposition; the sensory system must be able to form and maintain both patterns simultaneously and problems with one can interrupt the other. An excellent example of this is the Rx-β2cKO and β2 (TG) mouse, in which retinotopic mapping is disrupted only in binocular regions of the SC. The strongest evidence that the problems with retinotopy are a consequence of problematic eye-specific segregation is that all retinotopy from the remaining eye stayed intact in both the SC and LGN when one eye was removed at birth (Xu et al., 2011, 2015). As the ipsilateral projections are still present, they disrupt the activity from incorrectly terminating axons which can alter the retinotopic map.

GABAergic signalling is inhibitory before eye-opening

It is clear that synaptic fine-tuning uses specific features of spontaneous activity patterns, such as their frequency, amplitude and synchronicity. How does the immature brain shape these features? One prominent candidate is inhibitory signalling by inhibitory interneurons. These cells use the neurotransmitter GABA to prevent or reduce cell firing, either through inhibitory postsynaptic potentials or shunting inhibition. Interneurons are highly heterogeneous, and can be divided

into groups based on the proteins they express. These subtypes often have similar morphology, firing patterns and connectivity (Fig 3, adapted from van Versendaal & Levelt, 2016). This specificity of properties allows inhibitory cells to active as strong activity modulators in adults, capable of controlling activity through their connectivity and sensitivity to neuromodulators (Kepecs and Fishell, 2014; Markram et al., 2004; Tremblay et al., 2016; van Versendaal and Levelt, 2016). Until very recently, GABA was thought to act as an excitatory neurotransmitter, only switching to its adult inhibitory role as cells mature (Cherubini et al., 1991). Partly due to this theory, very little research had focused on the function of interneurons during development. Recently, GABAergic cells have been shown to exert an inhibitory effect on the cortical network from the end of the first postnatal week (Che et al., 2018; Kirmse et al., 2015; Minlebaev et al., 2007; Valeeva et al., 2016). GABAergic signalling is therefore a prime candidate to control spontaneous event patterning even before eye opening. In Chapter 2, we show that functional inhibition shapes properties of spontaneous activity. We even find that interneurons act in a subtype-

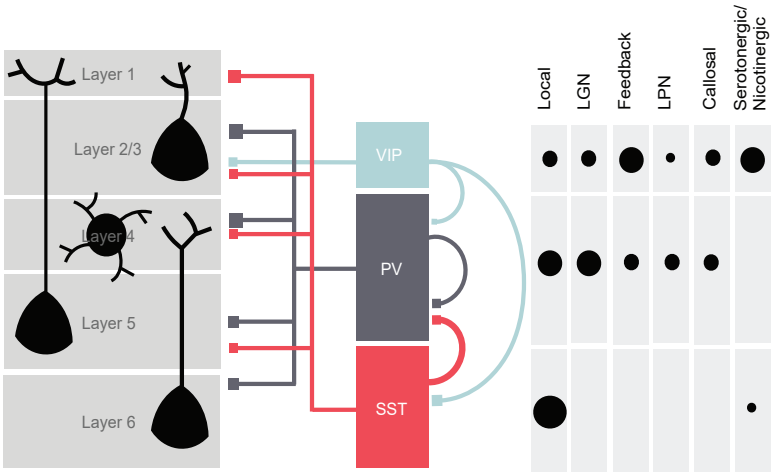

Figure 3, Schematic representation of the main projections to pyramidal cells from interneurons within primary visual cortex (V1) from van Versendaal & Levelt (2016).
SST = somatostatin, PV = parvalbumin, VIP = vasoactive intestinal peptide. Shown are rough estimates of projection densities (black circles) from local, thalamic (lateral geniculate nucleus (LGN) and the lateral posterior nucleus (LPN) of the thalamus), feedback and callosal projections onto different subtypes of interneurons. VIP interneurons are strongly responsive to nicotinergic and serotonergic neuromodulatory inputs and inputs from higher brain regions (feedback and callosal).

specific manner, where somatostatin cells control how many cells are recruited to an event.

The involvement of GABAergic signalling during this time opens up a wide range of new questions. As mentioned above, neuromodulators often exert their effects by targeting interneurons. Their involvement in spontaneous activity may mean that this activity is more plastic than we thought- rather than almost hard-coded, inevitable activity patterns, the exact features of spontaneous activity may respond to input. Recent work has shown that stimuli from the environment can indeed modulate spontaneous activity (Tiriac et al., 2018). Is spontaneous activity also responsive to the internal state of the animal? The state of the adult brain is controlled by neuromodulator release, for instance during the release of acetylcholine when the animal is in an attentive state (Giovannini et al., 2001; Paul et al., 2015), where it increases the sensitivity of neurons to those stimuli the animal is attending to (Muñoz and Rudy, 2014). To understand whether the internal state of the animal can change spontaneous activity features, we manipulated acetylcholine transmission with pharmacology in Chapter 3.

How does spontaneous activity shape young networks?

Accurate refinement will lead to clearly defined maps that can be seen at a macroscopic level. However, the actual process of refinement takes place at the single synapse, as each synapse is either protected or pruned. To accurately wire together these networks, plasticity mechanisms must both eliminate inaccurately targeted synapses and strengthen appropriate connections. We do not yet fully understand the mechanics behind these choices- exactly how altered temporal or spatial patterns can change the organization of the network.

In recent years there has been a surge in our understanding of the computational power of a neuron. The classic description of a neuron is as a linear integrator, summing inputs evenly regardless of their position along the dendritic tree. Recently, experimental evidence has come to support the idea that dendritic compartments can act as computational units, integrating inputs in a non-linear fashion (Poirazi and Mel, 2001), for review see (Branco and Haüsser, 2010; Govindarajan et al., 2006; Larkum and Nevian, 2008; Winnubst and Lohmann, 2012). Spatially clustered synapses can exert increased influence on cell output

when they are simultaneously active by generating NMDA dependent 'dendritic spikes'- large events whose charge exceeds the linear summation of the synapses involved. For this to have functional advantages, strategic organization of synapses along the dendrite is required. That dendritic specificity has great implications for the output of the cell has been demonstrated in adults (Lavzin et al., 2012; Sheffield and Dombeck, 2015). Spatial specificity also has consequences for refinement- it is not enough to ensure that certain cells are connected, these connections must also be strategically placed.

During development, synapses along the dendrite that are closer together (< 12µm) are more likely to be active simultaneously, and this organization disappears when spontaneous activity is blocked (Kleindienst and Lohmann, 2010). An 'out of sync, lose your link' plasticity mechanism underlies this organization, as synapses that show low synchronicity to their neighbours become depressed, with a significantly decreased transmission efficiency (Winnubst et al., 2015). This spatial clustering was found in both the visual cortex ***in vivo*** and the hippocampus ***in vitro.*** Though there are many similarities between the two, they have different temporal characteristics- whereas a burst in the hippocampus lasts only around 400 ms, bursts in the visual cortex have a longer duration of around 2 seconds. Interestingly, this was reflected in the plasticity rules guiding synaptic depression. When probing the time window during which two synapses were considered coactive, the hippocampus showed a much shorter integration window, of 400 ms, whereas in V1, depression of synapses was prevented if they were coactive within 2 seconds. Burst duration could be an important property of spontaneous activity, linking together only cells that are active within a certain time window.

As current techniques now allow us to directly measure changes at the level of the 'nuts and bolts' of the developing brain, we are set to begin to really understand the rules according to which the nervous system is built. Only by directly observing the plasticity mechanisms at work at these synapses can we really link the information content of activity to the structural and functional changes it causes. In Chapter 4 we describe the organization and plasticity rules observed at the level of the individual dendrite during the second postnatal week.

Thesis overview

Taken together, we can conclude that spontaneous activity contains essential information encoded in its features. But how are these features shaped by the young system, and in turn, how do they shape the brain at a synaptic level? Only by directly observing the plasticity mechanisms at work at these synapses can we really link the information content of activity to the structural and functional changes it causes.

In the following chapters, I will address several questions about spontaneous activity. The first experimental chapter (Chapter 2) aims to understand how inhibitory signalling in the young brain shapes spontaneous activity. By observing individual cells (≈10 um) and how they work together as a population, we investigate how inhibitory interneurons can control features of spontaneous activity, such as amplitude, frequency and network synchrony.

The second experimental chapter (Chapter 3) focuses on the plasticity of spontaneous activity itself, using large-scale imaging (≈ 5 mm^2). Does spontaneous activity respond to neuromodulation? We use pharmacology to probe the role of the neurotransmitter acetylcholine in spontaneous activity patterning.

Chapter 4 zooms in onto individual synaptic activations (≈ 1 um) on single cells. The focus of this chapter is on one of the most essential questions of spontaneous activity research; how synaptic strength and organisation is modulated by activity. Ultimately, large scale changes in refinement will have to occur synapse-by-synapse.

The final chapter (Chapter 5) is a technical section on manipulation of spontaneous activity using wireless optogenetics. This could allow us to change activity patterns in mouse pups while they are in the cage with their mother, and help us understand the functional consequences for the animal of long-term changes in spontaneous activity patterns.

References

Ackman, J.B., Burbridge, T.J., and Crair, M.C. (2012). Retinal waves coordinate patterned activity throughout the developing visual system. Nature *490*, 219–225.

Benjumeda, I., Escalante, A., Law, C., Morales, D., Chauvin, G., Muça, G., Coca, Y., Márquez, J., López-Bendito, G., Kania, A., et al. (2013). Uncoupling of EphA/ephrinA Signaling and Spontaneous Activity in Neural Circuit Wiring. J. Neurosci. *33*, 18208–18218.

Branco, T., and Hausser, M. (2010). The single dendritic branch as a fundamental functional unit in the nervous system. Curr.Opin.Neurobiol. *20*, 494–502.

Burbridge, T.J., Xu, H.-P., Ackman, J.B., Ge, X., Zhang, Y., Ye, M.-J., Zhou, Z.J., Xu, J., Contractor, A., and Crair, M.C. (2014). Visual Circuit Development Requires Patterned Activity Mediated by Retinal Acetylcholine Receptors. Neuron *84*, 1049–1064.

Cang, J., Kaneko, M., Yamada, J., Woods, G., Stryker, M.P., and Feldheim, D.A. (2005a). Ephrin-as guide the formation of functional maps in the visual cortex. Neuron *48*, 577–589.

Cang, J., Rentería, R.C., Kaneko, M., Liu, X., Copenhagen, D.R., and Stryker, M.P. (2005b). Development of Precise Maps in Visual Cortex Requires Patterned Spontaneous Activity in the Retina. Neuron *48*, 797–809.

Chandrasekaran, A.R., Plas, D.T., Gonzalez, E., and Crair, M.C. (2005). Evidence for an instructive role of retinal activity in retinotopic map refinement in the superior colliculus of the mouse. J Neurosci *%20;25*, 6929–6938.

Che, A., Babij, R., Iannone, A.F., Fetcho, R.N., Ferrer, M., Liston, C., Fishell, G., and García, N.V.D.M. (2018). Layer I Interneurons Sharpen Sensory Maps during Neonatal Development. Neuron *99*, 98–116.

Cherubini, E., Gaiarsa, J.L., and Ben-Ari, Y. (1991). GABA: an excitatory transmitter in early postnatal life. Trends Neurosci. *14*, 515–519.

Colonnese, M.T., Kaminska, A., Minlebaev, M., Milh, M., Bloem, B., Lescure, S., Moriette, G., Chiron, C., Ben-Ari, Y., and Khazipov, R. (2010). A Conserved Switch in Sensory Processing Prepares Developing Neocortex for Vision. Neuron *67*, 480–498.

Demas, J., Sagdullaev, B.T., Green, E., Jaubert-Miazza, L., McCall, M.A., Gregg, R.G., Wong, R.O., and Guido, W. (2006). Failure to maintain eye-specific segregation in nob, a mutant with abnormally patterned retinal activity. Neuron *50*, 247–259.

Godecke, I., Kim, D.S., Bonhoeffer, T., and Singer, W. (1997). Development of orientation preference maps in area 18 of kitten visual cortex. Eur.J Neurosci. *9*, 1754–1762.

Govindarajan, A., Kelleher, R.J., and Tonegawa, S. (2006). A clustered plasticity model of long-term memory engrams. Nat Rev Neurosci *7*, 575–583.

Grubb, M.S., Rossi, F.M., Changeux, J.P., and Thompson, I.D. (2003). Abnormal functional organization in the dorsal lateral geniculate nucleus of mice lacking the beta 2 subunit of the nicotinic acetylcholine receptor. Neuron *40*, 1161–1172.

Kepecs, A., and Fishell, G. (2014). Interneuron Cell Types: Fit to form and formed to fit. Nature *505*, 318–326.

Kirmse, K., Kummer, M., Kovalchuk, Y., Witte, O.W., Garaschuk, O., and Holthoff, K. (2015). GABA depolarizes immature neurons and inhibits network activity in the neonatal neocortex in vivo. Nat Commun *6*, 7750.

Kleindienst, T., and Lohmann, C. (2010). Simultaneous patch-clamping and calcium imaging in developing dendrites. J. Sharpe, R.O. Wong, and R. Yuste, eds. pp. 491–499.

Ko, H., Cossell, L., Baragli, C., Antolik, J., Clopath, C., Hofer, S.B., and Mrsic-Flogel, T.D. (2013). The emergence of functional microcircuits in visual cortex. Nature *496*, 96–100.

Larkum, M.E., and Nevian, T. (2008). Synaptic clustering by dendritic signalling mechanisms. Curr.Opin.Neurobiol. *18*, 321–331.

Lavzin, M., Rapoport, S., Polsky, A., Garion, L., and Schiller, J. (2012). Nonlinear dendritic processing determines angular tuning of barrel cortex neurons in vivo. Nature *490*, 397–401.

Leighton, A.H., and Lohmann, C. (2016). The Wiring of Developing Sensory Circuits-From Patterned Spontaneous Activity to Synaptic Plasticity Mechanisms. Front Neural Circuits *10*, 71.

Markram, H., Toledo-Rodriguez, M., Wang, Y., Gupta, A., Silberberg, G., and Wu, C. (2004). Interneurons of the neocortical inhibitory system. Nat.Rev.Neurosci *5*, 793–807.

McLaughlin, T., Torborg, C.L., Feller, M.B., and O'Leary, D.D.M. (2003). Retinotopic Map Refinement Requires Spontaneous Retinal Waves during a Brief Critical Period of Development. Neuron *40*, 1147–1160.

Meredith, R.M. (2015). Sensitive and critical periods during neurotypical and aberrant neurodevelopment: A framework for neurodevelopmental disorders. Neurosci Biobehav Rev *50C*, 180–188.

Minlebaev, M., Ben-Ari, Y., and Khazipov, R. (2007). Network mechanisms of spindle-burst oscillations in the neonatal rat barrel cortex in vivo. J. Neurophysiol. *97*, 692–700.

Mrsic-Flogel, T.D., Hofer, S.B., Creutzfeldt, C., Cloez-Tayarani, I., Changeux, J.P., Bonhoeffer, T., and Hubener, M. (2005). Altered map of visual space in the superior colliculus of mice lacking early retinal waves. J Neurosci *25*, 6921–6928.

Poirazi, P., and Mel, B.W. (2001). Impact of active dendrites and structural plasticity on the memory capacity of neural tissue. Neuron *29*, 779–796.

Rochefort, N.L., Garaschuk, O., Milos, R.I., Narushima, M., Marandi, N., Pichler, B., Kovalchuk, Y., and Konnerth, A. (2009). Sparsification of neuronal activity in the visual cortex at eye-opening. Proceedings of the National Academy of Sciences *106*, 15049–15054.

Rochefort, N.L., Narushima, M., Grienberger, C., Marandi, N., Hill, D.N., and Konnerth, A.

(2011). Development of Direction Selectivity in Mouse Cortical Neurons. Neuron *71*, 425–432.

Sheffield, M.E.J., and Dombeck, D.A. (2015). Calcium transient prevalence across the dendritic arbour predicts place field properties. Nature *517*, 200–204.

Siegel, F., Heimel, J.A., Peters, J., and Lohmann, C. (2012). Peripheral and Central Inputs Shape Network Dynamics in the Developing Visual Cortex In Vivo. Current Biology *22*, 253–258.

Simon, D.K., and O'Leary, D.D. (1992). Development of topographic order in the mammalian retinocollicular projection. J. Neurosci. *12*, 1212–1232.

Smith, S.L., and Trachtenberg, J.T. (2007). Experience-dependent binocular competition in the visual cortex begins at eye opening. Nat Neurosci *10*, 370–375.

Tiriac, A., Smith, B.E., and Feller, M.B. (2018). Light Prior to Eye Opening Promotes Retinal Waves and Eye-Specific Segregation. Neuron.

Torborg, C.L., and Feller, M.B. (2005). Spontaneous patterned retinal activity and the refinement of retinal projections. Prog.Neurobiol. *76*, 213–235.

Tremblay, R., Lee, S., and Rudy, B. (2016). GABAergic Interneurons in the Neocortex: From Cellular Properties to Circuits. Neuron *91*, 260–292.

Valeeva, G., Tressard, T., Mukhtarov, M., Baude, A., and Khazipov, R. (2016). An Optogenetic Approach for Investigation of Excitatory and Inhibitory Network GABA Actions in Mice Expressing Channelrhodopsin-2 in GABAergic Neurons. J. Neurosci. *36*, 5961–5973.

van Versendaal, D., and Levelt, C.N. (2016). Inhibitory interneurons in visual cortical plasticity. Cell. Mol. Life Sci. *73*, 3677–3691.

Winnubst, J., and Lohmann, C. (2012). Synaptic clustering during development and learning: The why, when and how. Frontiers in Molecular Neuroscience *5:70*.

Winnubst, J., Cheyne, J.E., Niculescu, D., and Lohmann, C. (2015). Spontaneous activity drives local synaptic plasticity in vivo. Neuron *87*, 399–410.

Xu, H., Furman, M., Mineur, Y.S., Chen, H., King, S.L., Zenisek, D., Zhou, Z.J., Butts, D.A., Tian, N., Picciotto, M.R., et al. (2011). An Instructive Role for Patterned Spontaneous Retinal Activity in Mouse Visual Map Development. Neuron *70*, 1115–1127.

Xu, H.-P., Burbridge, T.J., Chen, M.-G., Ge, X., Zhang, Y., Zhou, Z.J., and Crair, M.C. (2015). Spatial pattern of spontaneous retinal waves instructs retinotopic map refinement more than activity frequency. Dev Neurobiol *75*, 621–640.

Zhang, J., Ackman, J.B., Xu, H.P., and Crair, M.C. (2012a). Visual map development depends on the temporal pattern of binocular activity in mice. Nat Neurosci *15*, 298–307.

Zhang, J., Ackman, J.B., Xu, H.P., and Crair, M.C. (2012b). Visual map development depends on the temporal pattern of binocular activity in mice. Nat Neurosci *15*, 298–307.

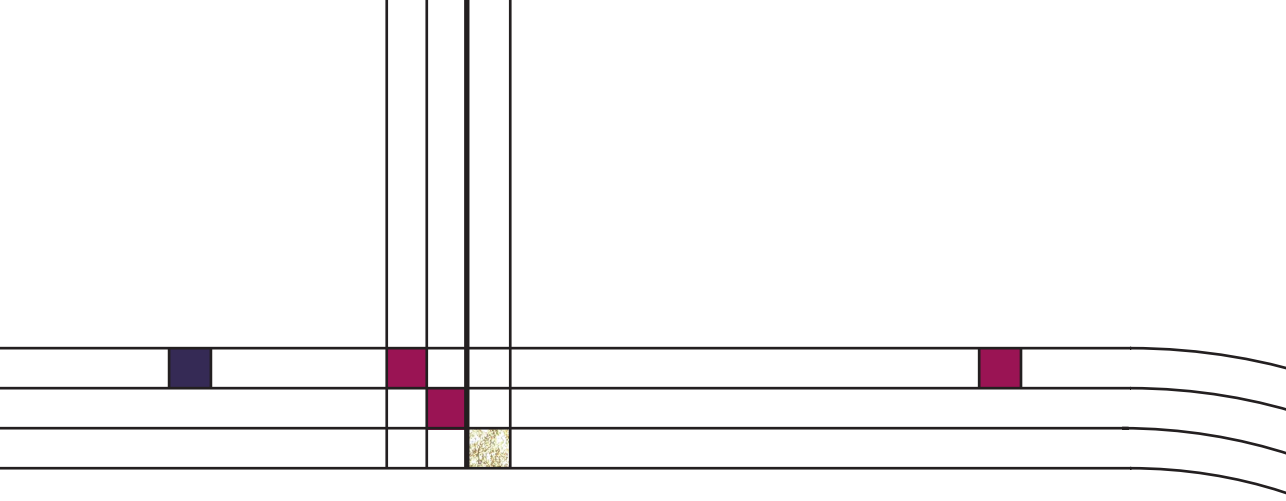

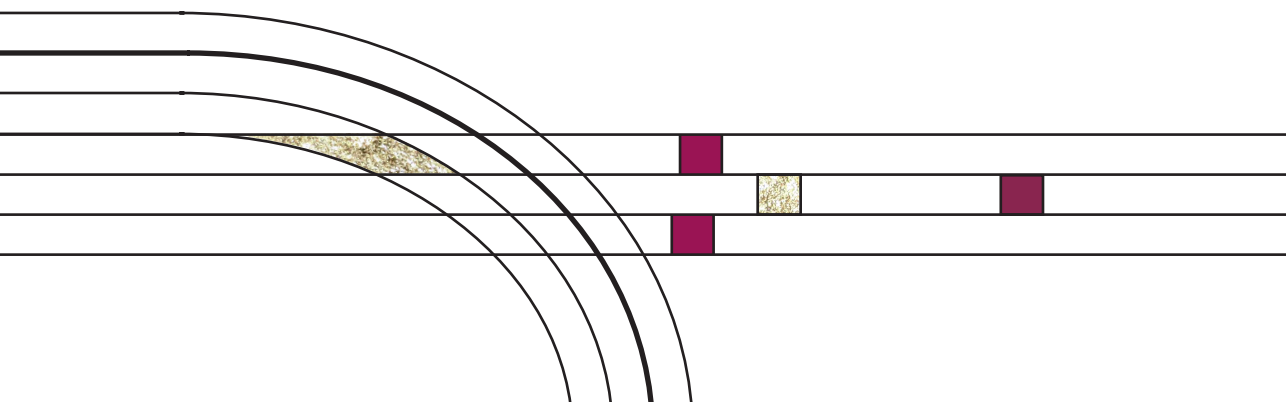

CHAPTER 2

Somatostatin interneurons restrict cell recruitment to retinally-driven spontaneous activity in the developing cortex

Authors

Alexandra H. Leighton, Juliette E. Cheyne, Gerrit J. Houwen, Paloma P. Maldonado, Fred De Winter, Christiaan N. Levelt, Christian Lohmann

ABSTRACT

During early development, before the eyes and ears even open, synaptic refinement of young sensory networks depends on activity generated by developing neurons themselves. In the mouse visual system, retinal cells spontaneously depolarize and recruit downstream neurons to bursts of activity, where the number of recruited cells determines the resolution of synaptic retinotopic refinement. Here we show that during the second postnatal week in mouse visual cortex, somatostatin (SST)-expressing interneurons control the recruitment of cells to a specific type of retinally-driven spontaneous activity. Suppressing SST interneurons at this age increases cell participation and allows events to spread further along the cortex. During the same developmental period, a second type of very high-participation, retina-independent events occur. During these events, we find that cells receive such large excitatory charge that inhibition is overwhelmed and large parts of the cortex participate in each burst. These results thus reveal a novel role of SST interneurons in restricting retinally-driven activity in the visual cortex, which may contribute to the refinement of retinotopy.

INTRODUCTION

Newborns can interact with their environment and perform sensorimotor tasks soon after birth, without any previous experience of patterned sensory input. These abilities rely on extensive preparation by the developing nervous system before the onset of sensory experience. Initially, neuronal networks are roughly outlined by molecular guidance cues, and subsequently refined by activity dependent processes Fs3. During this refinement phase, spontaneously depolarizing cells in the sensory organs and the brain (Blankenship and Feller, 2010) initiate and propagate patterned 'training' activity across the developing network, strengthening well-targeted synapses and weakening others.

In the mouse visual system, neonatal retinae generate bursts of activity which travel downstream and refine retinotopic maps as well as the segregation of contra- and ipsilateral afferents through Hebbian and non-Hebbian mechanisms (Kirkby et al., 2013). As a result of this fine-tuning, neurons in the mouse visual cortex can respond to visual information before the eyes open at postnatal day (P)14 (Cang et al., 2005; Ko et al., 2013; Rochefort et al., 2011; Zhang et al., 2012).

Spontaneous activity patterns can be described and distinguished by burst characteristics, such as frequency, duration, synchronicity of firing between cells, lateral spread, and the number of cells that participate (Ackman and Crair, 2014; Albert et al., 2008; Allene and Cossart, 2010; Colonnese and Phillips, 2018; Kerschensteiner, 2014; Luhmann and Khazipov, 2018). A growing body of work has shown that merely the presence of activity is not sufficient for refinement, but that these specific activity characteristics encode and transmit essential information required by the brain to develop normally (Kirkby et al., 2013; Leighton and Lohmann, 2016). The number of cells activated by each burst may determine the resolution with which spontaneous activity can refine connections between cells; for instance, if retinal waves recruit too many neurons, retinotopic map refinement is prevented (Burbridge et al., 2014, Xu et al., 2011, 2015). In contrast, eye-specific segregation can be impaired by changes in burst frequency (Burbridge et al., 2014; Xu et al., 2011).

Two types of spontaneous activity are found in the primary visual cortex (V1): retinally-driven, low-synchronicity events with low cell participation rates ('L-events') (Ackman et al., 2014; Gribizis et al., 2019; Siegel et al., 2012) and retina-independent, high-synchronicity events with high cell participation and amplitude ('H-events') (Gribizis et al., 2019; Hanganu et al., 2006; Siegel et al., 2012). It is possible that these different types of events work together to pattern the developing cortex, where sparse activation and retinal origin of L-events gives them the resolution required to shape the network according to the organization of the eye, whereas global ('H-events') could allow neurons to perform synaptic homeostasis, bringing synaptic strengths back to a workable range (Siegel et al., 2012). Indeed, computational modelling of this joint organization led to topographically refined receptive fields and sparsification of activity over time (Wosniack et al., 2021).

In adults, we have an increasing appreciation of the strong and specific regulation of network activity by interneuron subtypes (Kepecs and Fishell, 2014; Markram et al., 2004; Tremblay et al., 2016; van Versendaal and Levelt, 2016), but little is known about interneuron subtype activity in neonates. Recent work has shown that GABAergic cells exert an inhibitory effect on the cortical network as early as the start of the second postnatal week ***in vivo*** (Che et al., 2018; Kirmse et al., 2015;

Minlebaev et al., 2007; Valeeva et al., 2016) and that they are active in assemblies (Duan et al., 2020; Modol et al., 2020). GABAergic cells can regulate cortical activity patterns (Duan et al., 2020) and modelling the blocking of GABAergic transmission increased spontaneous activity cluster size (Rahmati et al., 2017) . During the same developmental window, somatostatin (SST)-expressing interneurons form strong synapses onto pyramidal cells, weakening to adult levels upon eye-opening (Guan et al., 2017). In the adult brain, SST interneurons can control the size of memory engrams in the adult hippocampus (Stefanelli et al., 2016) and exert lateral inhibitory control in the auditory (Kato et al., 2017) and visual cortex (Adesnik et al., 2012). We therefore investigated whether the strong inhibition mediated by SST interneurons before eye opening also restricts cell recruitment and event size during spontaneous activity.

We show that L-events cause highly localized activations in the visual cortex, associated with modest excitatory input, and that SST interneuron activity supports this confined activity by restricting cell participation to L-events. In contrast, we find that huge excitatory ion influx occurs during H-events, likely overwhelming inhibitory control and leading to widespread activation of the cortex.

RESULTS

L-events recruit fewer cells and show restricted lateral spread

L- and H-events were previously described using two-photon calcium imaging of populations of around 50 cell somas (Siegel et al., 2012). To understand how L-and H-characteristics match up to other reports of spontaneous activity, we measured their properties at a range of different scales. First, we used whole cell current-clamp recordings to compare cell recruitment between L- and H-events in V1 layer 2/3 neurons ***in vivo,*** in lightly anesthetized (0.7-1% isoflurane) mouse pups between P8 and P12 (Fig 1A). Simultaneous two-photon calcium imaging (using Oregon Green Bapta-AM) allowed identification of L- and H-events (Fig 1B), where events with over 80% participation were considered H-events (Siegel et al., 2012). We confirmed that L-events have lower cell participation, as patched cells almost always fired during H-events, but not during L-events (Fig 1C). Neurons also fired significantly more action potentials during H-events than during L-events, in correspondence with their higher calcium transient amplitude (Fig 1D). L-event duration (mean 4.6 seconds) was similar to the duration of retinal waves (summarized in Torborg and Feller, 2005), in line with their largely retinal origin.

To confirm our previous split of these events into two distinct groups (L and H) in a manner independent of calcium imaging, we performed hierarchical clustering using the number of action potentials fired and the duration of bursts (Fig 1E). Silhouette analysis revealed an optimum of two clusters (Fig 1F). This split (Fig 1G) corresponded well (76% overlap) to our original definition of L- and H-events, where events with between 20 and 80% participation classified as L-events, and those over 80% network participation were identified as H-events (Siegel et al., 2012). We therefore continued to use this 80% cut off to distinguish L- and H-events during two-photon network calcium imaging.

When using two-photon microscopy, H-events activated almost all neurons in the field of view. To measure lateral spread of events, we used *in utero* electroporation to widely express GCaMP6s, allowing us to record a much larger part of the visual cortex (4.9 mm^2) with wide-field imaging (Fig 1H). At this large population level, two types of events were still clearly detectable (Fig 1I). Silhouette analysis

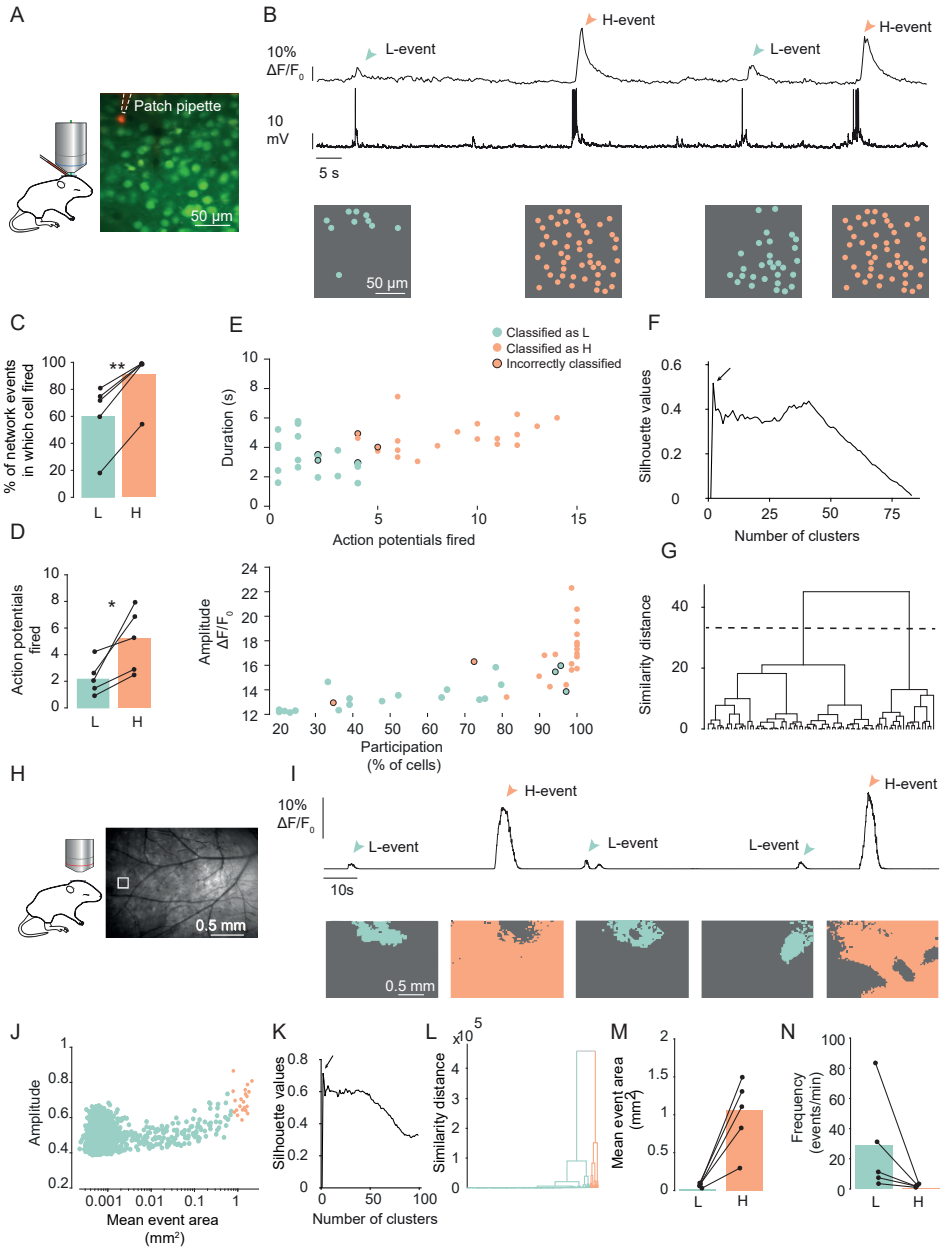
A
Patch pipette
50 µm
B
10% ΔF/F0
L-event
H-event
L-event
H-event
10 mV
5 s
50 µm
C
% of network events in which cell fired
**
L
H
D
Action potentials fired
*
L
H
E
Classified as L
Classified as H
Incorrectly classified
Duration (s)
Action potentials fired
Amplitude ΔF/F0
Participation (% of cells)
F
Silhouette values
Number of clusters
G
Similarity distance
H
0.5 mm
I
10% ΔF/F0
L-event
H-event
L-event
L-event
H-event
10s
0.5 mm
J
Amplitude
Mean event area (mm²)
K
Silhouette values
Number of clusters
L
x10^5
Similarity distance
M
Mean event area (mm²)
L
H
N
Frequency (events/min)
L
H

Figure 1, Distinct spontaneous activity patterns occur in the visual cortex during the second postnatal week

A. Cells in V1 L2/3 were loaded with the calcium indicator Oregon Green Bapta 1-AM (green) to track spontaneous activity patterns. The recorded cell was filled with Alexa 594 via the patch pipette for identification (red).
B. L-events (blue arrowheads) and H-events (orange arrowheads) shown as a calcium trace (average activity of all imaged cells) with simultaneous whole-cell current-clamp recording. The cells that participated in each event are displayed as filled circles below.
C. Cells fired action potentials during a higher percentage of H-events than L-events ($p = 0.001$, paired t-test, $n = 5$ cells).
D. More action potentials were fired during H-events than during L-events ($p = 0.03$, paired t-test, $n = 5$ cells).
E. Outcome of hierarchical clustering shown for all spontaneous events in a single cell, labelled by outcome of hierarchical clustering. Outlined events are those where the clustering outcome deviated from classification using the 80% network participation criterium. Top panel: the number of action potentials fired and the duration of the event (as measured in the whole-cell recording) were used to cluster events. Bottom panel: the network properties of the same events, shown as mean calcium amplitude in active cells against network participation of each event.
F. Silhouette analysis of hierarchical clustering using burst duration and action potentials fired.
G. Dendrogram of hierarchical clustering results for an example animal. Dashed line indicates cut-off at 2 clusters, distinguishing one group with many, small events and a second group with fewer, large events.
H. Epifluorescence imaging of the visual cortex expressing GCaMP-6s was used to image a larger field of view. White square indicates field of view in two-photon.
I. Mean calcium responses during L- and H-events (above) and area of activation (below).
J. Event amplitude by mean event area for all events detected in wide-field in an example animal, labelled according to classification by clustering.
K. Silhouette analysis of hierarchical clustering using amplitude and event size as parameters.
L. Dendrogram of hierarchical clustering results for an example animal.
M. Mean event areas of wide-field L- and H-events.
N. Frequency of each event type in activations per minute.

again revealed an optimal separation at two clusters (Fig 1J, K), splitting the data into events occurring locally and with low amplitudes (local events) and events with large spatial spread and with high amplitudes (Fig 1L, M), presumably corresponding to L- and H-events. Over the whole field of view, L-events occurred at higher frequencies than H-events (Fig 1N). To compare these measurements to the frequencies obtained with two-photon calcium imaging, we also measured event frequency at an area corresponding to the size of the field of view of our two-photon microscope. We found that widespread, putative H-events occurred at a frequency of 0.6 ± 0.25 events per minute in this smaller area, similar to the previously determined frequency in two-photon experiments (0.5 per minute; Siegel et al., 2012). For local L-events, we saw an average of 0.37 ± 0.12 events per minute in wide-field recordings, a lower frequency than the two-photon microscopy data (around 1 per minute) and in line with the reduced sensitivity of wide-field imaging to small, sparse activations of a few cells.

Taken together, L-events are characterized by low cell recruitment and local activation, as well as a low number of action potentials fired. In contrast, during H-events, large areas of the cortex are activated as a high density of cells fire in a burst of action potentials.

SST interneurons restrict spatial spread of spontaneous events

Given that in adulthood, SST interneurons control the size of memory engrams in the hippocampus (Stefanelli et al., 2016) as well as lateral inhibition in the auditory (Kato et al., 2017) and visual cortex (Adesnik et al., 2012), we asked whether SST interneurons also control the lateral spread of spontaneous activity during cortical development.

We selectively suppressed SST interneurons using a cre-dependent viral vector driving expression of an inhibitory hM4Di-DREADD (AAV-hSyn-DIO-hM4D(Gi)-mCherry) during calcium imaging of spontaneous activity in awake pups. 83 ± 8% of cells expressing the inhibitory hM4Di-DREADD also expressed SST (n = 4 animals, Fig 2A) and 79 ± 6% of SST interneurons expressed the hM4Di-DREADD. Activation of the hM4Di-DREADD with its fast-acting agonist clozapine reduced excitability of DREADD-expressing cells ***in vitro*** (Fig 2B,C) similar to the excitability-reducing

effect of hM4Di-DREADD activation in developing layer 2/3 pyramidal neurons described previously (Naskar et al., 2019).

By co-injecting the hM4Di-DREADD vector with pAAV-Syn-GCaMP6s, network activity was recorded in awake pups across a large part of the cortex with wide-field imaging (field of view: 4.9 mm^2, Fig 2D), before and after subcutaneous clozapine (0.5 mg/kg) injection. To control for possible hM4Di-DREADD independent effects of clozapine, results from a t-test are reported as significant only when a linear mixed-effects model with an interaction term (of injected virus type and clozapine administration) demonstrated a significantly better fit than one without the interaction term.

We first quantified activity origin and spread of all events (Fig 2E). Although all events are included in the figure, L-events strongly dominate the observed activity pattern as they are much more frequent than H-events. Both before and after SST interneuron suppression, most activity originating in V1 was confined to this area (Fig 2F), indicating that much of the observed spontaneous activity was restrained by V1 boundaries independently of SST interneuron signalling.

Upon SST interneuron suppression, network events activated a significantly larger area of V1 (Fig 2G, H). This was due to both an increase in the maximum lateral spread (Fig 2I) as well as the distance travelled during each event (Fig 2J). We detected no difference in the duration of events (Fig 2K), but their speed of propagation across the cortex increased (Fig 2L) and allowed them to travel further. We found no significant changes upon clozapine administration to control animals (Supplementary Figure 1).

The increase in event area could be due to an increase in the relative frequency of H-events, or increased recruitment of cells to each spontaneous event. Given that the event amplitude did not show a significant change (Fig 2M), and that the frequency of activity showed a trend to decrease (Fig 2N), it seems more likely that each spontaneous event recruits more active cells upon SST interneuron suppression. Event size before and after SST interneuron suppression shows a shift away from small events and towards larger events (Fig 2O).

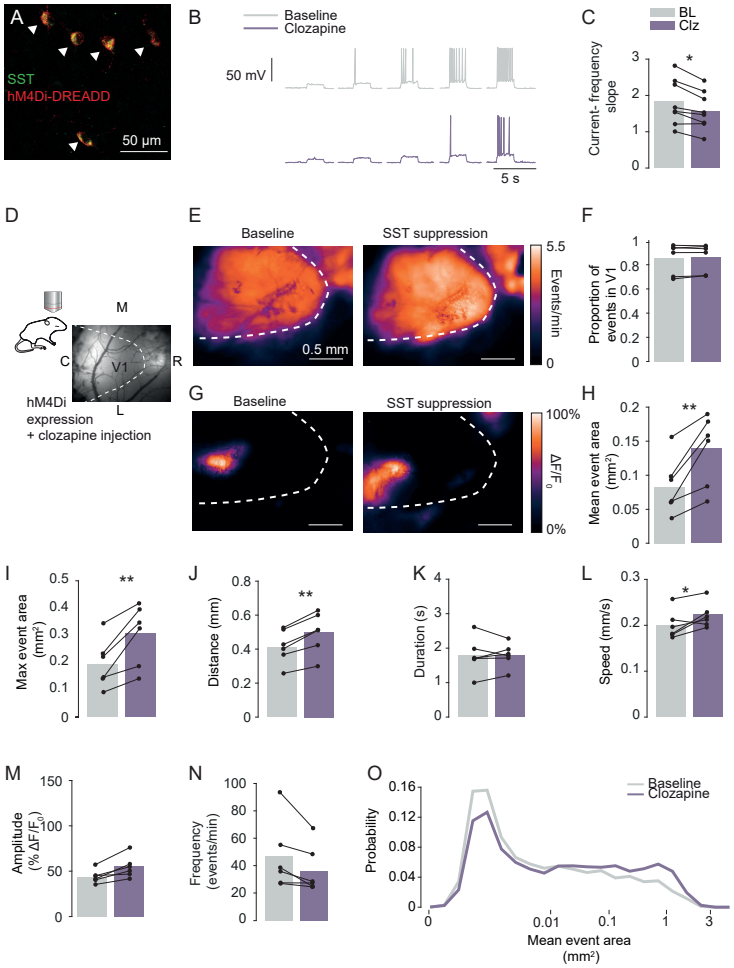

Figure 2, SST interneuron suppression selectively leads to larger event spread.

A. Section of the visual cortex of a P9 SST-cre mouse injected with AAV-hSyn-DIO-hM4D(Gi)-mCherry (red) with immunostaining for SST (green). All cells in the field of view were double-labeled.
B. Example cell firing at 30, 40, 50, 60 pA injection, before and after clozapine application.
C. Clozapine application in vitro significantly reduced excitability in SST interneurons expressing the hM4Di-DREADD construct (n = 8 cells, paired t-test, $p < 0.05$).
D. Wide-field imaging was used to record large scale activity patterns in animals expressing GCaMP6s and an hM4Di-DREADD construct in SST interneurons (M: medial, L: lateral, R: rostral, C: caudal). SST interneurons were suppressed with clozapine (Clz) injection.
E. Average activity frequency per pixel before (left) and after (right) clozapine injection to induce suppression of SST interneurons. Events were included only if they activated pixels within the V1 boundaries, but the entire field of view was used to measure event properties.
F. There was no significant change in the proportion of events that activated V1 upon clozapine injection to induce suppression of SST interneurons (n.s., paired t-test, n = 6 animals).
G. Example event before (left) and after (right) suppression of SST interneurons.

SST interneurons restrict cell recruitment to L-events

We repeated measurements of spontaneous activity during suppression of SST interneuron activity, using two-photon imaging (Fig 3A), again with co-injection of the hM4Di-DREADD vector with pAAV-Syn-GCaMP6s, or the pAAV-Syn-GCaMP6s vector alone in control animals. In control animals, clozapine injection did not significantly increase the frequency in any participation bin (Supplementary Figure 2A, B). Upon SST interneuron suppression, the frequency of events in low-participation bins did not change (Fig 3B-D). In contrast, suppressing SST interneurons specifically increased the frequency of events in the highest participation bin (Fig 3D). In this highest participation bin, a significant interaction effect was found between the expressed viral construct (1:1 hM4Di-DREADD with GCaMP6s compared to 1:1 diluted GCaMP6s) and clozapine injection (2-way ANOVA, interaction clozapine and viral injection, $p = 0.0008$).

This observation could either mean that SST interneuron suppression allows more 'true' H-events to occur in the network, or that SST interneuron suppression causes events to recruit more cells, increasing participation. Either explanation would increase the average area of events, as seen in the wide-field imaging (Fig 2H).

To distinguish between these scenarios, we assessed whether event amplitude (a proxy for the number of action potentials fired) increased upon SST interneuron suppression, as true H-events are associated with large event amplitudes. We did not detect an increase in mean event amplitude of participating cells, either as a

H. The mean area activated by each event increased upon suppression of SST interneurons ($p = 0.006$, paired t-test, $n = 6$ animals).
I. The maximum event area (the activated area during the largest frame of an event) was significantly higher after suppression of SST interneurons ($p = 0.006$, paired t-test, $n = 6$ animals).
J. Events traveled further across the cortex after suppression of SST interneurons through clozapine injection ($p = 0.00066$, paired t-test, $n = 6$ animals).
K. After suppression of SST interneurons, the duration of events did not change (n.s, one-way ANOVA comparing linear mixed-effects model with and without an interaction term, n.s. interaction of injected genotype and clozapine injection, $n = 6$ animals).
L. The speed of events increased after suppression of SST interneurons ($p = 0.049$, paired t-test, $n = 6$ animals).
M. No significant change in amplitude was detected after suppression of SST interneurons (one-way ANOVA comparing linear mixed-effects model with and without an interaction term, n.s. interaction of injected genotype and clozapine injection).
N. The frequency of events did not change significantly upon suppression of SST interneurons (n.s., paired t-test, $n = 6$ animals).
O. Distribution of mean area (over all active frames) of events before and after clozapine.

paired t-test comparing baseline with clozapine administration, or when taking the control experiments into account and testing for a significant interaction effect of injected construct and clozapine administration (Fig 3E, control in Supplementary Figure 2B), supporting the idea that SST interneuron suppression increases recruitment to events. In this scenario, events that would normally fall short of our detection threshold of 20% participation may cross into our definition of an event, explaining why we only detect this effect in the highest participation bin. Furthermore, careful analysis of neuronal participation and amplitude revealed that SST interneuron suppression specifically facilitated high participation events of low amplitude (Fig 3F, G, for controls see Supplementary Figure 2C), indicating increased recruitment of cells to L-events.

As the wide-field imaging data did not show an increase in event amplitude or frequency (Fig 2M, N), it seems likely that the increase in frequency seen in two-photon imaging experiments reflected a larger proportion of events entering the field of view due to their lateral spread, rather than a true increase in the number of events. SST interneuron suppression therefore changes cell recruitment without affecting the firing rate of active neurons. During baseline spontaneous activity, we did not detect a difference between the average participation of SST-expressing interneurons and the average participation of the rest of the cell population (Supplementary Figure 3A); SST expressing interneurons participated during both L- (Supplementary Figure 3B) and H- (Supplementary Figure 3C) events. Additionally, we did not detect a difference in amplitude during L- (Supplementary Figure 3D) or H- (Supplementary Figure 3E) events. Together, SST interneuron activity restricts the lateral spread and cell activation density of local L-events, but not their frequency or the overall firing rates of individual neurons during network events.

Excitatory and inhibitory balance during L- and H-events

Our observation that reducing SST interneuron-mediated inhibition affected the spread of L-events, without converting them (in terms of action potential firing frequency) into H-events, suggested that the difference between these two types of events was not caused simply by reduced recruitment of inhibition. More likely, differences in excitatory drive underlie the difference between L- and H-events, where SST interneurons participate in both events, but are overwhelmed by

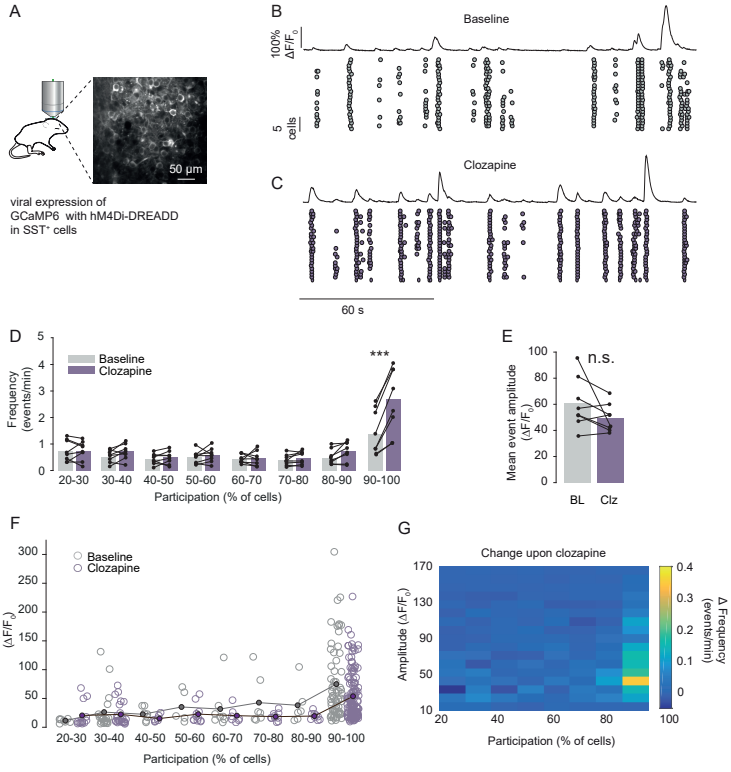

Figure 3, Suppressing SST interneuron activity selectively increases the number of high-participation low-amplitude events

A. Two-photon imaging was used to record calcium transients in animals expressing GCaMP6s and an inhibitory hM4Di-DREADD construct in SST interneurons. Clozapine was injected at low concentrations to activate the hM4Di-DREADD and reduce SST interneuron excitability.
B. Neurons were imaged in awake pups during the second postnatal week. Example recording before injection of clozapine. Shown is the average change in fluorescence over all cells in the field of view (above) and when each cell participated in an event (below). Each circle represents a calcium transient in a cell.
C. Example recording after SST interneuron suppression.
D. After SST interneuron suppression, there is a significant increase in the frequency of events only in the highest participation bin ($p = 0.0002$, threshold for significance at 0.0063 after Bonferroni correction for 8 comparisons, paired t-test, $n = 8$ animals). Number of 90-100% participation events, baseline condition: 261, clozapine condition: 607.
E. No change in amplitude was detected upon suppression of SST interneurons (n.s., paired t-test, $n = 8$ animals). Amplitude is measured as the average peak amplitude of all cells that participate in the event.
F. Mean amplitude of calcium peak of all active cells in each event, binned into participation bins of 20%, before and after clozapine in an example animal expressing hM4Di-DREADD. Filled circles represent mean amplitude value for each bin.
G. Heat map showing the change in frequency of activity in events/min after suppression of SST interneurons. The largest increase occurred in high-participation/low-amplitude events.

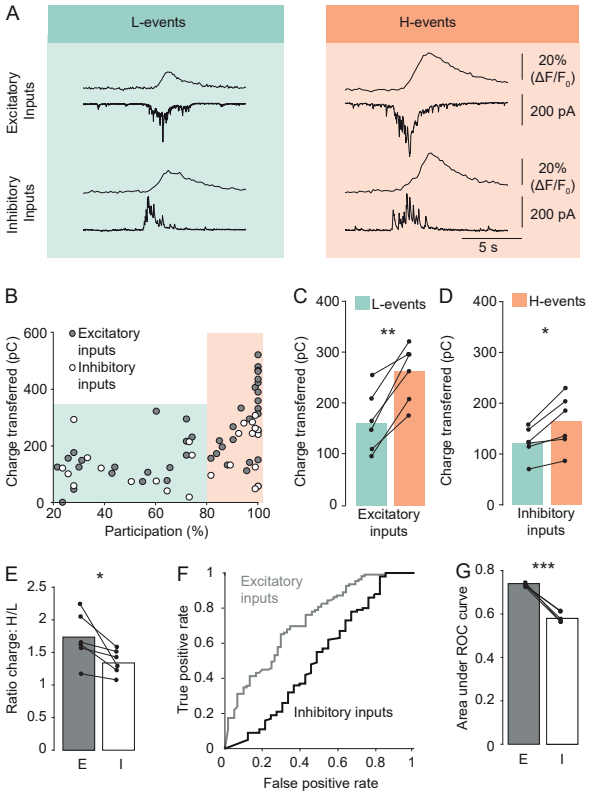

Figure 4, Excitatory and inhibitory synaptic inputs during L-and H-events

A. In vivo voltage-clamp recordings combined with network calcium imaging in layer 2/3 V1 neurons. Excitatory and inhibitory inputs were measured by switching the holding potential to the reversal potential of inhibitory or excitatory currents, respectively. Four events in an example cell, showing inhibitory and excitatory inputs received by the cell during an L-event and an H-event. Average calcium traces are shown from all imaged cells (above). Current traces (below) represent synaptic inputs onto the recorded neuron.

B. Absolute transferred charges of excitatory and inhibitory input currents during network events of different participations in one cell.

C. The excitatory charge transferred was significantly higher during H-events than during L-events ($p = 0.001$; paired t-test, $n = 6$ animals).

D. The inhibitory charge transferred was significantly higher during H-events than during L-events ($p = 0.016$, paired t-test, $n = 6$ animals).

E. The H:L ratio of charge transferred was significantly larger for excitatory than for inhibitory inputs ($p = 0.036$, paired t-test, $n = 6$ animals).

F. Example receiver operating characteristic (ROC) curve for one animal, showing a random forest classifier trained on excitatory or inhibitory data. The larger area under the curve for excitatory inputs indicates a higher success rate of classifying L- and H-events correctly when excitatory data was used compared to inhibitory data.

G. Quantification of the area under the ROC curve for all animals. The area under the curve is significantly higher for classifiers trained on excitatory input data than for those trained on inhibitory input data ($p = 0.0002$, paired t-test, $n = 5$ animals).

excitation during H-events. To test this directly, we recorded synaptic inputs received by the soma during L- and H-events in lightly anesthetized pups. We performed *in vivo* whole-cell recordings in voltage-clamp mode, while simultaneous calcium imaging of the network allowed identification of L- and H-events. As reported previously, events involved both glutamatergic and GABAergic synapses (Fig 4A, Colonnese, 2014; Hanganu et al., 2006; Minlebaev et al., 2007). In line with the higher network participation in H-events, both the excitatory and inhibitory charge transferred (defined as area under the curve of the synaptic currents during a burst) were larger during H-events than during L-events (Fig 4B-D). However, the ratio of excitatory charge transferred between H- and L-events was much larger than that of inhibitory charge transfer (Fig 4E). This confirms that H-events differ from L-events mainly due to a much stronger excitatory drive rather than to differences in inhibitory inputs.

To confirm directly that H- and L-events could be differentiated more reliably based on excitation or inhibition, we trained a random forest classifier (Breiman, 2001) using only electrophysiological measurements to decode whether an event was an L- or an H-event. Peak current amplitude, mean current amplitude, total charge transferred and duration of either inhibitory or excitatory current inputs were provided to the classifier. Training event classification was based on the original definition of 20-80% (L-events) and over 80% participation (H-events) in network events obtained with two-photon calcium imaging. For all animals, the classifier trained on the excitatory data performed significantly better than the classifier trained on the inhibitory data, as demonstrated by the larger area under the curve of the receiver-operator characteristics (ROC) curve (Fig 4F, G). We conclude that differences in excitatory drive underlie the main characteristics of H- and L-events while SST interneuron-mediated inhibition exerts much stronger control over L- than over H-events.

DISCUSSION

SST interneurons are crucial for activity-dependent maturation throughout the development of the nervous system. In the hippocampus and entorhinal cortex, long-range SST-expressing 'hub' cells synchronize spontaneous activity (Bonifazi et al., 2009; Mòdol et al., 2017) and activating SST interneurons can trigger synchronous

network depolarizations in slices (Flossmann et al., 2019). In the cortex, SST interneurons appear to be precocious (Pan et al., 2018), maturing before fast-spiking interneurons and even supporting the integration of fast-spiking interneurons into the network. SST interneurons in deep cortical layers receive dense but transient innervation from thalamocortical inputs during the first postnatal week (Marques-Smith et al., 2016; Tuncdemir et al., 2016), which facilitates the thalamocortical innervation of parvalbumin (PV)-expressing interneurons (Tuncdemir et al., 2016). SST interneurons also release the extracellular matrix protein Collagen XIX, which is required for PV-expressing cells to form the perisomatic inhibitory synapses that will give them such strong inhibitory control in the adult brain (Su et al., 2020).

In cortical L2/3, SST interneuron synapses onto pyramidal cells emerge at the beginning of the second postnatal week (Guan et al., 2017), when oxytocin release also increases SST interneuron excitability and sparsifies neuronal activity (Maldonado et al., 2021). At this age, SST interneuron-mediated inhibition is strong and can be readily recorded in the somas of cortical pyramidal neurons. After eye-opening, the strength of the synaptic connection from SST interneurons to pyramidal cells sharply decreases. Simultaneously, fast-spiking cells start to express PV and increase their synaptic strength onto pyramidal cells, perhaps taking over signalling functions from SST interneurons as the cortex matures (Guan et al., 2017). So far, the role of this strong SST interneuron-mediated inhibition during the second postnatal week is unknown.

Here, we found that during this period, suppression of SST interneurons increased the number of cells recruited to L-events and widened their lateral spread. This is in line with the strong influence of SST synapses and the early functional maturation of SST interneurons. Furthermore, this observation extends previous findings that interneurons restrict correlated activity to neuronal assemblies in the somatosensory cortex during early cortical development (Duan et al., 2020; Modol et al., 2020). It also matches the function of SST interneurons in adult mice, where they have extensive axonal arbours in L1 (Urban-Ciecko and Barth, 2016) and exert control over large distances through lateral inhibition in the visual (Adesnik et al., 2012) and auditory (Kato et al., 2017) cortex. Accordingly, upon suppression of SST interneurons during adulthood, cell recruitment in hippocampal engrams increases (Stefanelli et al., 2016) as does network synchronicity (Chen et al., 2015).

Under wide-field imaging, the largest events did not seem to increase their size, suggesting that H-events are less affected by the suppression of SST interneurons. However, specific pharmacological isolation of H-events would be necessary to understand whether SST interneuron suppression affects these events alongside L-events.

A large body of work has shown that the features of spontaneous activity patterns are instructive in wiring the developing brain (Feller, 1999; Katz and Shatz, 1996). Manipulations of the size or frequency of retinal waves have directly demonstrated the importance of accurate patterning of spontaneous activity for fine-tuning the ascending visual pathways (Burbridge et al., 2014; Xu et al., 2015). Using a wide range of techniques, we have described L-events as activity patterns during which relatively few cells are weakly activated. Since the spread of activity patterns constrains the degree of synaptic refinement, SST interneurons may optimize early activity patterns for establishing precise neuronal connections during the second postnatal week. We hypothesize that the largely retinal origin (Siegel et al., 2012) and restricted size of L-events allows them to mediate refinement of the network, as their localized nature maintains topographic specificity.

In contrast to local L-events, H-events are highly synchronized in time and drive substantial areas of the cortex to fire large numbers of action potentials. The high spatial spread and temporal synchronicity of H-events makes them less suitable to convey information about cell arrangement in the retina. Instead, H-events may perform synaptic homeostasis to maintain workable ranges of synaptic strength, perhaps in a similar mechanism as during slow-wave sleep (González-Rueda et al., 2018; Tononi and Cirelli, 2006). Indeed, (Wosniack et al., 2021) recently modelled how Hebbian plasticity rules allow L-events to refine cortical topography while H-events dynamically adapt their amplitude to keep synaptic strength in a workable range. We have previously shown that H- and L-events have distinct event characteristics, and that L-events and not H-events depend on retinal waves of activity. Here we find that in addition, H-events are also driven by much stronger excitatory influx than L-events, while inhibitory influx is only marginally larger. These observations may explain why suppression of SST interneurons did not turn L-events into H-events, as these events have similar inhibitory innervation, but different strength and sources of excitatory inputs. Most likely, the inhibitory inputs

that are able to constrain the spread of L-events during their weaker excitatory influx are simply overwhelmed by the strong excitatory influx during H-events.

In conclusion, we find that SST interneurons exert robust inhibitory control over network activity during the second postnatal week, even though inhibitory signalling is not fully strengthened until after eye opening. It seems that not only do interneurons exert inhibitory control over this early age, but they shape activity patterns crucial for driving fine-tuning of the developing network. It remains to be understood how other interneuron subtypes shape spontaneous activity, and future experiments involving prolonged suppression of SST interneuron activity during the second postnatal week may reveal the consequences for receptive field properties in the adult visual cortex.

METHODS

EXPERIMENTAL MODEL AND SUBJECT DETAILS

All experimental procedures were approved by the institutional animal care and use committee of the Royal Netherlands Academy of Sciences. All pups were aged between postnatal days (P) 8-14 and weight between 5 and 10g. Pups were housed in shared nests (two dams) with a maximum of 10 pups per cage. Animals were drug naïve. At the time of data collection, animals had previously undergone either viral injection at P0/P1 or *in utero* electroporation as embryos and subsequent toe-clipping for identification purposes, in order to achieve expression of the calcium sensor. Where the calcium sensor was acutely injected, animals had undergone no previous procedures. Where control animals were used, littermates were randomly assigned to experimental groups.

Genotypes

Wildtype mice were either C57BL/6J mice or C57BL/6J x CBA F1 mice. These mice open their eyes at P14. SST-IRES- cre (JAX 13044) mice were designed by Dr. Z. Josh Huang and ordered from Jackson Labs (SST-IRES-Cre; Taniguchi et al., 2011). To produce labelled SST interneurons, this line was crossed with a tdTomato-reporter mice (Ai14D, JAX 7908). These mice were maintained on a mixed C57Bl/6J x 129S background.

Surgeries

In Utero Electroporation

For wide-field calcium imaging shown in Figure 1 and Figure S4, pyramidal neurons in layer 2/3 of the visual cortex were transfected with GCaMP6s (2 mg/ml) and DsRed (2 mg/ml) at E16.5 using *in utero* electroporation (Harvey et al., 2009). Pregnant mice were anesthetized with isoflurane and a small incision (1.5–2 cm) was made in the abdominal wall. The uterine horns were carefully removed from the abdomen, and DNA was injected into the lateral ventricle of embryos using a sharp glass electrode. Voltage pulses (five square wave pulses, 30 V, 50-ms duration, 950-ms interval, custom-built electroporator) were delivered across the brain with tweezer electrodes covered in conductive gel. Embryos were rinsed with warm saline solution and returned to the abdomen, after which time the muscle and skin were sutured.

Virus injection

Pups (P0-P1) were anaesthetized using hypothermia (induced for 6 minutes). A small cut was made in the skin before insertion of a glass pipette and injection of 27 nl of virus in V1 (two-photon imaging) or 27 nl in V1 and a second injection of 27 nl in RL (to achieve greater spread, for wide-field imaging). Animals were injected with a mix of 1:1 AAV1-hSyn-DIO-hM4D(Gi)-mCherry and pAAV-Syn-GCaMP6s-WPRE-SV40 or a mixture of 1:1 PBS and pAAV-Syn-GCaMP6s-WPRE-SV40. pAAV-hSyn-DIO-hM4D(Gi)-mCherry was a gift from Bryan Roth (Krashes et al., 2011, Addgene plasmid # 44362).

Surgery for acute imaging

Animals were anesthetized with isoflurane (3% in 1 l/min O_2). After anaesthesia had become effective, lidocaine was used for local analgesia and a head bar with an opening (Ø 4 mm) above the visual cortex (0.5–2.5 mm rostral from lambda and 1–3 mm lateral from the midline) was attached to the skull with superglue and dental cement. For calcium imaging, a small craniectomy above the visual cortex was performed. The exposed cortical surface was kept moist with cortex buffer (125 mM NaCl, 5 mM KCl, 10 mM glucose, 10 mM HEPES, 2 mM MgSO4 and 2 mM CaCl2 [pH 7.4]). For recordings performed under anaesthesia (used during whole-cell recordings in Figure 1 and 4, and wide-field recordings in Figure 1), isoflurane

levels were lowered to 0.7–1%. Prior to awake imaging (Datasets in Figure 2, 3, S1-3), the animals were given 60 minutes to recover from anaesthesia.

Virus production

AAV vectors were produced as described previously (Verhaagen et al., 2018). In short, AAV1 serotype helper plasmid and pAAV-hSyn-DIO-hM4D(Gi)-mCherry or pAAV-Syn-GCaMP6s were co-transfected into HEK293T cells. Seventy-two hours later, the cells were harvested, lysed and centrifuged. Subsequently the viral particles were purified from the supernatant using an iodixanol density gradient and further concentrated using an Amicon Ultra-15 centrifugal filter. Titres were determined by quantitative PCR for the WPRE element in the viral genomes (vg). Primers for WPRE: 5′-CCCACTTGGCAGTACATCAA-3′ and 5′-GGAAAGTCCCATAAGGTCATGT-3′. Titres were 2E+12 vg/ml for pAAV-hSyn-DIO-hM4D(Gi)-mCherry and pAAV-Syn-GCAMP6s.

Calcium Imaging Methods

Calcium Sensors

Figure 1A-G, Figure 4 and Figure S3: The calcium-sensitive dye Oregon Green 488 BAPTA-1 AM (OGB-1, Invitrogen) was dissolved in 4 µl pluronic F-127, 20% solution in DMSO (Invitrogen) and further diluted (1 : 10) in dye buffer (150 mM NaCl, 2.5 mM KCl, and 10 mM HEPES) to yield a final concentration of 1 mM. The dye was then pressure-ejected at 10–12 psi for 12–13 min with a micropipette (3–5 MΩ) attached to a picospritzer (Toohey).

Fig 1H-N, Figure 2, 3, S1,2,4: Animals were injected (see: virus injection) with a mix of 1:1 AAV1-hSyn-DIO-hM4D(Gi)-mCherry and pAAV-Syn-GCaMP6s-WPRE-SV40 or (control animals) a mixture of 1:1 PBS and pAAV-Syn-GCaMP6s-WPRE-SV40.

Image acquisition

Two-photon

In vivo calcium imaging was performed on either a Nikon (A1R-MP) with a 0.8/16x water-immersion objective and a Ti:Sapphire laser (Chameleon II, Coherent) or a Movable Objective Microscope (Sutter Instruments) with a Ti:Sapphire laser (MaiTai HP, Spectra Physics) and a 0.8/40x water-immersion objective (Olympus) using Nikon or ScanImage software (Pologruto et al., 2003). Scan mirror positions

were recorded to synchronize calcium imaging and electrophysiology. Images of 330 by 330 μm were recorded at 5-10 Hz.

Epifluorescence

Epifluorescence was recorded at 20 Hz using custom-built LabVIEW software (National Instruments) using a digital CCD camera (QImaging), a 0.16/4x (Olympus) objective and a xenon-arc lamp (Sutter Instrument Company). To map the cortical surface and identify the location of V1, we labelled primary sensory areas post-hoc by immunohistochemistry for the thalamocortical axon marker vGlut2 (Supplementary Figure 4).

Dreadd activation

Animals expressing the above virus were first imaged at baseline. The fast DREADD agonist clozapine was then injected subcutaneously at 0.5 mg/kg. We expected to see effects in a relatively narrow time window and restricted our analyses to 30 minutes post-injection.

Electrophysiology Acquisition

In vivo: Current clamp

Membrane potential was recorded in current clamp at 10 kHz and filtered at 3 kHz (Multiclamp 700b; Molecular Devices). For current clamp recordings electrodes (4.5–6 MΩ) were filled with intracellular solution (105 mM K gluconate, 10 mM HEPES, 30 mM KCl, 10 mM phosphocreatine, 4 mM MgATP, and 0.3 mM GTP; Golshani et al., 2009). 10 μM Alexa 594 hydrazide (Invitrogen) was added to allow targeted whole-cell recordings. The mean network participation based on calcium imaging was 45% (L-events) and 94% (H-events). The patched cell participated (fired at least 1 action potential) in 70% of L-events and 100% of H-events. Taking a threshold of three action potentials or more gives participation rates similar to the calcium imaging (41% and 94%), implying that we can pick up cells that fire three action potentials or more.

In vivo: Voltage clamp

Synaptic currents were recorded in voltage clamp at 10 kHz and filtered at 3 kHz (Multiclamp 700b; Molecular Devices). For voltage clamp recordings, electrodes were filled with intracellular solution (120 mM $CsMeSO_3$, 8 mM NaCl, 15 mM $CsCl_2$,

10 mM TEA-Cl, 10 mM HEPES, 5 mM QX-314, 4 mM MgATP, 0.3 mM Na-GTP, Kwon et al., 2012).

The reversal potential for chloride was -28 mV and the reversal potential for excitatory currents was 0 mV, corrected for the measured liquid junction potential. The reversal potential for both excitatory and inhibitory inputs were checked empirically throughout each recording (by observing the direction of currents at a range of potentials) and found to correspond to the expected values. During whole-cell recording we alternated between measurements of inhibitory and excitatory current (5 minutes of each before switching) so that changes in patch quality over time would affect each condition equally.

In vitro: Current-clamp

Acute 300 µm coronal slices of the visual cortex were dissected. Pups were sacrificed by decapitation and their brains were immersed in ice-cold cutting solution (in mM): 2.5 KCl, 1.25 NaH_2PO_4, 26 $NaHCO_3$, 20 Glucose, 215 Sucrose, 1 $CaCl_2$, 7 $MgCl_2$ (Sigma), pH 7.3-7.4, bubbled with 95%/5% O_2/CO_2. Slices were obtained with a vibratome (VT1200 S, Leica) and subsequently incubated at 34°C in artificial cerebrospinal fluid (ACSF, in mM): 125 NaCl, 3.5 KCl, 1.25 NaH_2PO_4, 26 $NaHCO_3$, 20 Glucose, 2 $CaCl_2$, 1 MgCl2 (Sigma), pH 7.3-7.4. After 45 minutes, slices were transferred to the electrophysiology setup, kept at room temperature and bubbled with 95%/5% O_2/CO_2. For patch recordings, slices were transferred to a recording chamber and perfused (3 ml/min) with ACSF solution bubbled with 95%/5% O_2/CO_2 at 34°C.

Layer 2/3 SST^+ or SST^- cells were identified using a fluorescence/IR-DIC video microscope (Olympus BX51WI). SST^+ interneurons were identified by the mCherrry protein fluorescence from mice injected with pAAV-hSyn-DIO-hM4D(Gi)-mCherry. Current-clamp recordings were made with a MultiClamp 700B amplifier (Molecular Devices), filtered with a low pass Bessel filter at 10 kHz and digitized at 20-50 kHz (Digidata 1440A, Molecular Devices). Series resistance was assessed during recordings and neurons showing a series resistance > 30 MΩ or change > 30% were discarded. Digitized data were analyzed offline using Clampfit 10 (Molecular Devices) and Igor (WaveMetrics).

Electrodes were filled with an intracellular solution containing (in mM): 122 KGluconate, 10 Hepes, 13 KCl, 10 phosphocreatine disodium salt hydrate, 4 ATP magnesium salt, 0.3 GTP sodium salt hydrate (Sigma), pH 7.3. Clozapine 10 µM (Tocris) was bath applied. After breaking the seal, variable current injection was applied to keep cells at-60 mV. To test the excitability of the cells, current injection from-80 pA to 160 pA was applied in 10 pA increments.

QUANTIFICATION AND STATISTICAL ANALYSIS

Image processing

Two-photon

As described previously (Maldonado et al., 2021), two-photon image processing drift and movement artifacts were removed from each recording using NoRMCorre (Pnevmatikakis and Giovannucci, 2017). Delta F stacks were made using the mean fluorescence per pixel as baseline. ROIs were hand-drawn using the Fiji distribution of ImageJ2 (Rueden et al., 2017; Schindelin et al., 2012). Automated transient detection and further data processing was performed using custom-made MATLAB software (MathWorks).

Epifluorescence

Delta F stacks were made using the average fluorescence per pixel as baseline. V1 was identified based on activity coordinates and shape, after this method of identification was confirmed through immunohistochemistry for vGluT2 (Supplementary Figure 4).

Signal detection

Two-photon

In two-photon recordings (Fig 1C-F, Fig 3, Fig 4, FigS2, FigS3), activations within each cell were detected as in Siegel ***et al.,*** (2012) as a peak with both an absolute height and relative prominence of at least 5% $\Delta F/F_0$. When more than 20% of the total number of cells in the field of view were active simultaneously, the activation was considered an event.

Epifluorescence

In epifluorescence imaging (Fig 1G-L, Fig 2D-O, FigS1), events were detected as calcium peaks with an amplitude above 2x the standard deviation of the signal.

Connected component analysis was used to determine whether simultaneously occurring events were distinct, or part of one spreading activation. The total distance travelled by an event was measured by calculating the x and y coordinates of the center of mass of activation in each frame, and summing the difference between these coordinates for each successive frame. Speed was determined as this distance, divided by the number of seconds during which this event was detected (event duration). Analysis was restricted to events that activated at least one pixel in V1.

Electrophysiology

Electrophysiology measurements were aligned to images using custom-built MATLAB software. When an event was detected in calcium imaging, the corresponding electrophysiology trace was extracted from 8 seconds before and after the calcium peak. Contamination from events happening close together in time was removed by automatic detection and manual confirmation. Charge transferred during an excitatory or inhibitory input burst was measured as the area under the curve of the detected burst.

Receiver-operation characteristic curves and random forest classification were analyzed in MATLAB. A separate classifier was built for excitatory and inhibitory inputs for each recorded animal, using every event detected in that condition in that animal. Each run built 100 bagged classification trees. Out-of-bag prediction to classify events; i.e., for each event to be classified, only the trees in which that event was not featured was used to predict whether, based on the electrophysiology, the event was an L- or H-event. The success of this classification was then quantified by comparing it against whether the event was an L- or H-event, based on the participation as measured with calcium imaging, using the 80% cut-off to define an H-event. Success of out-of-bag prediction was used to compare the inhibitory and excitatory models. One animal was excluded from random forest classification due to insufficient inhibitory events to allow for good out-of-bag predictions.

Hierarchical clustering and silhouette analysis was performed in MATLAB. As described in Montijn et al., (2016), we used Ward's method (Ward, 1963) hierarchical clustering to construct dendrograms of all events. Clustering was based on the number of action potentials fired and duration (Fig. 1F) or the amplitude

and activated area (when performed on wide-field data). Hierarchical clustering was performed within each animal. Silhouette curves were made based on the dendrogram (Rousseeuw, 1987), where a single datapoint in a cluster was given a silhouette value of 0. The optimal number of clusters was taken as the overall maximum.

Statistical tests

The test used, n, and the definition of n for each test can be found in the figure legends. Where one paired measurement from each animal was used, we performed paired two-tailed t-tests.

In Figure 2B, each paired value represents a cell before and after application of clozapine. Input-output curves for the in vitro clozapine experiments were generated by calculating the cell firing rate at each current injection step in control and clozapine conditions.

In Figure 2 H-M, we additionally fit a multi-level model on all recorded events, that took the nested nature of this data into account (Aarts et al., 2014) and allowed us to test the interaction of the injected viral construct (either containing hMDi-DREADD or control) with the presence or absence of clozapine. We fitted a linear mixed-effects model using the lme4 package (Bates et al., 2014) in R (R Core Team, 2020) with baseline vs clozapine and DREADD vs control mice as fixed effects, with random intercepts and slopes for the metric that was being evaluated. To determine whether there was an interaction effect between the clozapine administration and the mouse line, we fitted a full model which included the interaction and a reduced model which did not. Whether there was a significant interaction was determined by comparing the full model with the reduced model using an ANOVA. Results of paired t-tests in Figure 2 are only shown where this ANOVA indicated a significant contribution of the interaction term. Similarly, in Figure 3D and E we performed a two-way ANOVA to confirm that the effects we detected were also significant relative to control animals.

In Supplementary Figure 3, we used the non-parametric two-sample Kolmogorov-Smirnov tests to compare distributions of amplitude and participation in both SST expressing and non-SST expressing cells.

Acknowledgements

The authors thank Cátia Silva, Alexander Heimel and Julijana Gjorgjieva for their comments on this manuscript, Monique van Mourik for technical assistance, Johan Winnubst and Guido Meijer for help with data analysis software. This work was supported by grants of the Netherlands Organization for Scientific Research (NWO, ALW Open Program grants, no. 822.02.006 and ALWOP.216; ALW Vici grant, no. 865.12.001) and the "Stichting Vrienden van het Herseninstituut".

Declaration of Interests

The authors declare no competing interests.

REFERENCES

Aarts, E., Verhage, M., Veenvliet, J.V., Dolan, C.V., and van der Sluis, S. (2014). A solution to dependency: using multilevel analysis to accommodate nested data. Nature Neuroscience *17*, 491–496.

Ackman, J.B., and Crair, M.C. (2014). Role of emergent neural activity in visual map development. Current Opinion in Neurobiology *24*, 166–175.

Ackman, J.B., Zeng, H., and Crair, M.C. (2014). Structured dynamics of neural activity across developing neocortex. BioRxiv 012237.

Adesnik, H., Bruns, W., Taniguchi, H., Huang, Z.J., and Scanziani, M. (2012). A neural circuit for spatial summation in visual cortex. Nature *490*, 226–231.

Albert, M.V., Schnabel, A., and Field, D.J. (2008). Innate Visual Learning through Spontaneous Activity Patterns. PLOS Computational Biology *4*, e1000137.

Allene, C., and Cossart, R. (2010). Early NMDA receptor-driven waves of activity in the developing neocortex: physiological or pathological network oscillations? J.Physiol *588*, 83–91.

Bates, D., Mächler, M., Bolker, B., and Walker, S. (2014). Fitting Linear Mixed-Effects Models using lme4. ArXiv:1406.5823 [Stat].

Blankenship, A.G., and Feller, M.B. (2010). Mechanisms underlying spontaneous patterned activity in developing neural circuits. Nat Rev Neurosci *11*, 18–29.

Bonifazi, P., Goldin, M., Picardo, M.A., Jorquera, I., Cattani, A., Bianconi, G., Represa, A., Ben-Ari, Y., and Cossart, R. (2009). GABAergic Hub Neurons Orchestrate Synchrony in Developing Hippocampal Networks. Science *326*, 1419–1424.

Breiman, L. (2001). Random Forests. Machine Learning *45*, 5–32.

Burbridge, T.J., Xu, H.-P., Ackman, J.B., Ge, X., Zhang, Y., Ye, M.-J., Zhou, Z.J., Xu, J., Contractor, A., and Crair, M.C. (2014). Visual Circuit Development Requires Patterned Activity Mediated by Retinal Acetylcholine Receptors. Neuron *84*, 1049–1064.

Cang, J., Renteria, R.C., Kaneko, M., Liu, X., Copenhagen, D.R., and Stryker, M.P. (2005). Development of Precise Maps in Visual Cortex Requires Patterned Spontaneous Activity in the Retina. Neuron *48*, 797–809.

Che, A., Babij, R., Iannone, A.F., Fetcho, R.N., Ferrer, M., Liston, C., Fishell, G., and García, N.V.D.M. (2018). Layer I Interneurons Sharpen Sensory Maps during Neonatal Development. Neuron *99*, 98–116.

Chen, N., Sugihara, H., and Sur, M. (2015). An acetylcholine-activated microcircuit drives temporal dynamics of cortical activity. Nature Neuroscience *18*, 892–902.

Chen, T.-W., Wardill, T.J., Sun, Y., Pulver, S.R., Renninger, S.L., Baohan, A., Schreiter, E.R., Kerr, R.A., Orger, M.B., Jayaraman, V., et al. (2013). Ultrasensitive fluorescent proteins for

imaging neuronal activity. Nature *499*, 295–300.

Colonnese, M.T. (2014). Rapid Developmental Emergence of Stable Depolarization during Wakefulness by Inhibitory Balancing of Cortical Network Excitability. J. Neurosci. *34*, 5477–5485.

Colonnese, M.T., and Phillips, M.A. (2018). Thalamocortical function in developing sensory circuits. Curr. Opin. Neurobiol. *52*, 72–79.

Duan, Z.R.S., Che, A., Chu, P., Modol, L., Bollmann, Y., Babij, R., Fetcho, R.N., Otsuka, T., Fuccillo, M.V., Liston, C., et al. (2020). GABAergic restriction of network dynamics regulates interneuron survival in the developing cortex. Neuron *105*, 75–92.

Feller, M.B. (1999). Spontaneous correlated activity in developing neural circuits. Neuron *22*, 653–656.

Flossmann, T., Kaas, T., Rahmati, V., Kiebel, S.J., Witte, O.W., Holthoff, K., and Kirmse, K. (2019). Somatostatin Interneurons Promote Neuronal Synchrony in the Neonatal Hippocampus. Cell Rep *26*, 3173-3182.e5.

Golshani, P., Goncalves, J.T., Khoshkhoo, S., Mostany, R., Smirnakis, S., and Portera-Cailliau, C. (2009). Internally Mediated Developmental Desynchronization of Neocortical Network Activity. J.Neurosci. *29*, 10890–10899.

González-Rueda, A., Pedrosa, V., Feord, R.C., Clopath, C., and Paulsen, O. (2018). Activity-Dependent Downscaling of Subthreshold Synaptic Inputs during Slow-Wave-Sleep-like Activity In Vivo. Neuron *97*, 1244–1252.

Gribizis, A., Ge, X., Daigle, T.L., Ackman, J.B., Zeng, H., Lee, D., and Crair, M.C. (2019). Visual Cortex Gains Independence from Peripheral Drive before Eye Opening. Neuron *0*.

Guan, W., Cao, J.-W., Liu, L.-Y., Zhao, Z.-H., Fu, Y., and Yu, Y.-C. (2017). Eye opening differentially modulates inhibitory synaptic transmission in the developing visual cortex. ELife *6*, e32337199661.

Hanganu, I.L., Ben Ari, Y., and Khazipov, R. (2006). Retinal waves trigger spindle bursts in the neonatal rat visual cortex. J Neurosci. *26*, 6728–6736.

Kato, H.K., Asinof, S.K., and Isaacson, J.S. (2017). Network-Level Control of Frequency Tuning in Auditory Cortex. Neuron *95*, 412–423.

Katz, L.C., and Shatz, C.J. (1996). Synaptic activity and the construction of cortical circuits. Science *274*, 1133–1138.

Kepecs, A., and Fishell, G. (2014). Interneuron Cell Types: Fit to form and formed to fit. Nature *505*, 318–326.

Kerschensteiner, D. (2014). Spontaneous Network Activity and Synaptic Development. Neuroscientist *20*, 272–290.

Kirkby, L.A., Sack, G.S., Firl, A., and Feller, M.B. (2013). A Role for Correlated Spontaneous

Activity in the Assembly of Neural Circuits. Neuron *80*, 1129–1144.

Kirmse, K., Kummer, M., Kovalchuk, Y., Witte, O.W., Garaschuk, O., and Holthoff, K. (2015). GABA depolarizes immature neurons and inhibits network activity in the neonatal neocortex in vivo. Nat Commun *6*, 7750.

Ko, H., Cossell, L., Baragli, C., Antolik, J., Clopath, C., Hofer, S.B., and Mrsic-Flogel, T.D. (2013). The emergence of functional microcircuits in visual cortex. Nature *496*, 96–100.

Krashes, M.J., Koda, S., Ye, C., Rogan, S.C., Adams, A.C., Cusher, D.S., Maratos-Flier, E., Roth, B.L., and Lowell, B.B. (2011). Rapid, reversible activation of AgRP neurons drives feeding behavior in mice. J. Clin. Invest. *121*, 1424–1428.

Leighton, A.H., and Lohmann, C. (2016). The Wiring of Developing Sensory Circuits-From Patterned Spontaneous Activity to Synaptic Plasticity Mechanisms. Front Neural Circuits *10*, 71.

Luhmann, H.J., and Khazipov, R. (2018). Neuronal Activity Patterns in the Developing Barrel Cortex. Neuroscience *368*, 256–267.

Maldonado, P.P., Nuno-Perez, A., Kirchner, J.H., Hammock, E., Gjorgjieva, J., and Lohmann, C. (2021). Oxytocin Shapes Spontaneous Activity Patterns in the Developing Visual Cortex by Activating Somatostatin Interneurons. Curr Biol *31*, 322–333.

Markram, H., Toledo-Rodriguez, M., Wang, Y., Gupta, A., Silberberg, G., and Wu, C. (2004). Interneurons of the neocortical inhibitory system. Nat.Rev.Neurosci *5*, 793–807.

Marques-Smith, A., Lyngholm, D., Kaufmann, A.-K., Stacey, J.A., Hoerder-Suabedissen, A., Becker, E.B.E., Wilson, M.C., Molnár, Z., and Butt, S.J.B. (2016). A Transient Translaminar GABAergic Interneuron Circuit Connects Thalamocortical Recipient Layers in Neonatal Somatosensory Cortex. Neuron *89*, 536–549.

Minlebaev, M., Ben-Ari, Y., and Khazipov, R. (2007). Network mechanisms of spindle-burst oscillations in the neonatal rat barrel cortex in vivo. J. Neurophysiol. *97*, 692–700.

Mòdol, L., Sousa, V.H., Malvache, A., Tressard, T., Baude, A., and Cossart, R. (2017). Spatial Embryonic Origin Delineates GABAergic Hub Neurons Driving Network Dynamics in the Developing Entorhinal Cortex. Cereb Cortex *27*, 4649–4661.

Modol, L., Bollmann, Y., Tressard, T., Baude, A., Che, A., Duan, Z.R.S., Babij, R., García, N.V.D.M., and Cossart, R. (2020). Assemblies of perisomatic GABAergic neurons in the developing barrel cortex. Neuron *105*, 93–105.

Montijn, J.S., Olcese, U., and Pennartz, C.M.A. (2016). Visual Stimulus Detection Correlates with the Consistency of Temporal Sequences within Stereotyped Events of V1 Neuronal Population Activity. The Journal of Neuroscience *36*, 8624–8640.

Naskar, S., Narducci, R., Balzani, E., Cwetsch, A.W., Tucci, V., and Cancedda, L. (2019). The development of synaptic transmission is time-locked to early social behaviors in rats. Nat Commun *10*, 1195.

Pan, N.C., Fang, A., Shen, C., Sun, L., Wu, Q., and Wang, X. (2018). Early Excitatory Activity-Dependent Maturation of Somatostatin Interneurons in Cortical Layer 2/3 of Mice. Cereb. Cortex.

Pnevmatikakis, E.A., and Giovannucci, A. (2017). NoRMCorre: An online algorithm for piecewise rigid motion correction of calcium imaging data. Journal of Neuroscience Methods *291*, 83–94.

Pologruto, T.A., Sabatini, B.L., and Svoboda, K. (2003). ScanImage: flexible software for operating laser scanning microscopes. Biomed.Eng Online. *2*, 13.

R Core Team (2020). R (Vienna, Austria: R Foundation for Statistical Computing).

Rahmati, V., Kirmse, K., Holthoff, K., Schwabe, L., and Kiebel, S.J. (2017). Developmental Emergence of Sparse Coding: A Dynamic Systems Approach. Scientific Reports *7*, 13015.

Rochefort, N.L., Narushima, M., Grienberger, C., Marandi, N., Hill, D.N., and Konnerth, A. (2011). Development of direction selectivity in mouse cortical neurons. Neuron *71*, 425–432.

Rousseeuw, P.J. (1987). Silhouettes: A graphical aid to the interpretation and validation of cluster analysis. Journal of Computational and Applied Mathematics *20*, 53–65.

Rueden, C.T., Schindelin, J., Hiner, M.C., DeZonia, B.E., Walter, A.E., Arena, E.T., and Eliceiri, K.W. (2017). ImageJ2: ImageJ for the next generation of scientific image data. BMC Bioinformatics *18*, 529.

Schindelin, J., Arganda-Carreras, I., Frise, E., Kaynig, V., Longair, M., Pietzsch, T., Preibisch, S., Rueden, C., Saalfeld, S., Schmid, B., et al. (2012). Fiji: an open-source platform for biological-image analysis. Nat Meth *9*, 676–682.

Siegel, F., Heimel, J.A., Peters, J., and Lohmann, C. (2012). Peripheral and central inputs shape network dynamics in the developing visual cortex in vivo. Current Biology *22*, 253–258.

Stefanelli, T., Bertollini, C., Lüscher, C., Muller, D., and Mendez, P. (2016). Hippocampal Somatostatin Interneurons Control the Size of Neuronal Memory Ensembles. Neuron *89*, 1074–1085.

Su, J., Basso, D., Iyer, S., Su, K., Wei, J., and Fox, M.A. (2020). Paracrine Role for Somatostatin Interneurons in the Assembly of Perisomatic Inhibitory Synapses. The Journal of Neuroscience JN-RM-0613-20.

Taniguchi, H., He, M., Wu, P., Kim, S., Paik, R., Sugino, K., Kvitsani, D., Fu, Y., Lu, J., Lin, Y., et al. (2011). A resource of cre driver lines for genetic targeting of GABAergic neurons in cerebral cortex. Neuron *71*, 995–1013.

Tononi, G., and Cirelli, C. (2006). Sleep function and synaptic homeostasis. Sleep Med.Rev *10*, 49–62.

Torborg, C.L., and Feller, M.B. (2005). Spontaneous patterned retinal activity and the

refinement of retinal projections. Prog.Neurobiol. *76*, 213–235.

Tremblay, R., Lee, S., and Rudy, B. (2016). GABAergic Interneurons in the Neocortex: From Cellular Properties to Circuits. Neuron *91*, 260–292.

Tuncdemir, S.N., Wamsley, B., Stam, F.J., Osakada, F., Goulding, M., Callaway, E.M., Rudy, B., and Fishell, G. (2016). Early Somatostatin Interneuron Connectivity Mediates the Maturation of Deep Layer Cortical Circuits. Neuron *89*, 521–535.

Urban-Ciecko, J., and Barth, A.L. (2016). Somatostatin-expressing neurons in cortical networks. Nat Rev Neurosci *17*, 401–409.

Valeeva, G., Tressard, T., Mukhtarov, M., Baude, A., and Khazipov, R. (2016). An Optogenetic Approach for Investigation of Excitatory and Inhibitory Network GABA Actions in Mice Expressing Channelrhodopsin-2 in GABAergic Neurons. J. Neurosci. *36*, 5961–5973.

Verhaagen, J., Hobo, B., Ehlert, E.M.E., Eggers, R., Korecka, J.A., Hoyng, S.A., Attwell, C.L., Harvey, A.R., and Mason, M.R.J. (2018). Small Scale Production of Recombinant Adeno-Associated Viral Vectors for Gene Delivery to the Nervous System. Methods Mol. Biol. *1715*, 3–17.

van Versendaal, D., and Levelt, C.N. (2016). Inhibitory interneurons in visual cortical plasticity. Cell. Mol. Life Sci. *73*, 3677–3691.

Ward, J.H. (1963). Hierarchical Grouping to Optimize an Objective Function. Journal of the American Statistical Association *58*, 236.

Winnubst, J., Cheyne, J.E., Niculescu, D., and Lohmann, C. (2015). Spontaneous activity drives local synaptic plasticity in vivo. Neuron *87*, 399–410.

Wosniack, M.E., Kirchner, J.H., Chao, L.-Y., Zabouri, N., Lohmann, C., and Gjorgjieva, J. (2021). Adaptation of spontaneous activity in the developing visual cortex. ELife *10*, e61619.

Xu, H.P., Furman, M., Mineur, Y.S., Chen, H., King, S.L., Zenisek, D., Zhou, Z.J., Butts, D.A., Tian, N., Picciotto, M.R., et al. (2011). An instructive role for patterned spontaneous retinal activity in mouse visual map development. Neuron *70*, 1115–1127.

Xu, H.-P., Burbridge, T.J., Chen, M.-G., Ge, X., Zhang, Y., Zhou, Z.J., and Crair, M.C. (2015). Spatial pattern of spontaneous retinal waves instructs retinotopic map refinement more than activity frequency. Dev Neurobiol *75*, 621–640.

Zhang, J., Ackman, J.B., Xu, H.P., and Crair, M.C. (2012). Visual map development depends on the temporal pattern of binocular activity in mice. Nat Neurosci *15*, 298–307.

SUPPLEMENTARY FIGURES

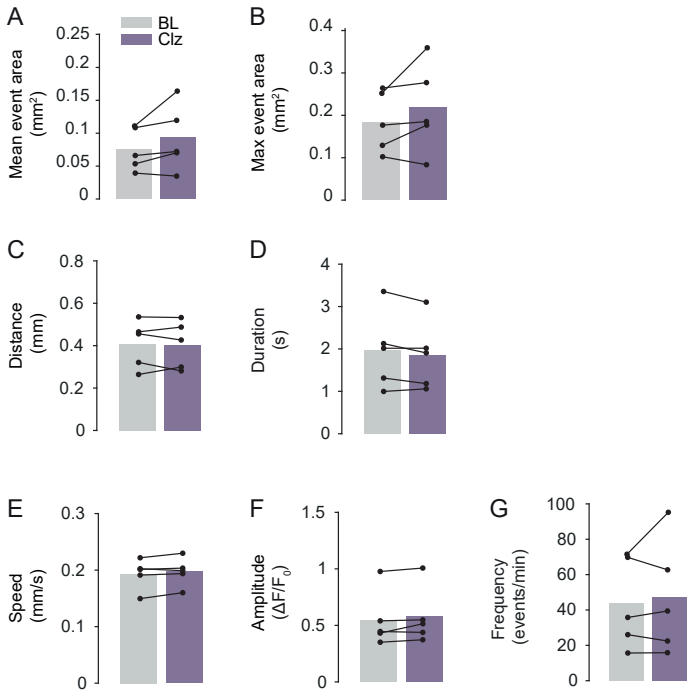

Supplementary Figure 1 , Wide-field recordings in control animals not injected with the hM4Di-DREADD construct

A. Upon clozapine administration, the mean total area activated by an event did not change in control animals (ns, paired two-tailed t-test, n = 5 animals).
B. We detected no change in the peak size of wide-field events upon clozapine administration in control animals (ns, paired two-tailed t-test, n = 5 animals).
C. The mean distance travelled across the cortex did not change after clozapine administration in control animals (ns, paired two-tailed t-test, n = 5 animals).
D. The mean duration of events did not change after clozapine administration in control animals (ns, paired two-tailed t-test, n = 5 animals).
E. We detected no change in the speed of events upon clozapine administration in control animals (ns, paired two-tailed t-test, n = 5 animals).
F. We detected no change in the mean amplitude of wide-field events upon clozapine administration in control animals (ns, paired two-tailed t-test, n = 5 animals).
G. We detected no change in the frequency of events upon clozapine administration in control animals (ns, paired two-tailed t-test, n = 5 animals).

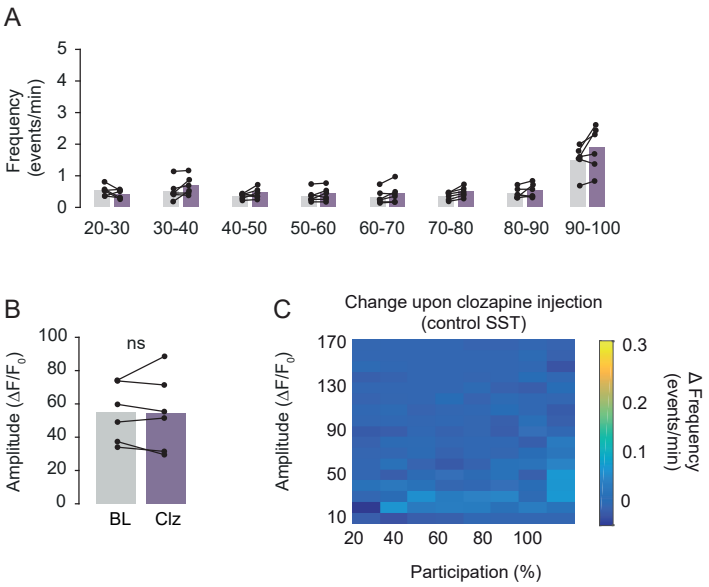

Supplementary Figure 2, Two-photon recordings in control animals not injected with the hM4Di-DREADD construct

A. No change in event frequency was found after administration of clozapine in control animals (ns, paired t-test, n = 6 animals).

B. No significant change in the amplitude of events was detected after administration of clozapine incontrol animals (ns, paired t-test, n = 6 animals).

C. A heatmap showing change over various amplitudes and participation ranges shows no change after clozapine administration in control animals.

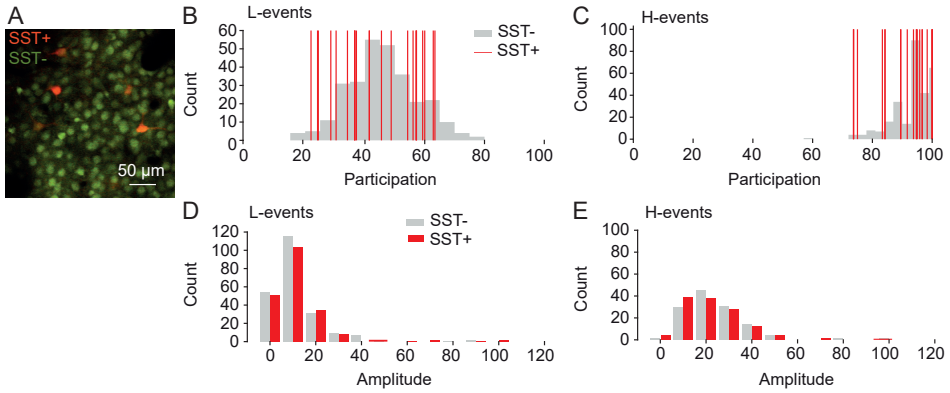

Supplementary Figure 3, Two-photon calcium imaging of SST+ and SST- cells during spontaneous activity

A. Cells expressing SST were labelled with the red fluorescent protein tdTomato
B. Distribution of the % of L-events in which each SST- cell participates. Red vertical lines are the values for each SST+ cell detected in these recordings. n = 283 SST- cells, 22 SST+ cells over 3 animals, Two-sample Kolmogorov–Smirnov test, n.s.
C. Distribution of the % of H-events in which each SST- cell participates. Red vertical lines are the values for each SST+ cell detected in these recordings. n = 283 SST- cells, 22 SST+ cells over 3 animals, Two-sample Kolmogorov–Smirnov test, n.s.
D. No significant difference was detected between the distribution of the mean amplitudes of SST- and SST+ cells during L- events, n = 221 L-events, Two-sample Kolmogorov–Smirnov test, n.s.
E. No significant difference was detected between the distribution of the mean amplitudes of SST- and SST+ cells during H- events, n = 128 H-events, Two-sample Kolmogorov–Smirnov test, n.s.

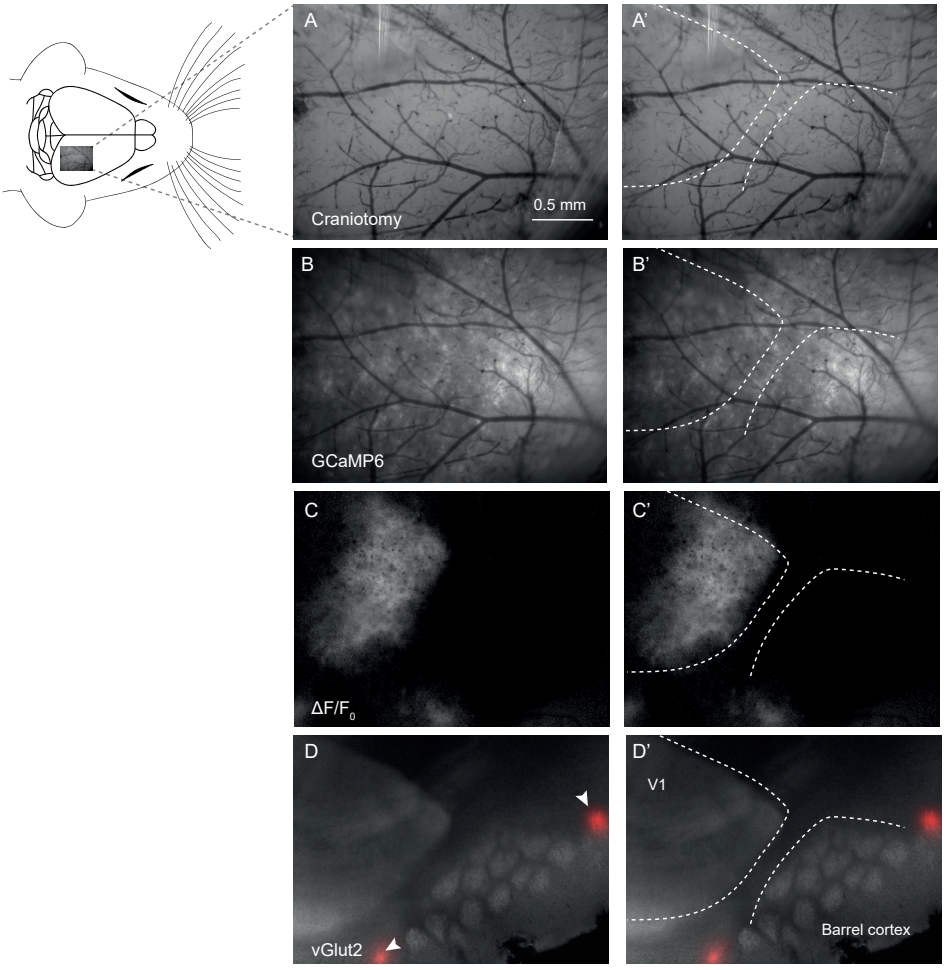

Supplementary Figure 4, Mapping primary sensory cortices using post-hoc vglut2 immunohistochemistry

A, A'. Craniotomy with exposed surface of the cortex.

B, B'. GCaMP6 expressing neurons

C, C'. Spontaneous activity event expressed as DF/F0.

D, D'. Posthoc immunohistochemistry for vGlut2 reveals boundaries of primary sensory areas (V1, barrel cortex). Arrow heads show injected fluorescent marker for aligning the posthoc labeling with the in vivo imaging.

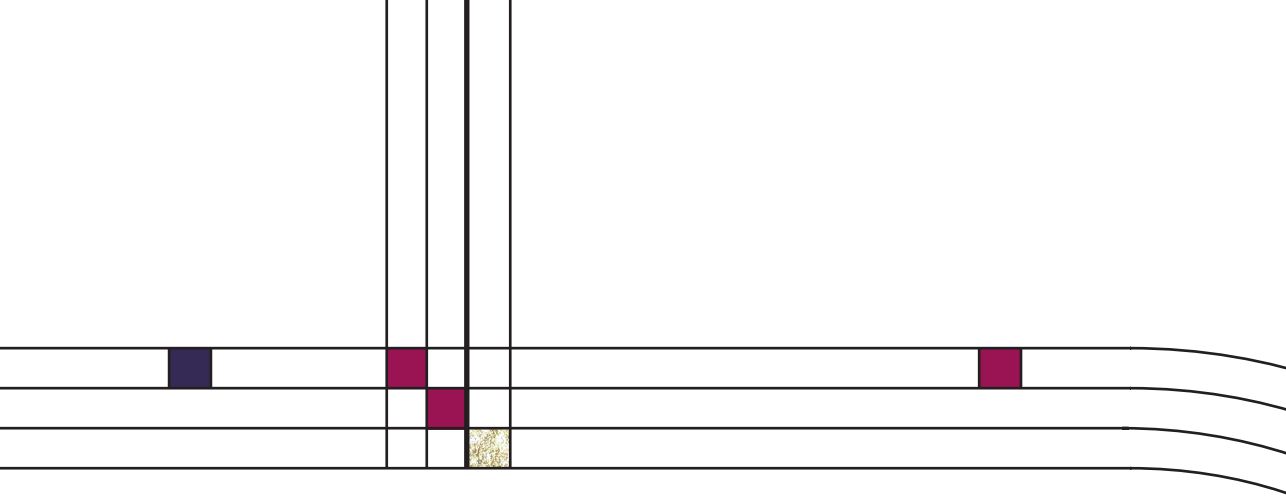

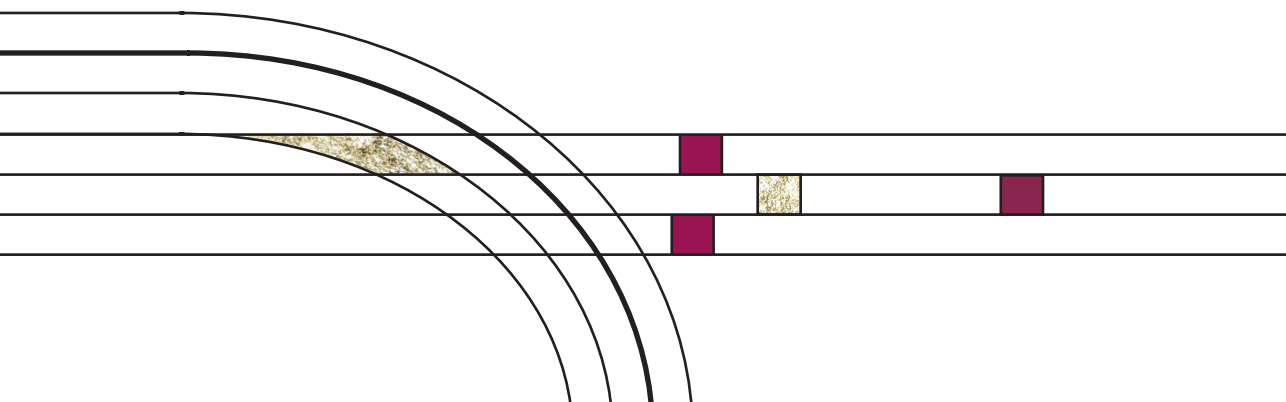

CHAPTER 3

Cholinergic modulation of spontaneous activity during the second postnatal week

Authors

Alexandra H. Leighton, Gerrit J. Houwen and Christian Lohmann

INTRODUCTION

Adapting to the environment is essential for survival, and so the brain is constantly adjusting the internal state of the animal to match external influences. Some adaptations occur very quickly, such as a fast rush of adrenaline upon encountering danger. Other adaptations, such as behavioural changes or learning new skills, can take place over much slower timescales. One way in which the brain adapts is through the release of neuromodulators; chemical messengers that can have widespread influence on neuronal activity. One such neuromodulator is acetylcholine, which can influence neuronal responses through both inhibitory interneuron activity and presynaptic modulation of excitatory synapses (Chen et al., 2015; Goard and Dan, 2009; Pinto et al., 2013). Acetylcholine is released into the cortex by the basal forebrain during heightened attention (Giovannini et al., 2001; Paul et al., 2015), and increases the sensitivity of neurons to those stimuli the animal is attending to (Muñoz and Rudy, 2014). This allows the animal to focus on a salient input, such as an approaching predator. Cholinergic signalling is also involved in learning and memory, where high acetylcholine levels may favour memory formation by strengthening feedforward inputs and reducing excitatory feedback inputs (Hasselmo, 2006). For instance, cholinergic-mediated disinhibition of auditory cortex pyramidal cells will facilitate fear conditioning in response to a complex tone, linking environmental information to cortical response (Letzkus et al., 2011). Acetylcholine can be seen as an uncertainty marker, signalling unreliability of predictive cues (Picciotto et al., 2012). In the context of the Bayesian brain model, in which sensory information is represented as a probability distribution (Knill and Pouget, 2004), acetylcholine may signal when information is low, indicating a need to route more information from the environment to update and enrich probability distributions. Acetylcholine is therefore associated with steering information flow to optimally match the state of the animal; when acetylcholine release is high, information from the periphery is prioritised and excitatory intracortical connections are simultaneously suppressed in a bid to obtain more data.

Acetylcholine binds to both metabotropic muscarinic receptors and ionotropic nicotinic receptors, and each are responsible for a different aspect of modulating information flow. Activating muscarinic receptors suppresses intracortical connections, whereas activated nicotinic receptors mediate enhanced thalamic input to the cortex (Hasselmo, 2006). Muscarinic receptors occur at pre- and

postsynaptic sites (Groleau et al., 2015) whereas nicotinic receptors are found spread across the cell body, presynaptic terminals and axons (Picciotto et al., 2012). The release site, postsynaptic receptor type and location, as well as the concentration of acetylcholine esterase (the enzyme that will break down released acetylcholine) will interact to produce the neuromodulatory effects of acetylcholine.

Before the senses are active, young neuronal circuits are shaped by spontaneous activity, which is generated by the nervous system itself rather than evoked by an external stimulus. In the mouse visual system, bursts of activity generated in the retina refine retinotopic maps and the segregation of contra- and ipsilateral afferents through Hebbian and non-Hebbian mechanisms (Kirkby et al., 2013). As a result of this fine-tuning, neurons in the mouse visual cortex respond with striking acuity to visual information as soon as the eyes open at postnatal day (P)14 (Cang et al., 2005; Ko et al., 2013; Rochefort et al., 2011; Zhang et al., 2012). Spontaneous activity occurs in different patterns, which can be described in terms of frequency, synchronicity, amplitude, number of cells participating and other characteristics (Ackman and Crair, 2014; Kerschensteiner, 2014). These specific characteristics encode and transmit essential information required by the brain to develop normally (Kirkby et al., 2013; Leighton and Lohmann, 2016). For instance, if retinal waves are too large, retinotopic map refinement is prevented, whereas eye-specific segregation can be impaired by changes in event frequency (Burbridge et al., 2014; Xu et al., 2011). At this developmental stage, cholinergic projections already innervate V1 (Groleau et al., 2015; Latsari et al., 2002). However, we do not yet know whether or how spontaneous activity is modulated by acetylcholine. The molecular guidance pathways that set out the initial organisation of the brain are often considered to be 'hard-coded', relatively impervious to outside influences. In contrast, critical periods exist during which development is very sensitive to the environment. It is not clear to what extent the features of spontaneous activity are fully deterministic, or whether they can be shaped by experience. If spontaneous activity features can be altered by the state of the animal via neuromodulators, this could give experience and behavioural state during very early life the opportunity to permanently shape the organisation of the brain.

We and others have previously described patterns of activity in the visual cortex which are driven by retinal waves (Ackman et al., 2012) and reduced upon

enucleation (Hanganu et al., 2006; Siegel et al., 2012). We refer to these cortical events as low participation events ('L-events') as they activate relatively few neurons. Their retinal origin, combined with their comparative sparsity, gives them the potential to shape the network according to the organization of the eye. During the same postnatal period, a second set of events can be seen, which are not affected by retinal manipulations. These high participation events ('H-events') are patterned differently to L-events, as they are highly synchronized in time and drive a calcium response in almost all cells in the field of view. This activity pattern may allow them to perform synaptic homeostasis, bringing synaptic strengths back to a workable range (Siegel et al., 2012).

These events occur during the second postnatal week. At this time, cholinergic axons innervate the visual cortex (Groleau et al., 2015; Latsari et al., 2002), where cells can respond to cholinergic signalling (Kassam et al., 2008). As early as the first postnatal week, cholinergic signalling can modulate event frequency, and stimulating the basal forebrain increases the chances of recording an event in the visual cortex (Hanganu et al., 2007).

Here, we used wide-field calcium imaging to record from cortex during spontaneous activity in awake mice between postnatal day (P) 9 and P12. Pharmacological agents were applied to manipulate acetylcholine binding to both nicotinic and muscarinic receptors. We detected no effects of mecamylamine, a non-competitive nicotinic receptor antagonist, on event patterns. However, we found that atropine, a competitive muscarinic receptor antagonist, caused events to be shorter and larger, resulting in a 'flash'-like appearance. Additionally, atropine caused waves to travel in a stereotypical direction.

MATERIALS AND METHODS

Animals

All experimental procedures were approved by the institutional animal care and use committee of the Royal Netherlands Academy of Arts and Sciences. Mice (C57BL/6J) of both sexes were used. All animals were aged between postnatal days (P) 8-12. These mice open their eyes at P14.

Surgery

Animals were anesthetized with isoflurane (3% in 1 l/min O_2). After anaesthesia had become effective, lidocaine was used for local analgesia and a head bar with an opening (Ø 4mm) above the visual cortex (0.5–2.5 mm rostral from lambda and 1–3 mm lateral from the midline) was attached to the skull with superglue and dental cement. For calcium imaging, a craniotomy above the visual cortex was performed. The exposed cortical surface was kept moist with cortex buffer (125 mM NaCl, 5 mM KCl, 10 mM glucose, 10 mM HEPES, 2 mM MgSO4 and 2 mM CaCl2 [pH 7.4]). For calcium imaging under anaesthesia, isoflurane levels were lowered to 0.7–1%. Prior to awake imaging, the animals were given 60 minutes to recover from anaesthesia.

In utero electroporation

For wide-field calcium imaging, pyramidal neurons in layer 2/3 of the visual cortex were transfected with GCaMP6s (2 mg/ml) and DsRed (2 mg/ml) at E16.5 using ***in utero*** electroporation (Harvey et al., 2009). Pregnant mice were anesthetized with isoflurane and a small incision (1.5–2 cm) was made in the abdominal wall. The uterine horns were carefully removed from the abdomen, and DNA was injected into the lateral ventricle of embryos using a sharp glass electrode. Voltage pulses (five square wave pulses, 30 V, 50-ms duration, 950-ms interval, custom-built electroporator) were delivered across the brain with tweezer electrodes covered in conductive gel. Embryos were rinsed with warm saline solution and returned to the abdomen, after which time the muscle and skin were sutured.

Imaging

Epifluorescence was recorded using custom-built LabVIEW software (National Instruments) using a digital CCD camera (QImaging), a 0.16/4x (Olympus) objective and a xenon-arc lamp (Sutter Instrument Company) with a movable objective microscope (Sutter Instrument Company). Delta F stacks were made using the average fluorescence per pixel as baseline. V1 was identified based on activity coordinates and shape after this method of identification was confirmed through immunohistochemistry for vGluT2.

Pharmacology

Baseline condition was measured for 40 minutes before applying atropine (1 mM) dissolved in cortex buffer onto the cortical surface. Imaging began 30 minutes

after atropine application. After 40 minutes of recording in the atropine condition, mecamylamine (final concentration 10μM) was added to the atropine mix and applied to the cortical surface. In recordings without atropine, mecamylamine was dissolved directly in cortex buffer.

Statistics

For all tests, events were averaged per animal and n was taken as the number of individual animals in a dataset. Paired two-tailed t-tests were used to compare events before and after application with no corrections of significance thresholds for multiple comparisons.

RESULTS

Application of mecamylamine alone does not alter event properties

We combined pharmacology with wide-field imaging to observe the effect of manipulating cholinergic signalling on large scales (4.9 mm^2, Fig 1A). To isolate the effect of nicotinic signalling, we applied the nicotinic receptor antagonist mecamylamine (Fig 1) to the cortex. Upon mecamylamine application we detected no change in event duration (Fig 1B) or average size (Fig 1C). When compared to baseline, no changes were detected in amplitude (Fig 1D). We measured how far each event travelled across the surface of the brain by calculating the centre of mass of each frame in an event. The amount by which this centre of mass moved over all frames of the event was quantified as distance. This measurement was also not affected by mecamylamine (Fig 1E), neither was the frequency of events (Fig 1F). A histogram of event sizes (Fig 1G) shows that mecamylamine does not change event size distribution.

Atropine increases event area and decreases event duration

In a subsequent set of animals, atropine (1 mM in cortex buffer), a muscarinic receptor antagonist, was applied to the cortical surface (Fig 2A). Atropine significantly decreased the duration of events (Fig 2B), and events increased to take up a larger average area (Fig 2C), resulting in events that quickly flashed into appearance rather than moving as a wave across the cortex. The mean amplitude

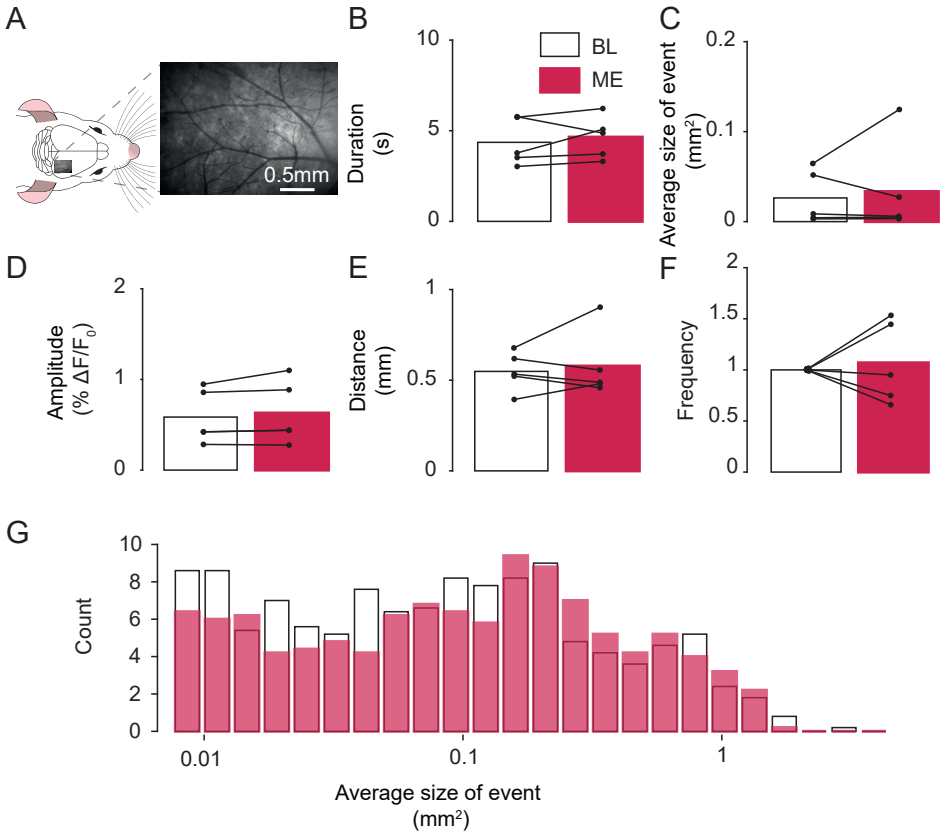

Fig 1, Cortical application of the nicotinic blocker mecamylamine

A. Wide field imaging of 4.9 mm^2 above the visual cortex.

B. No change in mean event duration was detected upon mecamylamine application.

C. No change in event area was detected after mecamylamine application.

D. No change in event amplitude was detected after mecamylamine application.

E. No change in distance travelled by the center of mass of an event was detected after mecamylamine application.

F. The frequency of overall events was the same in the baseline and mecamylamine condition. Frequency shown normalized to baseline frequency.

G. Distribution of event size (averaged per animal) before and after mecamylamine.

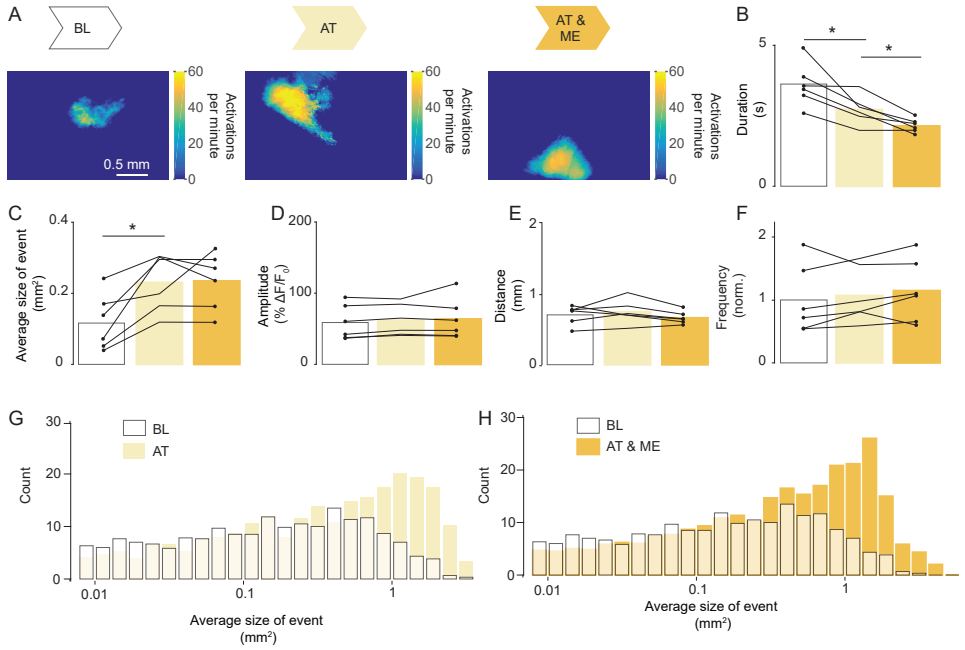

Figure 2, Blocking cholinergic signalling increases event size and shortens event duration

A. Wide-field imaging was used to measure the large-scale effects of pharmacological manipulation of cholinergic signalling. Pharmacological agents were applied directly to the cortex. BL= baseline, AT =atropine, AT & ME = atropine with mecamylamine.

B. Atropine decreases event duration ($p<0.05$). Atropine with Mecamylamine further decrease event duration compared to baseline and compared to the atropine condition ($p<0.05$).

C. The average size of an event (measured as the average number of mm^2 taken up by each event) is increased upon atropine application ($p<0.05$). It remains increased compared to baseline once atropine with mecamylamine is applied ($p<0.05$), but does not increase further due to the addition of mecamylamine.

D. We detected no significant change in amplitude upon either atropine or atropine with mecamylamine.

E. The distance travelled by an event did not change after administration of either atropine or atropine with mecamylamine.

F. We detected no change in the frequency of events after administration of either atropine or atropine with mecamylamine.

G. Distribution of the mean size of an event before and after application of atropine.

H. Distribution of the mean size of an event before and after application of atropine and mecamylamine. Note that the baseline is a repeat of the data in 2G.

of an event did not change (Fig 2D), and the distance measurement was also not affected by atropine (Fig 2E). Application of atropine had no effect on overall frequency (Fig 2F).

After recording the effect of atropine, the nicotinic antagonist mecamylamine was added (Fig 2A). Besides blocking all cholinergic signalling, this addresses the concern that atropine may increase acetylcholine release by targeting presynaptic muscarinic inhibitors (Kilbinger, 1984). When both muscarinic and nicotinic antagonists were applied, events further decreased in duration (Fig 2B) compared to atropine alone. Mean event size was larger than baseline (Fig 2C), but not increased compared to atropine. Mecamylamine did not change event amplitude, distance or frequency compared to atropine (Fig 2D, E, F). As in Figure 1, it seems that mecamylamine application does not have a large impact on wave properties.

The distributions of activation size after pharmacological manipulations (Fig 2G, H) showed a relative increase in large events due to atropine, which was maintained after mecamylamine application. To investigate this difference, we next used hierarchical clustering to group events into L- and H-events.

Cholinergic signalling modulates both L- and H-events

Knowing the relative importance of cholinergic signalling for L- and H- events may help us understand their relative origins. If H-events are intracortical, we would expect them to be affected by muscarinic signalling due to its role in suppressing intracortical connections. L-events may be more sensitive to nicotinic signalling, which can modulate thalamic input to the cortex (Hasselmo, 2006). Hierarchical clustering was performed per animal on event amplitude and maximum area activated during an event (Fig 3A, B). After atropine application, the data split into two groups at a different point (Fig 3C, D), specifically at higher event size, suggesting that L-events become more H-like in characteristics, but that the split into two activity patterns is maintained.

Upon atropine application, both L- and H-events became significantly shorter (Fig 3E, J) in duration. The mean area of L-events showed a trend to increase (Fig 3F), and the mean size of H-events increased significantly (Fig 3K). In both L- and H-events, the amplitude remained the same before and after atropine application

(Fig 3G, L). The distance travelled only decreased significantly in H-events (Fig 3H, M). Upon atropine application, we detected no change in L-event frequency (Fig 3I) and only a trend for H-event frequency to increase (Fig 3N). Taken together, it seems that both types of event can be modulated by atropine.

Upon mecamylamine application in addition to atropine, the duration of both L- and H- events decreased further (Fig 3E, J). There was no difference in the size of events (Fig 3F, K) or the amplitude (Fig 3G, L). We saw that H-events travelled significantly shorter distances across the cortex when compared to the atropine condition (Fig 3H). There was no significant change in frequency of either L-events (Fig 3I) or H-events (Fig 3N). It seems likely that the changes upon mecamylamine application are due to continued exposure to atropine and that mecamylamine does not change event properties in either L or H events.

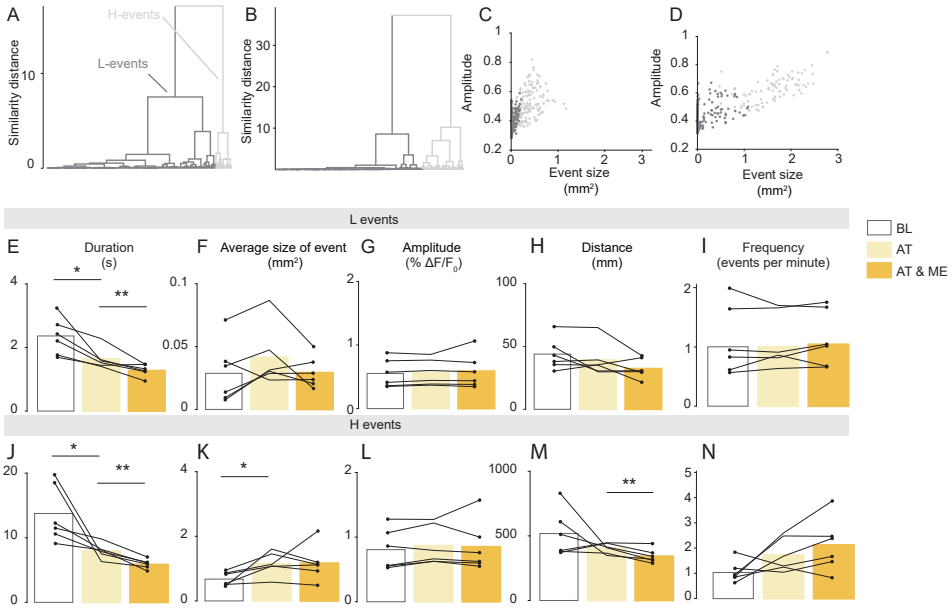

Figure 3, Cholinergic signalling affects both L- and H-events

A. Dendrogram of hierarchical clustering of baseline activity.

B. Dendrogram of hierarchical clustering after atropine application.

C. Event area by amplitude with labelled L- and H-events in baseline condition of one example animal.

D. Event area by amplitude with labelled L- and H-events after atropine application in the same example animal as Fig 2K.

E. The duration of L-events is decreased by atropine ($p<0.05$) and further decreased by atropine with mecamylamine ($p<0.01$).

F. We detected no change in mean L-event area either upon atropine or atropine with mecamylamine application.

G. The mean event amplitude of L-events showed a trend to increase after atropine ($p= 0.08$) but showed no change upon atropine with mecamylamine.

H. The distance travelled by an L-event was not altered by atropine.

I. The frequency of L-events was not changed by atropine or by atropine with mecamylamine application.

J. The duration of H-events is decreased by atropine ($p<0.05$) and further decreased by atropine with mecamylamine ($p<0.01$).

K. Upon atropine, the mean event size of H-events increased ($p<0.05$). Atropine with mecamylamine had no further effect.

L. Mean H-event amplitude did not change after atropine or atropine with mecamylamine application.

M. H-event distance did not change after atropine application, but reduced upon atropine with mecamylamine application ($p<0.01$).

N. The frequency of H-events did not change after atropine or atropine with mecamylamine application.

Atropine changes activity direction

Given that atropine could modulate spontaneous activity feature patterning, we further investigated the properties of spontaneous activity after atropine application, aiming to understand whether cholinergic signalling affects the direction of activity movement. Though not all spontaneous activity appears wave-like under wide-field imaging, many activations do move across the cortex, and their direction can therefore be tracked. We found that atropine did not affect the movement of events along the medio-lateral axis, either overall (Fig 4A) or when the data was split into L- and H-events (Fig 4C, E). In contrast, atropine caused events to on average travel further in a caudal to rostral direction (Fig 4B). This was only a trend in L-events (Fig 4D), but did have a significant effect on H-events (Fig 4F). The effect on direction is summarised as a polar histogram of all animals in Fig 4G, showing the shift towards the caudal – rostral direction. This is the same direction that H-events were found to preferentially travel in under two-photon (Siegel et al., 2012).

DISCUSSION

These results depict cholinergic signalling as a powerful modulator of activity as early as the second postnatal week. Though blocking nicotinic signalling through mecamylamine had no clear effect, the muscarinic antagonist atropine lead to larger, shorter events that travelled in a stereotypical direction.

Atropine prevents acetylcholine binding to muscarinic receptors, mimicking a resting or inattentive state which is typically associated with synchronized activity (Harris and Thiele, 2011). Indeed, we see that each event takes up a larger area of the cortex, indicating that more cells participate in each event. The duration of activity is reduced; activity tends to appear as short, large flashes. It seems as though atropine increases both timing and spatial correlations. Activation of muscarinic receptors would typically suppress intracortical signalling (Hasselmo, 2006; Kimura, 2000, Fig 5A, B). Atropine may prevent this effect, maintaining strong intracortical connections that increase correlations. Preventing muscarinic signalling with atropine made events more H-like, suggesting that these events use intracortical connections to achieve their large cortical spread and high synchronicity (Fig 5C). As H-events sweep across large parts of the cortex, they may

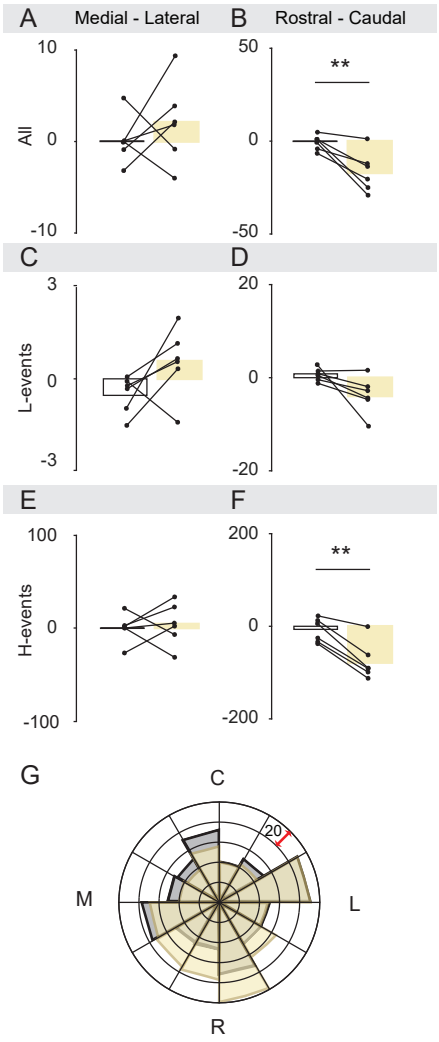

Figure 4, Atropine application causes events to travel in caudal-to-rostral direction

A. There is no change in the mean distance travelled in the medio-lateral direction over all events.

B. Upon atropine application, more events travel in a caudal to rostral direction.

C. L-events do not change the mean distance travelled in medio-lateral direction upon atropine application.

D. After atropine, L-events do not significantly change direction, though there is a trend for events to increase caudal to rostral distance travelled.

E. H-events do not change the mean distance travelled in medio-lateral direction upon atropine or atropine with mecamylamine application.

F. H-events travel further along the caudal-rostral axis upon atropine application ($p<0.01$).

G. Distribution of event directions for all animals before and after atropine application.

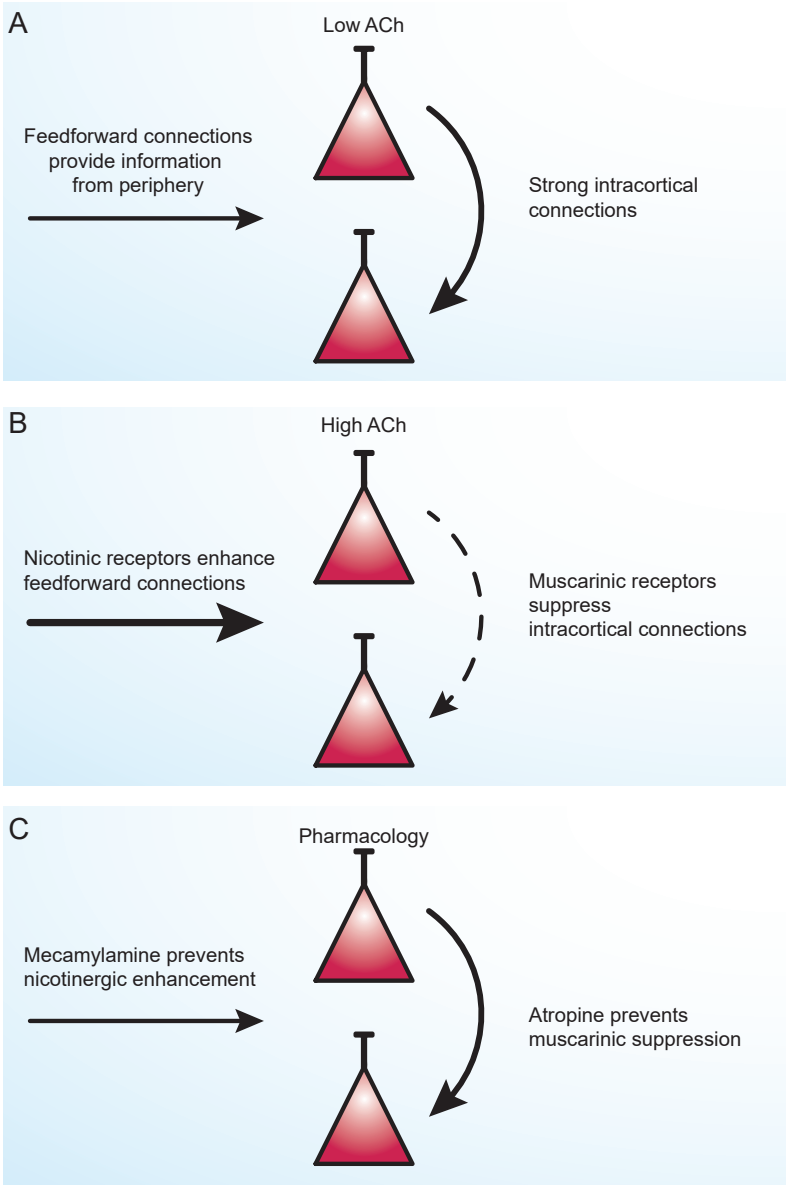

Figure 5, Modulation of feedforward and intracortical connection strength by acetylcholine

A. During low acetylcholine, strong intracortical connections promote information transfer between cortical neurons. Feedforward connections are not strengthened.

B. During high acetylcholine release, muscarinic receptors cause suppression of intracortical connections. Nicotinergic receptors promote feedforward information flow, likely from the periphery or thalamus.

C. Atropine is a muscarinic receptor antagonist, whereas mecamylamine is a nicotinergic antagonist. These compounds compete with acetylcholine and may prevent the normal action of the neuromodulator.

only be able to occur under low-acetylcholine conditions, when the muscarinic 'brake' on intracortical connections is absent. It would be interesting to test whether increasing cholinergic tone could promote L-event characteristics or decorrelate the cortex. This could support the previously hypothesized role for L- and H-events, in which L-events pattern the cortex according the retina, and H-events provide synaptic homeostasis. If acetylcholine indeed signals uncertainty (Yu and Dayan, 2005), i.e. the need to update information, this signal should promote the routing of L-events as these carry information about the periphery. It may be the case that L- and H-events prepare the cortex to be able to process visual inputs during different behavioural states after eye-opening.

After atropine application, waves travelled further in the caudal to rostral direction. Under two-photon microscopy, L-events were found to travel in all directions, whereas H-events preferentially followed the caudal-rostral direction (Siegel et al., 2012). This could be further evidence that waves became more H-like after atropine application, though we do not see this baseline tendency for caudal to rostral travel of H-events in our wide-field imaging here.

Broadly speaking, the effects of mecamylamine with atropine were similar to those of atropine alone. Only in duration was the atropine with mecamylamine condition significantly different to atropine. Given that mecamylamine applied alone had no detectable effects, it seems most likely that this further decrease in duration was due to prolonged or increased application of atropine rather than due to nicotinic activation. This is surprising, given that in pilot experiments with both atropine and mecamylamine under two-photon, a large increase in event frequency was found. Though it remains to be seen what caused this discrepancy, it is imaginable that mecamylamine has effects that are not detectable at the scale of wide-field imaging scale, but which could be picked up with a method such as two-photon calcium imaging in which changes can be seen at individual cell level. A thorough approach testing different concentrations or perhaps different nicotinic antagonists would be necessary before conclusions could be drawn on the contribution of nicotinic signalling to the patterning of spontaneous activity.

In order to understand the impact of cholinergic modulation of spontaneous activity on animal development, it is important to link cholinergic release to behavioural

state. State modulation develops postnatally, with consistent modulation of cortical spontaneous and evoked activity by state only appearing around P11/12 (Cirelli and Tononi, 2015; Colonnese et al., 2010), though animals do show sleep-wake cycles much earlier. Perhaps the relative occurrence of L- and H-events varies depending on whether the mouse is resting or alert. Though acetylcholine is released during the attentive state, acetylcholine release from the nucleus basalis may be able to specifically target different cortical areas (Yu and Dayan, 2005) rather than causing an overall increase of acetylcholine in the whole cortex. To properly interpret these findings, it is essential to understand how much endogenous cholinergic modulation happens specifically in the visual cortex at this time, specifically in the absence or paucity of incoming visual stimulation.

Taken together, these results demonstrate that cholinergic signalling can modulate the patterning of spontaneous activity during the second postnatal week. To refine our understanding of how this works, future experiments could use pharmaco- or optogenetics to activate or silence cholinergic inputs into the cortex from basal forebrain neurons, for instance using the ChaT promotor. The most interesting and ambitious project would be to link changes in endogenous cholinergic signalling, through changes in the patterning of spontaneous activity, to anatomical and functional refinement.

REFERENCES

Ackman, J.B., Burbridge, T.J., and Crair, M.C. (2012). Retinal waves coordinate patterned activity throughout the developing visual system. Nature *490*, 219–225.

Cang, J., Renteria, R.C., Kaneko, M., Liu, X., Copenhagen, D.R., and Stryker, M.P. (2005). Development of Precise Maps in Visual Cortex Requires Patterned Spontaneous Activity in the Retina. Neuron *48*, 797–809.

Chen, N., Sugihara, H., and Sur, M. (2015). An acetylcholine-activated microcircuit drives temporal dynamics of cortical activity. Nature Neuroscience *18*, 892–902.

Cirelli, C., and Tononi, G. (2015). Cortical development, EEG rhythms, and the sleep/wake cycle. Biol Psychiatry *77*, 1071–1078.

Colonnese, M.T., Kaminska, A., Minlebaev, M., Milh, M., Bloem, B., Lescure, S., Moriette, G., Chiron, C., Ben-Ari, Y., and Khazipov, R. (2010). A Conserved Switch in Sensory Processing Prepares Developing Neocortex for Vision. Neuron *67*, 480–498.

Giovannini, M.G., Rakovska, A., Benton, R.S., Pazzagli, M., Bianchi, L., and Pepeu, G. (2001). Effects of novelty and habituation on acetylcholine, GABA, and glutamate release from the frontal cortex and hippocampus of freely moving rats. Neuroscience *106*, 43–53.

Goard, M., and Dan, Y. (2009). Basal forebrain activation enhances cortical coding of natural scenes. Nat Neurosci *12*, 1444–1449.

Groleau, M., Kang, J.I., Huppé-Gourgues, F., and Vaucher, E. (2015). Distribution and effects of the muscarinic receptor subtypes in the primary visual cortex. Front Synaptic Neurosci *7*.

Hanganu, I.L., Ben Ari, Y., and Khazipov, R. (2006). Retinal waves trigger spindle bursts in the neonatal rat visual cortex. J Neurosci. *26*, 6728–6736.

Hanganu, I.L., Staiger, J.F., Ben Ari, Y., and Khazipov, R. (2007). Cholinergic Modulation of Spindle Bursts in the Neonatal Rat Visual Cortex In Vivo. J.Neurosci. *27*, 5694–5705.

Harris, K.D., and Thiele, A. (2011). Cortical state and attention. Nature Reviews Neuroscience *12*, 509.

Hasselmo, M.E. (2006). The Role of Acetylcholine in Learning and Memory. Curr Opin Neurobiol *16*, 710–715.

Kassam, S.M., Herman, P.M., Goodfellow, N.M., Alves, N.C., and Lambe, E.K. (2008). Developmental excitation of corticothalamic neurons by nicotinic acetylcholine receptors. J. Neurosci. *28*, 8756–8764.

Kilbinger, H. (1984). Presynaptic muscarine receptors modulating acetylcholine release. Trends in Pharmacological Sciences *5*, 103–105.

Kimura, F. (2000). Cholinergic modulation of cortical function: A hypothetical role in shifting the dynamics in cortical network. Neuroscience Research *38*, 19–26.

Kirkby, L.A., Sack, G.S., Firl, A., and Feller, M.B. (2013). A Role for Correlated Spontaneous

Activity in the Assembly of Neural Circuits. Neuron *80*, 1129–1144.

Knill, D.C., and Pouget, A. (2004). The Bayesian brain: the role of uncertainty in neural coding and computation. Trends in Neurosciences *27*, 712–719.

Ko, H., Cossell, L., Baragli, C., Antolik, J., Clopath, C., Hofer, S.B., and Mrsic-Flogel, T.D. (2013). The emergence of functional microcircuits in visual cortex. Nature *496*, 96–100.

Latsari, M., Dori, I., Antonopoulos, J., Chiotelli, M., and Dinopoulos, A. (2002). Noradrenergic innervation of the developing and mature visual and motor cortex of the rat brain: a light and electron microscopic immunocytochemical analysis. J. Comp. Neurol. *445*, 145–158.

Letzkus, J.J., Wolff, S.B.E., Meyer, E.M.M., Tovote, P., Courtin, J., Herry, C., and Luthi, A. (2011). A disinhibitory microcircuit for associative fear learning in the auditory cortex. Nature *480*, 331–335.

Muñoz, W., and Rudy, B. (2014). Spatiotemporal specificity in cholinergic control of neocortical function. Current Opinion in Neurobiology *26*, 149–160.

Paul, S., Jeon, W.K., Bizon, J.L., and Han, J.-S. (2015). Interaction of basal forebrain cholinergic neurons with the glucocorticoid system in stress regulation and cognitive impairment. Front. Aging Neurosci. *7*.

Picciotto, M.R., Higley, M.J., and Mineur, Y.S. (2012). Acetylcholine as a neuromodulator: cholinergic signaling shapes nervous system function and behavior. Neuron *76*, 116–129.

Pinto, L., Goard, M.J., Estandian, D., Xu, M., Kwan, A.C., Lee, S.-H., Harrison, T.C., Feng, G., and Dan, Y. (2013). Fast modulation of visual perception by basal forebrain cholinergic neurons. Nat. Neurosci. *16*, 1857–1863.

Rochefort, N.L., Narushima, M., Grienberger, C., Marandi, N., Hill, D.N., and Konnerth, A. (2011). Development of direction selectivity in mouse cortical neurons. Neuron *71*, 425–432.

Siegel, F., Heimel, J.A., Peters, J., and Lohmann, C. (2012). Peripheral and central inputs shape network dynamics in the developing visual cortex in vivo. Current Biology *22*, 253–258.

Yu, A.J., and Dayan, P. (2005). Uncertainty, Neuromodulation, and Attention. Neuron *46*, 681–692.

Zhang, J., Ackman, J.B., Xu, H.P., and Crair, M.C. (2012). Visual map development depends on the temporal pattern of binocular activity in mice. Nat Neurosci *15*, 298–307.

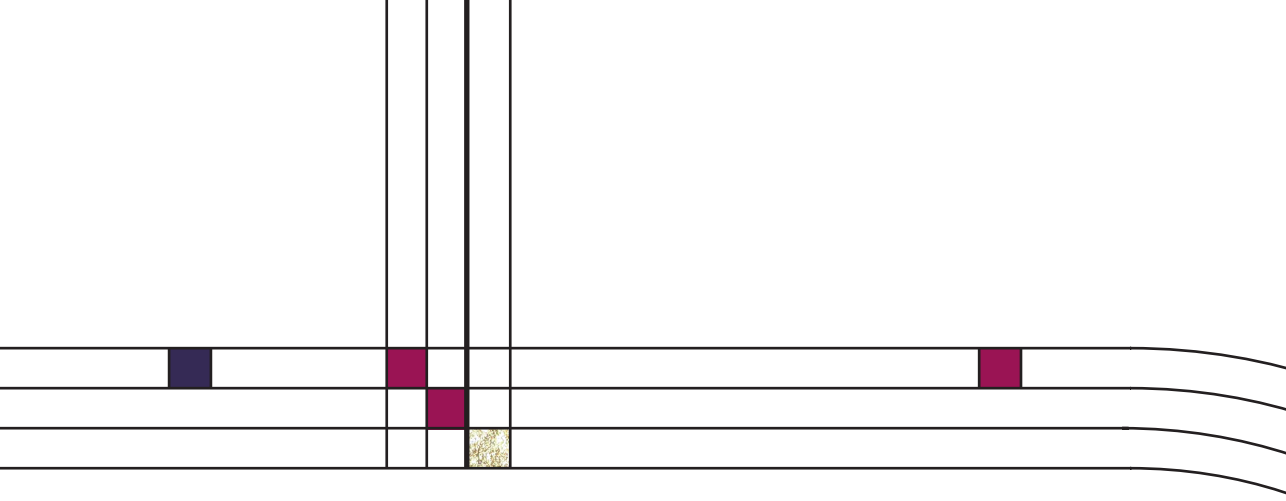

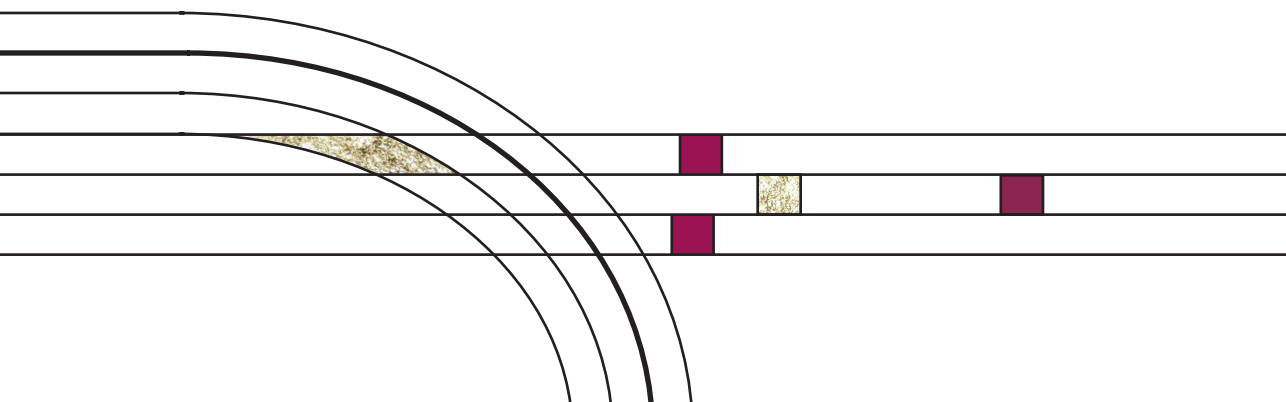

CHAPTER 4

Spatially structured synaptic inputs in the developing visual cortex before eye opening

Authors

Alexandra H. Leighton, Juliette E. Cheyne and Christian Lohmann

ABSTRACT

The complex spatial organization of excitatory synapses on cortical dendrites is important for high level sensory processing, however, it is essentially unknown how dendritic input structure develops. Here, we combine ***in vivo*** voltage-clamp recordings and two-photon calcium imaging across populations of individual synapses in the neonatal mouse visual cortex to investigate the emergence of dendritic input structure before eye opening. At postnatal day 8, the density of functional synapses is very low and synaptic transmission events are rare. During the second postnatal week, synaptic density increases whilst synapses become organized into dendritic domains surrounding particularly active synapses. Synapses in domains have higher activity levels, are more co-active with their neighbours and increase in activity when they are coactive with their neighbours. Synapses outside domains are prone to undergo synaptic depression and elimination. The emergence of domains before sensory experience may establish dendritic units for functional integration to facilitate high-level computations of visual inputs after eye opening.

INTRODUCTION

The majority of synaptic inputs target the dendritic arbour, where they are integrated and can trigger action potential outputs. As predicted by theoretical studies (Poirazi and Mel, 2001), this integration is not linear, and the relative influence of inputs can be controlled through local mechanisms (reviewed in: Larkum and Nevian, 2008; Major et al., 2013; Sjostrom et al., 2008; Stuart and Spruston, 2015; Tran-Van-Minh et al., 2015). For example, the dendrites of hippocampal and cortical pyramidal cells can integrate local synaptic inputs supra-linearly (Branco and Hausser, 2011; Harnett et al., 2012; Losonczy and Magee, 2006; Makara and Magee, 2013). In vivo studies indicate that local non-linear dendritic integration serves sensory processing, probably by greatly enhancing the ability of pyramidal neurons to differentiate between different input patterns (Lavzin et al., 2012; Palmer et al., 2014; Smith et al., 2013; Xu et al., 2012).

The initial spatial organization of synapses arises during early development, when synaptic connections between young neurons are formed and refined into functional networks. During the first postnatal week, synapses form at high rates

in the rodent cortex (Blue and Parnavelas, 1983; De Felipe J. et al., 1997). By the time the ears and eyes open, networks are ready to process the incoming sensory information. For example, in the mouse visual system, receptive fields are present at eye opening by the end of the second postnatal week. Even features such as receptive field size and structure, as well as orientation and direction tuning, are indistinguishable from those in mature animals (Ko et al., 2013; Rochefort et al., 2011).

Since local dendritic integration and thus the fine-scale subcellular input structure of cortical neurons underlies sensory processing, these observations raise the question of how the fine-scale connectivity in the visual cortex arises in the absence of patterned visual input. Before sensory information is available, the neonatal cortex relies on spontaneously generated bursts of activity to accurately wire up developing networks (Blankenship and Feller, 2010; Katz and Shatz, 1996; Kerschensteiner, 2014; Kirkby et al., 2013; Leighton and Lohmann, 2016; Seabrook et al., 2017). In the visual system, spontaneous activity is generated in the retina and travels across developing networks, transmitting information about retinal organization to the central visual system (Ackman et al., 2012; Colonnese and Khazipov, 2010; Gribizis et al., 2019; Hanganu et al., 2006; Shen and Colonnese, 2016; Siegel et al., 2012). Specific manipulations of retinal wave properties affect the wiring of the central visual system, including the primary visual cortex (Burbridge et al., 2014; Cang et al., 2005; Triplett et al., 2009; Zhang et al., 2012).

The local nature of dendritic integration mechanisms places high importance on the spatial organization of synapses. Indeed, recent studies have shown that synaptic inputs are spatially structured; during development, synapses that are frequently co-active during spontaneous activity will cluster together along dendrites of hippocampal and cortical neurons (Kleindienst et al., 2011; Takahashi et al., 2012; Winnubst et al., 2015). In adults, synapses are closer together if they are both driven by particular features of sensory input (Iacaruso et al., 2017; Lee et al., 2019). Additionally, learning often occurs through clustered structural changes of spine synapses (Cichon and Gan, 2015; Fu et al., 2012; Gambino et al., 2014; Makino and Malinow, 2011; McBride et al., 2008).

These observations suggest that structured spontaneous activity regulates the formation of synapses along developing dendrites, with more co-active synapses developing closer together. However, it is unknown when and how dendrites develop the precise spatial and temporal organization required to perform useful local dendritic computations. Here, we used in vivo patch-clamping and synaptic calcium imaging during the course of the second postnatal week to show the emergence of spatial structure in the functional synaptic inputs along dendrites of V1 layer 2/3 pyramidal neurons. We observe that functional synapses form across the entire dendritic tree, but they become stabilized preferentially in the neighbourhood of highly active synapses, which are typically located on spines. Within these dendritic domains, emerging synapses become stabilized when they are co-active with their neighbours. Thus, the development of synaptic inputs follows specific rules that can help prepare developing neurons for performing high-level computations and sensory processing upon eye opening.

RESULTS

Synaptic density and activity increase during the second postnatal week

To visualize the activity and spatial organization of synapses in the developing mouse V1, we imaged spontaneously occurring synaptic calcium transients on apical dendrite stretches of pyramidal cells in L2/3 ***in vivo*** using the calcium indicator GCaMP-6s (Fig 1A).

We mapped synaptic inputs across 12 dendritic stretches from 11 mice, aged between postnatal day (P)8 and P13, the day before eye opening (Fig 1B). These stretches all contained branch points. To track ongoing spontaneous network activity, input currents were measured at the soma. Spontaneous network activity occurred in bursts lasting 2.26 ± 1.62 s. During each burst, the corresponding active synapses on the imaged dendritic area were identified (Fig 1C). A synapse was considered active if a local increase in fluorescence was observed with a centre of activation that remained in a consistent location over at least 3 consecutive imaging frames. To prevent inclusion of false positive synapses, we used a conservative definition of a functional synapse by restricting the dataset to those synapses that were active at least 3 times during the recording period and had

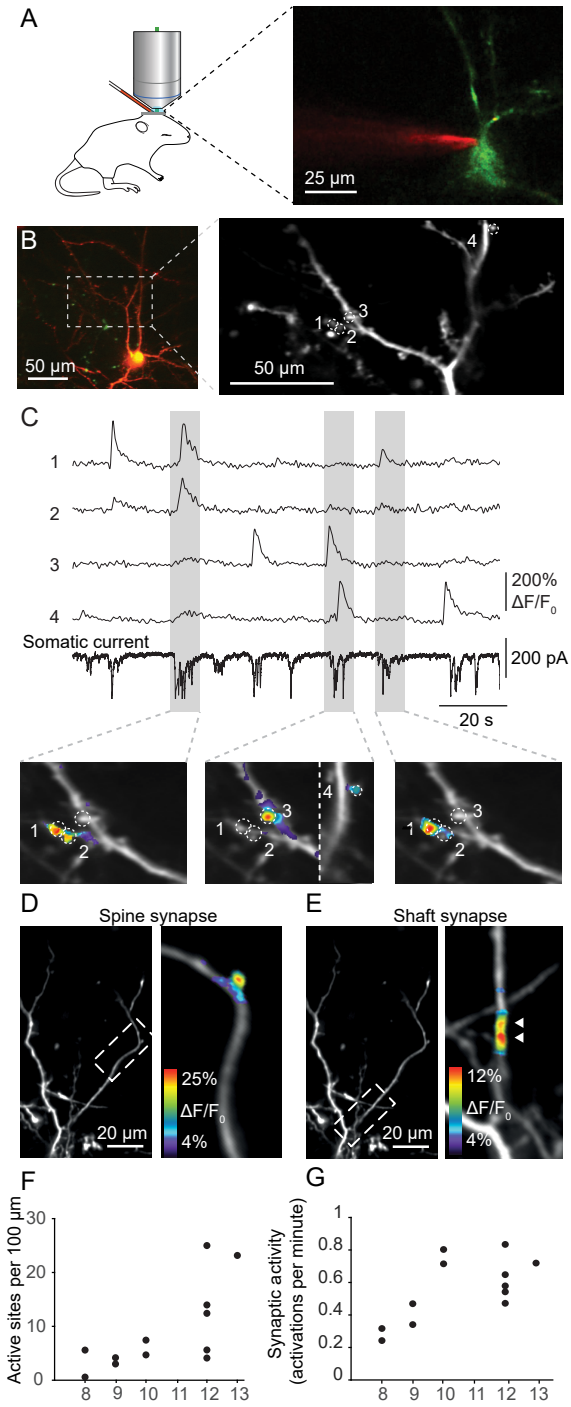

Figure 1, Synaptic density increases during the second postnatal week

A. Pyramidal cells in LII/III of P8-P13 mouse visual cortex, expressing dsRed and GCaMP-6s, were targeted in vivo under two-photon guidance. Pipettes were coated in Alexa 594 for visualization.

B. Whole cell recordings were made from the soma in voltage clamp configuration. Dendritic branches were imaged and synapses were identified by local increases in fluorescence.

C. Spontaneous bursts of activity were visible both as local increases in fluorescence at synapses and as barrages of synaptic input in the somatic recording. Example bursts showing that the participation of individual synapses could be detected clearly and that neighbouring synapses could be distinguished.

D. Active synapses were considered spines if the increase in fluorescence occurred in a protrusion that separated them from the main dendritic shaft.

E. Shaft synapses were observed, which occurred directly onto the dendritic shaft with no discernable morphology.

F. The density of active synapses (both shaft and spine synapses) increased during the second postnatal week (n = 12, Spearman rank coefficient 0.70, p = 0.01).

G. The mean activity of synapses increased during the second postnatal week (n = 12, Spearman's rank coefficient 0.68, p = 0.01)

a minimum activation frequency of 0.06 activations per minute. Together, these dendritic stretches carried 178 functional synapses (Supplementary Figure 1). As expected, the number of active synapses during each burst correlated highly with the total charge transferred (Supplementary Fig 2A).

In the mature cortex, most synapses are located on spines with morphologically distinct spine heads (Berry and Nedivi, 2017). Their shape provides some chemical and electrical isolation from the dendrite and leads to clearly detectable calcium signals (Fig 1D). However, during development, many cortical synapses are formed directly onto the shaft where synaptic calcium transients are easily eclipsed by back-propagating action potentials. To prevent action potential firing, we held layer 2/3 pyramidal neurons at-40 mV in voltage-clamp mode during imaging. This allowed us to image calcium transients at both spine and shaft synapses (Fig 1E).

During the second postnatal week, the density of active synapses overall increased (Fig 1F). Both the density of spine and shaft synapses increased (Supplementary Figure 2B). The frequency of transmission events at active synapses increased with age (Fig 1G). The percentage of spine synapses over all dendritic stretches was 50.7 ± 15.4% (mean ± SD) and did not differ much across ages (Supplementary Figure 2C). Most dendritic stretches contained structural spine heads that were not active (Supplementary Figure 2D).

Synapses become spatially organized according to their activity levels

Though average activity levels increased with age, we found that the shape of the distribution of activity frequencies remained similar throughout the second postnatal week. Most synapses were infrequently active, but the distribution was heavy-tailed on the right (Fig 2A, B) revealing a subset of very highly active synapses. For each dendritic stretch, approximately 20% of synapses were located in this tail. We labelled these 20% most active synapses of each dendritic stretch 'high-activity synapses', and considered the remaining 80% of synapses 'standard' synapses. Most high-activity synapses were on morphologically distinct spines (79.9 ± 22%), in contrast to the remaining 80% of synapses, of which 42.5 (± 26%) were on spines.

We mapped the spatial location of each synapse along the dendritic stretches (Fig 2C, D). Synapses with high activity levels were typically surrounded by other synapses, many of which were highly active as well. This effect was seen in dendritic stretches of all ages (Supplementary Figure 1), but seemed most consistent and striking in dendritic stretches imaged towards the end of the second postnatal week.

To investigate whether synapses were indeed spatially organized according to their activity level, we tested whether high activity synapses also had more highly active neighbours (synapses within a radius of 12 µm). We calculated the mean activity of synapses in the neighbourhood of high-activity synapses, and compared that to the mean activity of synapses in the neighbourhood of standard synapses. At the beginning of the second postnatal week, in dendritic stretches from mice aged P8-P10, neighbours of high activity and neighbours of standard synapses had comparable mean activity frequencies (Fig 2E). In contrast, by the end of the second postnatal week (P12-P13) an activity-based organization had emerged where synapses surrounding high-activity synapses were significantly more active than those surrounding standard synapses (Fig 2E). There was no difference detected in the number of surrounding sites (Fig 2F).

We varied both the radius in which synapses were considered neighbours and the cut-off for high-activity synapses and found that the results were robust within a

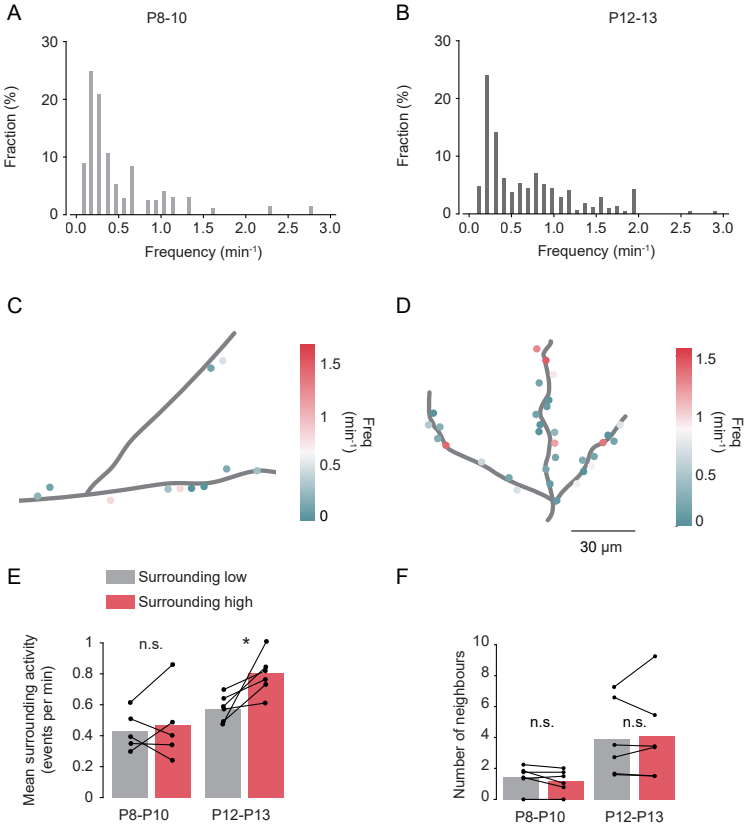

Figure 2, High activity synapses create dendritic domains with increased activity

A. Distribution of synaptic transmission frequency for dendritic stretches from animals at the beginning (P8-P10) of the second postnatal week.

B. Distribution of synaptic transmission frequency for dendritic stretches from animals at the end (P12-13) of the second postnatal week.

C. The synaptic transmission frequency (mean number of activations per minute) mapped for each synapse on a dendritic stretch from an example P8 animal.

D. The synaptic transmission frequency (mean number of activations per minute) mapped for each synapse on a dendritic stretch from an example P12 animal.

E. The mean activity of synapses within a radius of 12 µm from a standard synapse compared to the mean activity of synapses with a radius of 12 µm from a highly active synapse. At P8-P10 there is no difference between the mean surrounding activity (left, n = 6, two-tailed paired t-test, n.s.). At P12-P13, highly active synapses have higher surrounding activity than standard synapses (n = 6, two-tailed paired t-test, p = 0.025).

F. No significant difference was detected between the number of sites surrounding high active and low active sites, either at P8-P10 or P12-P13 (n = 6 at both ages, two-tailed paired t-test, n.s.).

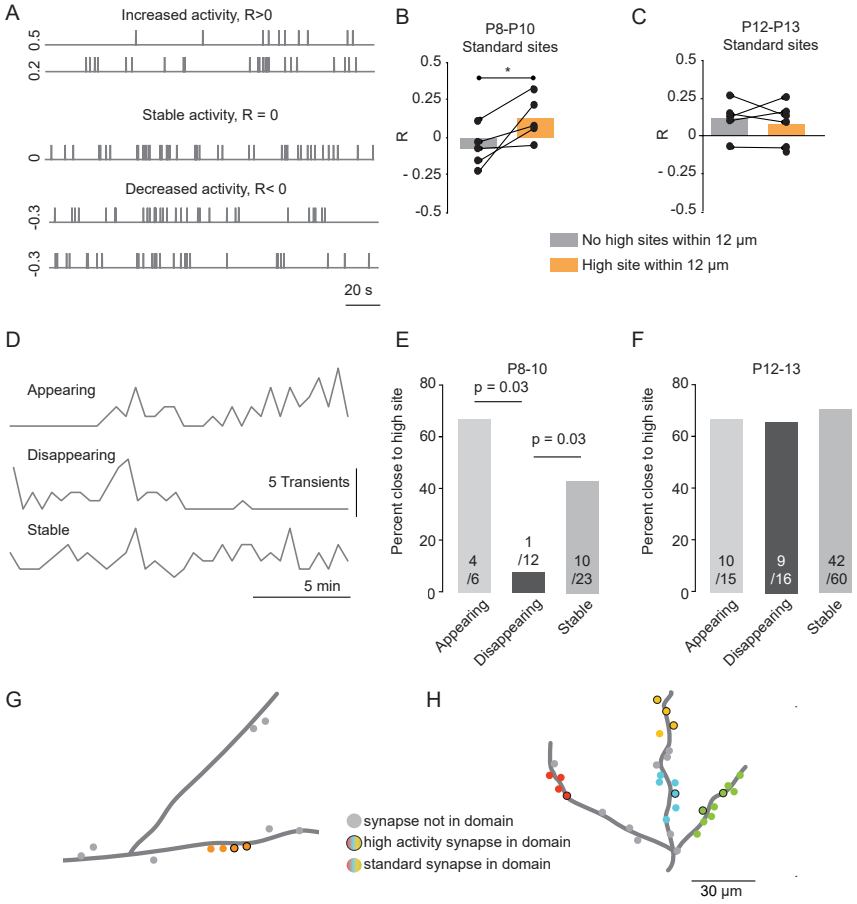

Figure 3, High-activity synapses protect neighbouring synapses from suppression

A. Activations during a recording from 5 example synapses. Correlating the smoothed activity trace with time results in a correlation coefficient R, quantifying the activity change in a single synapse during the recording.

B. In dendritic stretches from animals aged P8-P10, standard synapses within 12 µm of a highly active synapse had higher R values than standard synapses without a neighbouring highly active synapse (n = 6, two-tailed paired t-test, p = 0.04).

C. At P12-P13, there was no difference between the R values of standard synapses with or without a neighbouring highly active synapse (n = 6, two-tailed paired t-test, n.s.).

D. Activity was binned into 1-minute intervals. Synapses that were inactive for the first three 3-minute recordings were labelled as appearing, disappearing synapses were inactive during the three last recordings and stable synapses were active during the last and first three 3-minute recordings.

E. The distribution of appearing, disappearing and stable synapses differed between domains and inter-domain dendritic stretches at P8-P10 (Pearson's chi-squared test).

F. The distribution of appearing, disappearing and stable synapses did not differ between domains and inter-domain dendritic stretches at P12-P13 (Pearson's chi-squared test).

G. Example dendritic domains from a P9 dendritic stretch. 3H. Example dendritic domains imaged at P12.

range of parameters (Supplementary Figure 3A,B). The largest effect was found within a radius of 12 µm, the distance over which we previously found activity-dependent clustering (Winnubst et al., 2015). We continued to use 12 µm as the distance between two synapses within which they are considered neighbouring synapses. In line with the finding that many highly active synapses are also morphological spines, the mean activity of neighbours of active spine synapses is higher than those surrounding shaft synapses (Supplementary Figure 3C). However, when the mean neighbouring activity of any morphological spine synapse (active and non-active spines) is compared to the activity surrounding shaft synapses, we detect no difference (Supplementary Figure 3D), suggesting that morphology alone does not lead to this spatial organization.

Synapses become preferentially stabilized within dendritic domains

What plasticity rule could cause this organization by activity to emerge over the days before eye-opening? We hypothesized that high activity synapses may convey some advantage to their neighbouring synapses, causing them to be stabilized when compared to synapses which lack a neighbouring highly active synapse. We therefore measured how the activity of an individual synapse changed over the total length of the recording, and whether this was related to its spatial location.

To quantify the direction and degree of synaptic activity changes during each experiment, we determined the correlation coefficient 'R' of activity frequency and time for each synapse (Fig 3A). A positive R value indicated an increase in the frequency of transmissions of a given synapse during the experiment, and a negative value indicated a decrease of transmissions.

We then asked how this measure of synaptic activity change varied across synapses, depending on whether or not they had a neighbouring high synapse. In P8-10 animals, standard synapses with a highly active neighbour were likely to show an increase in activity over time (Fig 3B). In contrast, standard synapses that did not have a highly active neighbour often had R values below zero, indicating a decrease in activity. P12-13 animals did not show this effect (Fig 3C). We did not detect an effect of having a high-activity neighbour on the R value of high synapses themselves (Supplementary Figure 4A,B).

While most standard synapses were active throughout the entire recording, some synapses appeared or disappeared during the duration of an experiment (Fig 3D). We asked whether in these extreme cases, the fate of a synapse was still dependent on its location relative to a highly-active synapse. We pooled standard synapses for dendritic stretches from animals aged P8-P10 (Fig 3E) and P12-P13 (Fig 3F). At P8-P10, the distribution of stable, disappearing and appearing synapses differed depending on the presence of a neighbouring highly-active synapse, where a higher proportion of synapses without a highly active neighbour disappeared than synapses with a highly active neighbour. This was not the case in older dendritic stretches.

Taken together, we found that dendritic segments differed in their ability to stabilize synapses depending on the presence of a neighbouring highly active synapse. It seems that dendritic domains form around highly active synapses, in which synapses are more likely to stabilize their activity at the beginning of the second postnatal week. The relative benefit afforded by dendritic domains was observable even during the 27.6 (± 7.1) minutes of imaging recorded from each dendritic stretch. Synapses outside of these domains are more likely to undergo synaptic depression. By the end of the second postnatal week, an organization of activity has emerged where synapses within a domain have higher activity levels than outside.

Synapses inside domains have high local co-activity

We hypothesized that the relative advantage offered by domains could be high local coactivity. We showed previously in the hippocampus and visual cortex (Niculescu et al., 2018; Winnubst et al., 2015) that developing synapses with low local coactivity become depressed, reducing their transmission frequency. This mechanism takes place over a radius of 12 µm.

We mapped local coactivity per synapse over each dendritic stretch (Fig 4A) and confirmed that synapses within dendritic domains had higher local coactivity values than synapses outside domains at both P8-P10 and P12-P13 (Fig 4B, C). At P12-13, the overall difference between coactivity inside and outside a domain was lower (Fig 4C), presumably reflecting the sparsification of spontaneous activity that occurs before eye-opening (Rochefort et al., 2009). To test whether increased

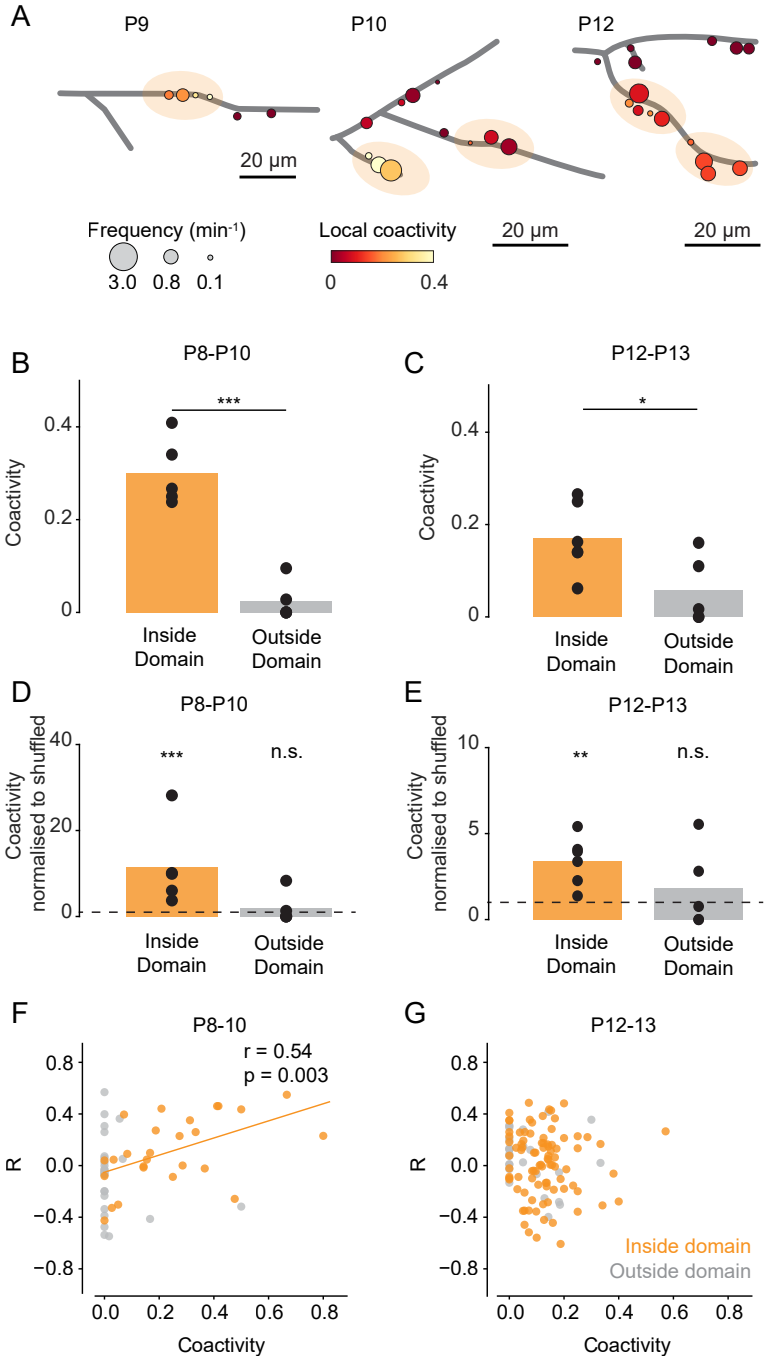
A
P9
P10
P12
20 µm
Frequency (min-1)
3.0 0.8 0.1
Local coactivity
0 0.4
20 µm
20 µm
B
P8-P10
***
Coactivity
0.4
0.2
0
Inside Domain
Outside Domain
C
P12-P13
*
Coactivity
0.4
0.2
0
Inside Domain
Outside Domain
D
P8-P10
Coactivity normalised to shuffled
40
20
0
***
n.s.
Inside Domain
Outside Domain
E
P12-P13
Coactivity normalised to shuffled
10
5
0
**
n.s.
Inside Domain
Outside Domain
F
P8-10
r = 0.54
p = 0.003
R
0.8
0.4
0.0
−0.4
−0.8
0.0 0.2 0.4 0.6 0.8
Coactivity
G
P12-13
R
0.8
0.4
0.0
−0.4
−0.8
Inside domain
Outside domain
0.0 0.2 0.4 0.6 0.8
Coactivity

Figure 4, High coactivity within a domain protects synapses

A. Example dendritic stretches at three different ages. Each active synapse is labeled by a disk whose diameter represents its activation frequency and the color its local coactivity. Domains are marked with a faint orange oval. Typically, local coactivity values are higher inside domains than outside domains.

B. Local coactivity inside a domain is higher than outside a domain for dendritic stretches from animals aged P8-P10 ($n = 6$ dendritic stretches, two-tailed unpaired t-test, $p<0.001$).

C. Local coactivity inside a domain is higher than outside a domain for dendritic stretches from animals aged P12-P13 ($n = 6$ dendritic stretches, two-tailed unpaired t-test, $p = 0.04$).

D. Measured coactivity divided by shuffled coactivity at P8-10. There was no difference between shuffled activity and the measured data for synapses outside of domains. In contrast, synapses within a domain had significantly higher coactivity with their neighbours than in the shuffled data (observed versus shuffled data, $n = 6$ dendritic stretches, two-tailed unpaired t-test, $p = 0.0017$).

E. Measured coactivity divided by shuffled coactivity at P12-13. There was no difference between shuffled activity and the measured data for synapses outside of domains. In contrast, synapses within a domain had significantly higher coactivity with their neighbours than in the shuffled data (observed versus shuffled data, $n = 6$ dendritic stretches, two-tailed unpaired t-test, $p = 0.02$).

F. Mean pairwise coactivity with neighbouring synapses was significantly correlated with the change in activity during a recording ('R') for in-domain synapses, but not for synapses located outside domains in P8-P10 animals (Spearman's rank correlation).

G. There was no significant correlation detected between local coactivity and R in P12 -13 animals (Spearman's rank correlation).

coactivity was due to the presence of highly active sites increasing the chance of co-activity, we compared the observed coactivity levels with values for each dendritic stretch, preserving the spatial location and activity levels of each synapse but shuffling the burst of inputs during which they were active. Synapses outside domains had similar co-activity levels to shuffled activity patterns. In contrast, in-domain synapses showed significantly higher coactivity levels than the shuffled data at both ages (Fig 4D, E). This finding demonstrates that increased local coactivity was not a secondary consequence of higher synaptic activity inside domains, but rather that inputs from neurons with similar activity patterns became specifically organized into domains.

In P8-P10 animals, within domains, the local coactivity of synapses correlated with their R values, the index of synaptic activity change (Fig 4F), where synapses that were frequently active out-of-sync with their neighbours had lower R values. Synapses outside domains almost always had coactivity values of 0, preventing a fair estimation of the relationship between R and local coactivity outside domains. In animals aged P12-P13, coactivity and change of synaptic activity appeared to be unrelated (Fig 4G).

Taken together, we see that high-activity synapses form highly co-active dendritic domains. Given that low local coactivity reduces synaptic transmission, synapses within domains are preferentially stabilized and less likely to be eliminated when compared to synapses outside of domains.

DISCUSSION

Recent evidence suggests that specific patterns of synaptic inputs enable neurons in the sensory cortex to process information independently on individual dendritic segments (Iacaruso et al., 2017; Jia et al., 2010; Lee et al., 2019; Wilson et al., 2016) and to perform high-level computations of sensory inputs (Lavzin et al., 2012; Palmer et al., 2014; Smith et al., 2013; Xu et al., 2012). Here, we show that inputs to V1 neurons become organized into domains of synchronized synapses even before the onset of vision. These domains may be the precursors of individual computational units in dendrites of the mature visual system.

In line with previous anatomical findings in both mouse and rat cortex (Blue and Parnavelas, 1983; Defelipe, 1997), we observed that the density of functional synapses more than doubled during the course of the second postnatal week, supporting the idea that this is a particularly critical time for synapse formation. Both shaft and spine synaptic synapses were present in roughly equal proportions at this age. This is in contrast to the adult brain, where almost all excitatory synapses are located on spines (Berry and Nedivi, 2017; Ju and Zhou, 2018). How the system moves from predominantly shaft-based signalling to spine-based is unknown, and we did not observe the formation of new spines during the recording periods. It seems likely that, rather than shaft synapses being converted into spine synapses (Miller and Peters, 1981), spine synapses appear adjacent to shaft synapses, perhaps using synaptogenic signals caused by local high activity (Reilly et al., 2011). The domains we describe could encourage spinogenesis in specific regions, maintaining organization as the system shifts from shaft- to spine-based connections.

The majority of synapses we recorded from were active at low frequencies, and only a subset of synapses showed very high activity levels. In adults, synaptic strength also occurs with a skewed distribution; most synapses are weak, but a handful have much higher synaptic strength (Cossell et al., 2015; Markram et al., 1997). These exceptionally strong connections are those synapses formed between cells with similar receptive fields (Cossell et al., 2015). It is possible that the high-activity synaptic sites we describe are also formed between cells that are tuned to similar input, their shared feedforward inputs and increased chance of co-activity having protected their connection over time. These cells may even be clonally related,

i.e. generated from the same progenitor (Li et al., 2012; Ohtsuki et al., 2012), as clonally related cells share gap-junction connections early in development, and are more likely to be synaptically connected once chemical synapses take over signalling (Yu et al., 2012). By actively promoting local co-activity with clonally related synapses, a young network could prune retinotopically incorrect synapses and promote proximity between synapses with similar receptive field properties, as seen in the adult (Iacaruso et al., 2017).

Since a large proportion of synaptic inputs of sensory cortex layer 2/3 neurons represent local horizontal connections (Petreanu et al., 2009), V1 inputs most likely contributed many of the synapses we mapped in the present study. In contrast to the mostly low activity levels of synapses shown here, almost all V1 neurons participate in spontaneous activity events frequently (Siegel et al., 2012). Why do the activity levels differ so obviously between V1 neurons and their synapses? The most straightforward explanation is that while presynaptic action potential firing frequencies are similar across all input neurons, the release probabilities differ strongly across their synapses. In fact, previous ***in vitro*** studies showed that release probabilities vary considerably across both the input and output synapses of individual developing neurons (Markram et al., 1997; Walz et al., 2009). Furthermore, since spontaneous activity drives plasticity of transmission success rate at developing synapses (Branco et al., 2008; Winnubst et al., 2015), a broad distribution of synaptic release probabilities provides a large dynamic range for fine-tuning developing neuronal networks through spontaneous activity.

We propose that the initial formation of high-activity synapses outside domains occurs through activity-independent processes that allow synapses from some neurons - perhaps those that are clonally related to the postsynaptic neuron - to establish and strengthen synapses without the need of local co-activity. These synapses may then become the starting points for emerging domains along the developing dendrite. In fact, in our data set from younger dendritic stretches, we observed a few synapses that were located outside domains and were isolated or locally de-synchronous with neighbour synapses, but nevertheless, showed strong increases in transmission frequency during our recordings. These synapses may shape the strong connectivity between specific neurons at the beginning of the second postnatal week. Highly active synapses themselves did not follow

the same pattern as standard sites. A recent ultrastructural study (de Vivo et al., 2017) reported that the largest 20% of synapses were not reduced after sleep, in contrast to the remaining 80% of synapses which became scaled according to size. Protecting high-activity sites from suppression could increase the signal to noise ratio in the developing network (González-Rueda et al., 2018).

During the second postnatal week, highly active synapses become surrounded by increasing numbers of synapses. In addition, synapses in domains show higher coactivity with their neighbours than synapses outside domains. We found that the increased local coactivity within domains cannot be explained by the increased synaptic density or activity inside domains. Local coactivity was correlated with increases in activity levels for synapses inside, but not outside domains. Thus, synapses inside domains are most likely selected based on their activity patterns, through a synaptic plasticity mechanism involving proBDNF-mediated synaptic depression, and mature BDNF-mediated synaptic stabilization (Kirchner and Gjorgjieva, 2019; Niculescu et al., 2018; Winnubst et al., 2015).

Co-activity with neighbours is correlated with changes in activity only at the beginning of the second postnatal week. At the period just before eye opening, we no longer saw a relationship between the activity change of a synapse and its coactivity or location relative to a high-activity synapse. By having a specific time window for this plasticity rule, domains can be maintained even if their coactivity reduces in line with the sparsification of spontaneous activity before eye-opening (Rochefort et al., 2009). Independently of the function of temporally controlled synaptic plasticity in dendrites, our observations suggest a central role of spatially (in-domain vs. outside domain synapses) and temporally (early vs. late second postnatal week) controlled synaptic plasticity for generating structured synaptic inputs.

Organizing synapses into domains could prepare the visual cortex for high level sensory processing. Theoretical work suggests that local synaptic integration can boost a neuron's computational power by dramatically increasing its capacity to differentiate across multiple inputs patterns (Poirazi and Mel, 2001). Recent ***in vivo*** experiments indicate that, indeed, local supra-linear integration of synaptic inputs contributes to sensory sensitivity (Lavzin et al., 2012; Palmer et al., 2014; Smith

et al., 2013; Xu et al., 2012). Synaptic clustering of synapses with similar tuning properties, a prerequisite for local dendritic computations, has been demonstrated recently in the mature mouse visual cortex (Iacaruso et al., 2017). Here, we show that clustered synapses emerge in specific dendritic domains. While our previous "out of sync-lose your link" model of synaptic clustering demonstrated how inputs from neurons with similar activity patterns are stabilized (Niculescu et al., 2018; Winnubst et al., 2015), it could not explain how run-away clustering across the entire dendritic tree can be prevented. Since we show here that locally synchronized synapses become stabilized in domains, but not in inter-domains stretches, synapses of different input patterns could cluster independently in each domain. The independent emergence of domains constrains the extension of individual domains until they reach the nearest neighbour domain and may prevent one input pattern from taking over the entire dendritic arborization of a neuron.

Together, our findings show that synapses form with very high spatio-temporal precision even before the eyes open, as spontaneous activity prepares the visual cortex for the onset of vision by shaping synaptic synapses into domains with high synaptic density and coactivity.

METHODS

Animals

All experimental procedures were approved by the Institutional Animal Care and Use Committee of the Royal Netherlands Academy of Arts and Sciences. We used 11 C57BL/6J mouse pups between P8 and P13.

Plasmids

For *in utero* electroporation, GCaMP6s (Addgene plasmid 40753; Douglas Kim) (Chen et al., 2013) was cloned into pCAGGS and used in combination with DsRed in pCAGGS (Winnubst et al., 2015, gift from Christiaan Levelt). Cells co-expressed the fluorescent protein dsRed for somatic targeting and structural information.

In Utero Electroporation

Constructs were introduced through *in utero* electroporation at E16.5. Pyramidal neurons in layer 2/3 of the visual cortex were transfected with GCaMP6s (2mg/ml) and DsRed (0.5-2 mg/ml) at E16.5 using *in utero* electroporation (Harvey et al., 2009). Pregnant mice were anesthetized with isoflurane and a small incision (1.5–2 cm) was made in the abdominal wall. The uterine horns were removed from the abdomen, and DNA was injected into the lateral ventricle of embryos using a sharp glass electrode. Voltage pulses (five square waves, 30 V, 50-ms duration, 950-ms interval, custom-built electroporator) were delivered across the brain with tweezer electrodes covered in conductive gel. Embryos were rinsed with warm saline solution and returned to the abdomen, after which time the muscle and skin were sutured.

In Vivo Electrophysiology and Calcium Imaging

The surgery and stabilization for the *in vivo* calcium imaging experiments were performed as described previously (Siegel et al., 2012; Winnubst et al., 2015). Animals were anesthetized with 2% isoflurane, which was reduced to 0.7%–1% after surgery. We previously reported that although this low level of anaesthesia does reduce the frequency of spontaneous network events, relative to that seen in wake animals, it does not change the basic properties of spontaneous network activity, such as participation rates and event amplitudes (Siegel et al., 2012). Electrodes (4.5–6 M Ω) were fluorescently coated with BSA-Alexa 594 to allow targeted whole-cell recordings (Sasaki et al., 2012). To visualize synaptic inputs,

action potentials were blocked with QX314 in the intracellular solution (120 mMCsMeSO3, 8 mM NaCl, 15 mM CsCl2, 10 mM TEA-Cl, 10 mM HEPES, 5 mMQX-314 bromide, 4 mM MgATP, and 0.3 mM Na-GTP; Takahashi et al., 2012; Winnubst et al., 2015). Currents were recorded in voltage clamp at 10 kHz and filtered at3 kHz (Multiclamp 700b; Molecular Devices). The liquid junction potential was corrected for. Bursts were identified as a sharp negative deflection in the current, followed by a return to baseline, which consisted of multiple synaptic currents.

Image acquisition

In vivo calcium imaging was performed on either a Nikon (A1R-MP) with a 0.8/16x water-immersion objective and a Ti:Sapphire laser (Chameleon II, Coherent) or a Movable Objective Microscope (Sutter Instruments) with a Ti:Sapphire laser (MaiTai HP, Spectra Physics) and a 0.8/40x water-immersion objective (Olympus) using Nikon or ScanImage software (Pologruto et al., 2003). We recorded the movement signal of the scan mirrors to synchronize calcium imaging and electrophysiology.

Image processing

To remove drift and movement artifacts from each recording, we performed image alignment using NoRMCorre (Pnevmatikakis and Giovannucci, 2017). Each recording was aligned to the first recording in the series to remove any movements between recording sessions. Delta F stacks were made using the average fluorescence per pixel as baseline. ROIs were hand-drawn using ImageJ (NIH). Automated transient detection and further data processing was performed using custom-made Matlab software (MathWorks).

Statistical Analysis

We limited our domain analysis to synaptic synapses with at least one neighbouring synapse. N = experiments (image dendritic areas) unless stated otherwise. One dendritic stretch was imaged from each animal except once, when two dendritic stretches were imaged in a single cell in a P12 animal. We used only synapses that were active with a frequency of at least 0.06 activations per minute, and were active at least three times during a recording. Data are presented as mean ± SD.

Synapses were labelled as ‘appearing’ if they first became active from nine minutes after the beginning of an experiment (i.e. after three consecutive three-minute

recordings), and as 'disappearing' if they were inactive for at least the last 9 minutes. Remaining synapses were considered stable.

For normally distributed data and data with relatively low sample numbers (6-8), where normality test are underpowered, we used t-tests as recommended (de Winter, 2013). We used paired t-tests when observations were compared within the same dendritic stretch, except when missing observations made that impossible. For data that were not normally distributed we used non-parametric statistical comparisons, Man-Whitney-U tests for independent samples and Wilcoxon signed-rank tests for paired data.

To test whether the coactivity values we observed inside and outside domains were higher than expected by chance considering synaptic density and activity levels, we shuffled synaptic activity 1000x. Synaptic location and the overall number of times each synapse was active was maintained, but the bursts during which these activations took place was shuffled and local coactivity was calculated.

Acknowledgments

This work was supported by grants of the Netherlands Organization for Scientific Research (NWO, ALW Open Program grants, no. 819.02.017, 822.02.006 and ALWOP.216; ALW Vici, no. 865.12.001), the "Stichting Vrienden van het Herseninstituut" (all C. L.).

REFERENCES

Ackman, J.B., Burbridge, T.J., and Crair, M.C. (2012). Retinal waves coordinate patterned activity throughout the developing visual system. Nature *490*, 219–225.

Berry, K.P., and Nedivi, E. (2017). Spine dynamics: Are they all the same? Neuron *96*, 43–55.

Blankenship, A.G., and Feller, M.B. (2010). Mechanisms underlying spontaneous patterned activity in developing neural circuits. Nat. Rev. Neurosci. *11*, 18–29.

Blue, M.E., and Parnavelas, J.G. (1983). The formation and maturation of synapses in the visual cortex of the rat. II. Quantitative analysis. J. Neurocytol. *12*, 697–712.

Branco, T., and Hausser, M. (2011). Synaptic integration gradients in single cortical pyramidal cell dendrites. Neuron *69*, 885–892.

Branco, T., Staras, K., Darcy, K.J., and Goda, Y. (2008). Local dendritic activity sets release probability at hippocampal synapses. Neuron *59*, 475–485.

Burbridge, T.J., Xu, H.-P., Ackman, J.B., Ge, X., Zhang, Y., Ye, M.-J., Zhou, Z.J., Xu, J., Contractor, A., and Crair, M.C. (2014). Visual Circuit Development Requires Patterned Activity Mediated by Retinal Acetylcholine Receptors. Neuron *84*, 1049–1064.

Cang, J., Renteria, R.C., Kaneko, M., Liu, X., Copenhagen, D.R., and Stryker, M.P. (2005). Development of Precise Maps in Visual Cortex Requires Patterned Spontaneous Activity in the Retina. Neuron *48*, 797–809.

Cichon, J., and Gan, W.-B. (2015). Branch-specific dendritic Ca2+ spikes cause persistent synaptic plasticity. Nature *520*, 180–185.

Colonnese, M.T., and Khazipov, R. (2010). "Slow Activity Transients" in Infant Rat Visual Cortex:A Spreading Synchronous Oscillation Patterned by Retinal Waves. J. Neurosci. *30*, 4325–4337.

Cossell, L., Iacaruso, M.F., Muir, D.R., Houlton, R., Sader, E.N., Ko, H., Hofer, S.B., and Mrsic-Flogel, T.D. (2015). Functional organization of excitatory synaptic strength in primary visual cortex. Nature *518*, 399–403.

De Felipe J., Marco, P., Fairen, A., and Jones, E.G. (1997). Inhibitory synaptogenesis in mouse somatosensory cortex. Cereb.Cortex *7*, 619–634.

Fu, M., Yu, X., Lu, J., and Zuo, Y. (2012). Repetitive motor learning induces coordinated formation of clustered dendritic spines in vivo. Nature *483*, 92–95.

Gambino, F., Pagès, S., Kehayas, V., Baptista, D., Tatti, R., Carleton, A., and Holtmaat, A. (2014). Sensory-evoked LTP driven by dendritic plateau potentials in vivo. Nature *515*, 116–119.

González-Rueda, A., Pedrosa, V., Feord, R.C., Clopath, C., and Paulsen, O. (2018). Activity-Dependent Downscaling of Subthreshold Synaptic Inputs during Slow-Wave-Sleep-like Activity In Vivo. Neuron *97*, 1244–1252.

Gribizis, A., Ge, X., Daigle, T.L., Ackman, J.B., Zeng, H., Lee, D., and Crair, M.C. (2019). Visual

Cortex Gains Independence from Peripheral Drive before Eye Opening. Neuron *0*.

Hanganu, I.L., Ben Ari, Y., and Khazipov, R. (2006). Retinal waves trigger spindle bursts in the neonatal rat visual cortex. J Neurosci *26*, 6728–6736.

Harnett, M.T., Makara, J.K., Spruston, N., Kath, W.L., and Magee, J.C. (2012). Synaptic amplification by dendritic spines enhances input cooperativity. Nature *491*, 599–602.

Iacaruso, M.F., Gasler, I.T., and Hofer, S.B. (2017). Synaptic organization of visual space in primary visual cortex. Nature *547*, 449–452.

Jia, H., Rochefort, N.L., Chen, X., and Konnerth, A. (2010). Dendritic organization of sensory input to cortical neurons in vivo. Nature *464*, 1307–1312.

Ju, J., and Zhou, Q. (2018). Dendritic Spine Modifications in Brain Physiology. Neuroplast. - Insights Neural Reorganization.

Katz, L.C., and Shatz, C.J. (1996). Synaptic activity and the construction of cortical circuits. Science *274*, 1133–1138.

Kerschensteiner, D. (2014). Spontaneous Network Activity and Synaptic Development. Neurosci. Rev. J. Bringing Neurobiol. Neurol. Psychiatry *20*, 272–290.

Kirchner, J.H., and Gjorgjieva, J. (2019). A unifying framework for synaptic organization on cortical dendrites. BioRxiv 771907.

Kirkby, L.A., Sack, G.S., Firl, A., and Feller, M.B. (2013). A Role for Correlated Spontaneous Activity in the Assembly of Neural Circuits. Neuron *80*, 1129–1144.

Kleindienst, T., Winnubst, J., Roth-Alpermann, C., Bonhoeffer, T., and Lohmann, C. (2011). Activity-dependent clustering of functional synaptic inputs on developing hippocampal dendrites. Neuron *72*, 1012–1024.

Ko, H., Cossell, L., Baragli, C., Antolik, J., Clopath, C., Hofer, S.B., and Mrsic-Flogel, T.D. (2013). The emergence of functional microcircuits in visual cortex. Nature *496*, 96–100.

Larkum, M.E., and Nevian, T. (2008). Synaptic clustering by dendritic signalling mechanisms. Curr. Opin. Neurobiol. *18*, 321–331.

Lavzin, M., Rapoport, S., Polsky, A., Garion, L., and Schiller, J. (2012). Nonlinear dendritic processing determines angular tuning of barrel cortex neurons in vivo. Nature *490*, 397–401.

Lee, K.-S., Vandemark, K., Mezey, D., Shultz, N., and Fitzpatrick, D. (2019). Functional Synaptic Architecture of Callosal Inputs in Mouse Primary Visual Cortex. Neuron.

Leighton, A.H., and Lohmann, C. (2016). The Wiring of Developing Sensory Circuits-From Patterned Spontaneous Activity to Synaptic Plasticity Mechanisms. Front. Neural Circuits *10*, 71.

Li, Y., Lu, H., Cheng, P. lin, Ge, S., Xu, H., Shi, S.H., and Dan, Y. (2012). Clonally related visual

cortical neurons show similar stimulus feature selectivity. Nature *486*, 118–121.

Losonczy, A., and Magee, J.C. (2006). Integrative Properties of Radial Oblique Dendrites in Hippocampal CA1 Pyramidal Neurons. Neuron. *50*, 291–307.

Major, G., Larkum, M.E., and Schiller, J. (2013). Active properties of neocortical pyramidal neuron dendrites. Annu. Rev. Neurosci. *36*, 1–24.

Makara, J.K., and Magee, J.C. (2013). Variable Dendritic Integration in Hippocampal CA3 Pyramidal Neurons. Neuron *80*, 1438–1450.

Makino, H., and Malinow, R. (2011). Compartmentalized versus Global Synaptic Plasticity on Dendrites Controlled by Experience. Neuron *72*, 1001–1011.

Markram, H., Lubke, J., Frotscher, M., Roth, A., and Sakmann, B. (1997). Physiology and anatomy of synaptic connections between thick tufted pyramidal neurones in the developing rat neocortex. J Physiol-Lond. *500*, 409–440.

McBride, T.J., Rodriguez-Contreras, A., Trinh, A., Bailey, R., and DeBello, W.M. (2008). Learning drives differential clustering of axodendritic contacts in the barn owl auditory system. J.Neurosci *28*, 6960–6973.

Niculescu, D., Michaelsen-Preusse, K., Güner, Ü., Dorland, R. van, Wierenga, C.J., and Lohmann, C. (2018). A BDNF-mediated push-pull plasticity mechanism for synaptic clustering. Cell Rep. *24*, 2063–2074.

Ohtsuki, G., Nishiyama, M., Yoshida, T., Murakami, T., Histed, M., Lois, C., and Ohki, K. (2012). Similarity of Visual Selectivity among Clonally Related Neurons in Visual Cortex. Neuron *75*, 65–72.

Palmer, L.M., Shai, A.S., Reeve, J.E., Anderson, H.L., Paulsen, O., and Larkum, M.E. (2014). NMDA spikes enhance action potential generation during sensory input. Nat. Neurosci. *17*, 383–390.

Petreanu, L., Mao, T., Sternson, S.M., and Svoboda, K. (2009). The subcellular organization of neocortical excitatory connections. Nature *457*, 1142–1145.

Pnevmatikakis, E.A., and Giovannucci, A. (2017). NoRMCorre: An online algorithm for piecewise rigid motion correction of calcium imaging data. J. Neurosci. Methods *291*, 83–94.

Poirazi, P., and Mel, B.W. (2001). Impact of active dendrites and structural plasticity on the memory capacity of neural tissue. Neuron *29*, 779–796.

Pologruto, T.A., Sabatini, B.L., and Svoboda, K. (2003). ScanImage: flexible software for operating laser scanning microscopes. BiomedEng Online *2*, 13.

Reilly, J.E., Hanson, H.H., and Phillips, G.R. (2011). Persistence of excitatory shaft synapses adjacent to newly emerged dendritic protrusions. MolCell Neurosci.

Rochefort, N.L., Garaschuk, O., Milos, R.-I., Narushima, M., Marandi, N., Pichler, B., Kovalchuk,

Y., and Konnerth, A. (2009). Sparsification of neuronal activity in the visual cortex at eye-opening. Proc. Natl. Acad. Sci. *106*, 15049–15054.

Rochefort, N.L., Narushima, M., Grienberger, C., Marandi, N., Hill, D.N., and Konnerth, A. (2011). Development of direction selectivity in mouse cortical neurons. Neuron *71*, 425–432.

Sasaki, T., Matsuki, N., and Ikegaya, Y. (2012). Targeted axon-attached recording with fluorescent patch-clamp pipettes in brain slices. Nat. Protoc. *7*, 1228–1234.

Seabrook, T.A., Burbridge, T.J., Crair, M.C., and Huberman, A.D. (2017). Architecture, Function, and Assembly of the Mouse Visual System. Annu. Rev. Neurosci. *40*, 499–538.

Shen, J., and Colonnese, M.T. (2016). Development of Activity in the Mouse Visual Cortex. J. Neurosci. Off. J. Soc. Neurosci. *36*, 12259–12275.

Siegel, F., Heimel, J.A., Peters, J., and Lohmann, C. (2012). Peripheral and central inputs shape network dynamics in the developing visual cortex in vivo. Curr. Biol. *22*, 253–258.

Sjostrom, P.J., Rancz, E.A., Roth, A., and Hausser, M. (2008). Dendritic excitability and synaptic plasticity. Physiol Rev *88*, 769–840.

Smith, S.L., Smith, I.T., Branco, T., and Häusser, M. (2013). Dendritic spikes enhance stimulus selectivity in cortical neurons in vivo. Nature *503*, 115–120.

Stuart, G.J., and Spruston, N. (2015). Dendritic integration: 60 years of progress. Nat. Neurosci. *18*, 1713–1721.

Takahashi, N., Kitamura, K., Matsuo, N., Mayford, M., Kano, M., Matsuki, N., and Ikegaya, Y. (2012). Locally Synchronized Synaptic Inputs. Science *335*, 353–356.

Tran-Van-Minh, A., Cazé, R.D., Abrahamsson, T., Cathala, L., Gutkin, B.S., and DiGregorio, D.A. (2015). Contribution of sublinear and supralinear dendritic integration to neuronal computations. Front. Cell. Neurosci. *9*, 67.

Triplett, J.W., Owens, M.T., Yamada, J., Lemke, G., Cang, J., Stryker, M.P., and Feldheim, D.A. (2009). Retinal input instructs alignment of visual topographic maps. Cell *139*, 175–185.

de Vivo, L., Bellesi, M., Marshall, W., Bushong, E.A., Ellisman, M.H., Tononi, G., and Cirelli, C. (2017). Ultrastructural Evidence for Synaptic Scaling Across the Wake/sleep Cycle. Science *355*, 507–510.

Walz, C., Elssner-Beyer, B., Schubert, D., and Gottmann, K. (2009). Properties of glutamatergic synapses in immature layer Vb pyramidal neurons: coupling of pre- and postsynaptic maturational states. ExpBrain Res.

Wilson, D.E., Whitney, D.E., Scholl, B., and Fitzpatrick, D. (2016). Orientation selectivity and the functional clustering of synaptic inputs in primary visual cortex. Nat. Neurosci. *19*, 1003–1009.

Winnubst, J., Cheyne, J.E., Niculescu, D., and Lohmann, C. (2015). Spontaneous activity drives

local synaptic plasticity in vivo. Neuron *87*, 399–410.

de Winter, J. (2013). Using the Student's t-test with extremely small sample sizes. Pract. Assess. Res. Eval. *18*.

Xu, N.L., Harnett, M.T., Williams, S.R., Huber, D., O'Connor, D.H., Svoboda, K., and Magee, J.C. (2012). Nonlinear dendritic integration of sensory and motor input during an active sensing task. Nature *492*, 247–251.

Yu, Y.C., He, S., Chen, S., Fu, Y., Brown, K.N., Yao, X.H., Ma, J., Gao, K.P., Sosinsky, G.E., Huang, K., et al. (2012). Preferential electrical coupling regulates neocortical lineage-dependent microcircuit assembly. Nature *486*, 113–117.

Zhang, J., Ackman, J.B., Xu, H.P., and Crair, M.C. (2012). Visual map development depends on the temporal pattern of binocular activity in mice. Nat Neurosci *15*, 298–307.

SUPPLEMENTARY FIGURES

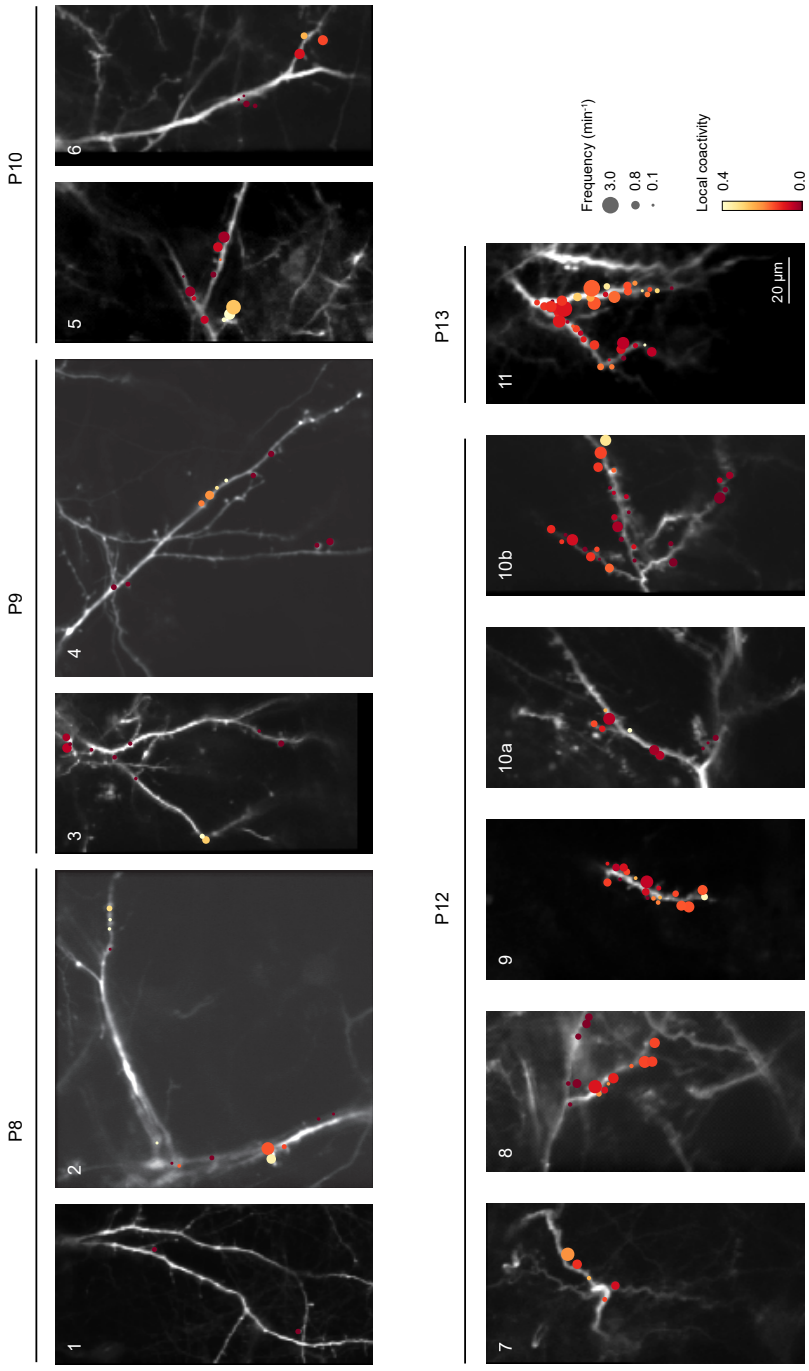

Supplementary Figure 1
S1 Overview of all imaged dendritic areas. Each synapse is represented as a disk where the size represents the transmission frequency and the colour the local coactivity.

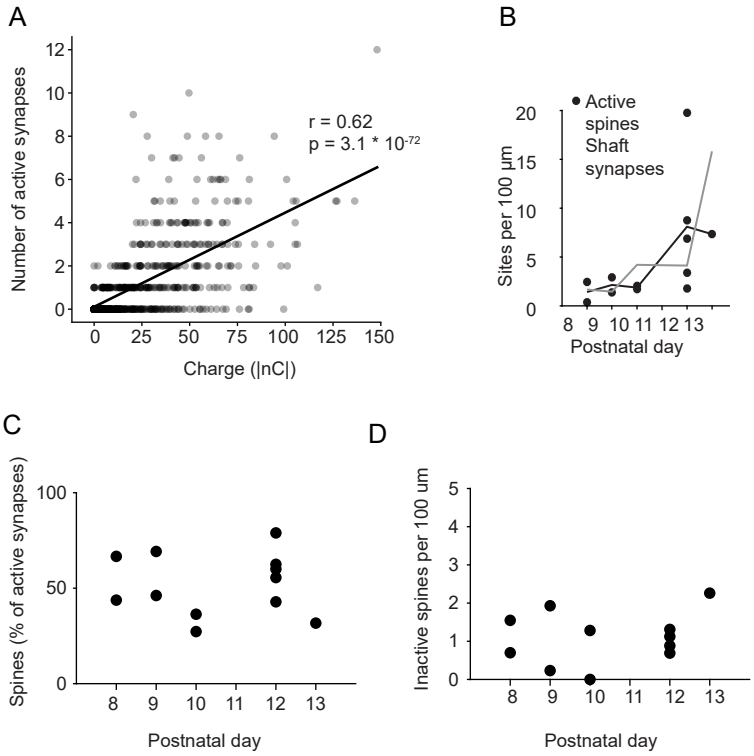

Supplementary Figure 2

A. The number of observed active synapses in an imaged dendritic area was positively correlated with the total charge received by the postsynaptic neuron during the coincident burst of spontaneous synaptic currents measured in voltage-clamp.

B. In the second postnatal week, the age of the animal correlated significantly to the measured number of active spiny synapses (n = 12, Spearman rank coefficient 0.69, p = 0.01) and shaft synapses (n = 12, Spearman rank coefficient 0.63, p = 0.02).

C. The percentage of active synapses that have spine morphology rather than shaft morphology does not change with age age (n = 12, Spearman rank coefficient 0.22, n.s.).

D. The density of inactive morphological spines does not change with age (n = 12, Spearman rank coefficient 0.018, n.s.)

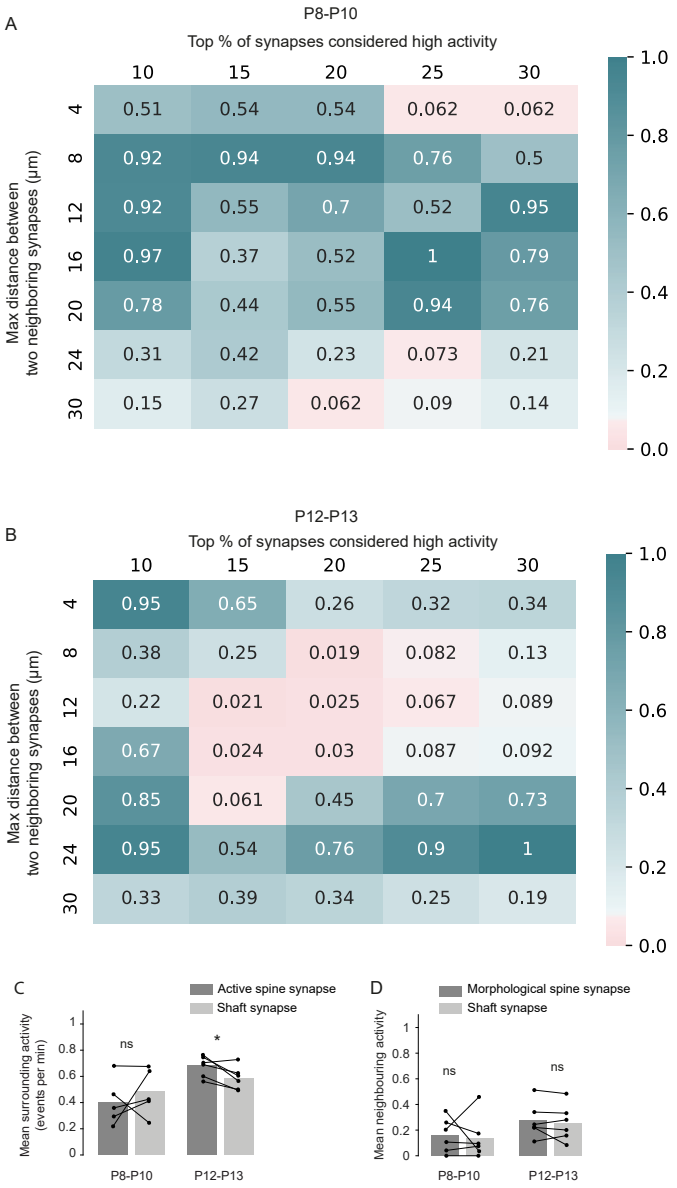

Supplementary Figure 3

A. For animals aged P8-P10, p values of a paired t-test comparing the activity of synapses surrounding high-activity synapses to those surrounding low-activity synapses, with varying thresholds for what is considered a neighboring site and what is considered a highly active site.

B. For animals aged P12-P13, p values of a paired t-test comparing the activity of synapses surrounding high-activity synapses to those surrounding low-activity synapses, with varying thresholds for what is considered a neighboring site and what is considered a highly active site.

C. At P8-P10 there is no difference between the mean activity of synapses within 12 µm of active spine synapses and the mean activity of synapses within 12 µm of active shaft synapses (n = 6 dendritic stretches, two-tailed paired t-test, n.s.). At P12-P13, active spine synapses have significantly higher surrounding activity (n = 6 dendritic stretches, two-tailed paired t-test, p = 0.032) than shaft synapses.

D. Neither at P8-P10 nor P12-P13 did we detect a difference between the mean activity of synapses within 12 µm of a morphological spine synapse when compared to the mean activity of synapses surrounding an active shaft synapse (n = 6 dendritic stretches, two-tailed paired t-test, n.s.).

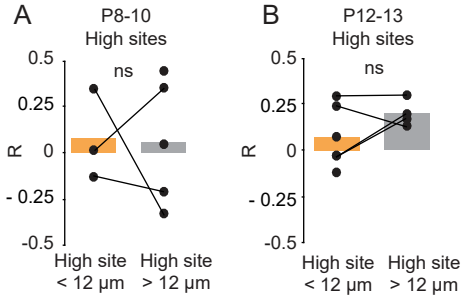

Supplementary Figure 4

A. R values for high-activity synapses inside and outside domains did not differ significantly at P8-10 (n =6, two-tailed paired t-test, n.s.).

B. R values for high-activity synapses inside and outside domains did not differ at P12-13 (n =6, two-tailed paired t-test, n.s.).

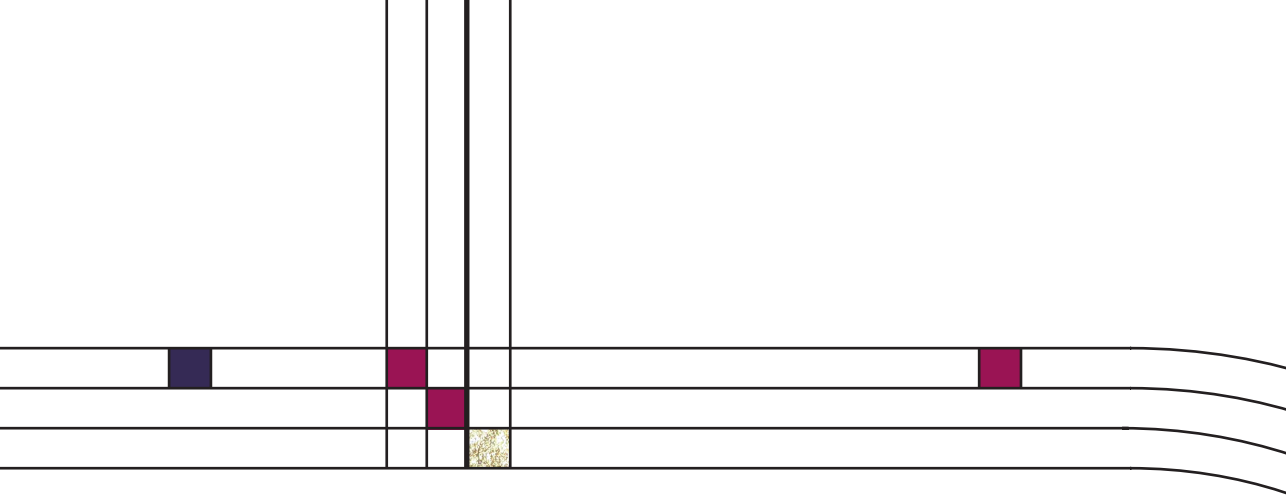

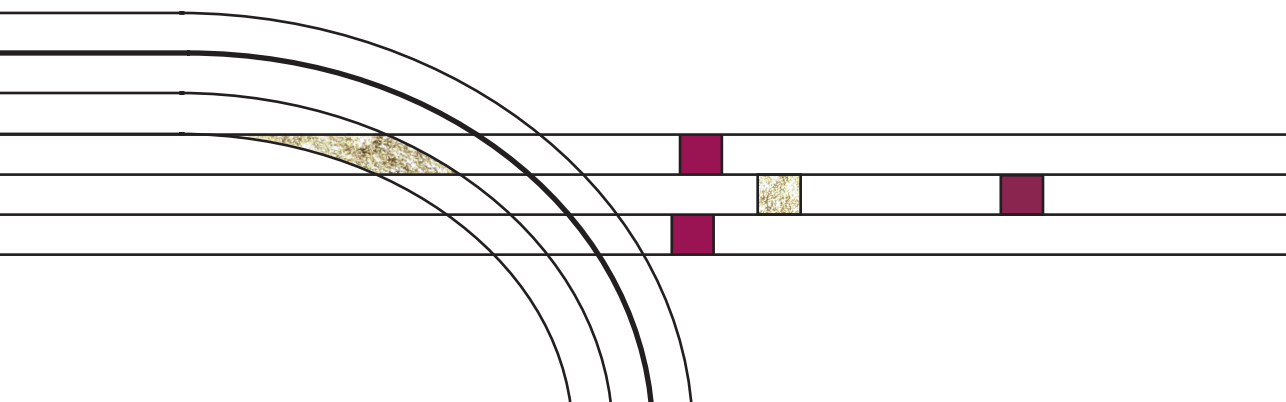

CHAPTER 5

Lightweight, wireless LED implant for chronic manipulation in vivo of spontaneous activity in neonatal mice

Authors

Alexandra H. Leighton, Victoria Busch, Joris E. Coppens and Christian Lohmann

ABSTRACT

Manipulation of activity in the neonatal rodent brain can help us understand healthy development. However, experimental procedures at this age come with a set of challenges unique to the neonatal animal. As pups are small, cannot be separated from their mother for long periods of time, and must be housed in a nest, many traditional techniques are unusable during the first two postnatal weeks. Here, we describe the use of magnetic resonance induction to allow wireless and chronic optogenetic manipulation of spontaneous activity in mouse pups during the second postnatal week. Pups were implanted with a lightweight receiver coupled to an LED and successfully returned to the homecage. A transmitting magnetic field surrounding the homecage drives the implanted LED and is regulated by a microcontroller to allow flexible, precisely-timed and wireless control over neuronal manipulation.

INTRODUCTION

During early development, the connections between young neurons are refined into functionally useful networks in an activity-dependent manner. Bursts of spontaneously generated activity travel through the brain, pruning unwanted synapses and strengthening well-targeted connections (Luhmann et al., 2016; Simon and O'Leary, 1992). Understanding how spontaneous activity controls these crucial choices teaches us about the fundamental processes that underlie the formation of the brain, and may also help us understand and treat neurodevelopmental disorders (Cheyne et al., 2019; Goncalves et al., 2013).

Experimental manipulation of spontaneous activity is one of the most direct and powerful ways to test the consequences of activity patterns on the network. However, attempting to manipulate activity in very young rodents comes with unique challenges. Firstly, neonatal animals are too small for conventional methods that require heavy head plates or batteries. At ten days old a mouse will weigh around 6 grams (Greenham, 1977) preventing use of most modern headstages. Secondly, repeatedly removing pups from the mother is a stressful experience that can have consequences for neural and behavioural development in a manner that is difficult to predict (Orso et al., 2019; Tractenberg et al., 2016) and is therefore best avoided if possible.

Chemogenetic manipulations are one possibility (Urban and Roth, 2015), and can be performed with one or two daily injections of the agonist, preventing long absences from the mother. However, chemogenetic manipulations are best suited to applications where a blanket change is required, such as an overall reduction in signalling from one neuron type or a specific subset. Spontaneous activity is carefully patterned; the frequency, participation and synchrony of the activity are not random characteristics, but contain information that give spontaneous activity the ability to shape the network (Kirkby et al., 2013; Leighton and Lohmann, 2016). Therefore, mimicking or manipulating this activity would ideally involve specifically timed changes in firing. To circumvent these difficulties, we describe here an extremely lightweight, wireless optogenetic tool, which allows precise and reliable induction of spikes in pups between postnatal days (P) 8-14. To our knowledge, this is the first description of a method that allows pups to return to the nest environment while receiving induction of neuronal activity.

METHODS

Animals

All experimental procedures were approved by the institutional animal care and use committee of the Royal Netherlands Academy of Sciences. Mice of both sexes were used. All animals were aged between postnatal days (P) 8-14. Wild-type mice were either C57BL/6J mice or C57BL/6J x CBA F1. These mice open their eyes at P14.

In utero Electroporation

Pyramidal neurons in layer 2/3 of the visual cortex were transfected with plasmid DNA driving expression of Channelrhodopsin 2 (ChR2) (2 mg/ml, 15753- pCAGGS-ChR2-Venus (AddGene) and DsRed (2 mg/ml) at E16.5 using ***in utero*** electroporation (Harvey et al., 2009). Pregnant mice were anesthetized with isoflurane and a small incision (1.5–2 cm) was made in the abdominal wall. The uterine horns were carefully removed from the abdomen, and DNA was injected into the lateral ventricle of embryos using a sharp glass electrode. Voltage pulses (five square wave pulses, 30 V, 50-ms duration, 950-ms interval, custom-built electroporator) were delivered across the brain with tweezer electrodes covered in conductive

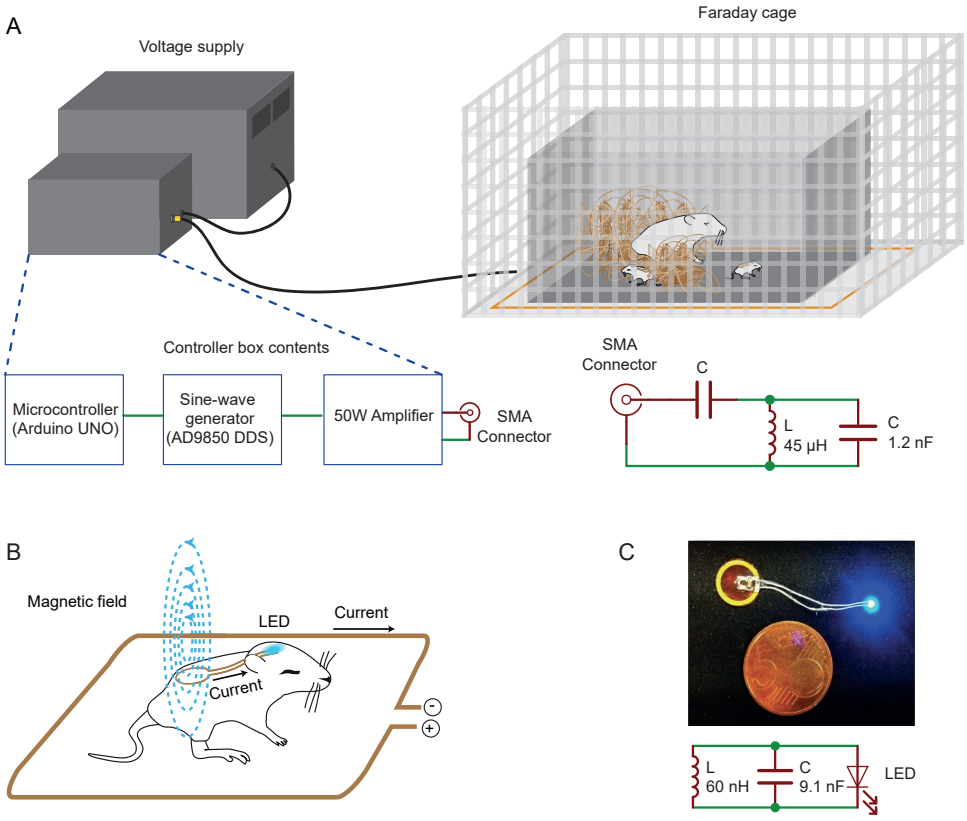

Figure 1, Resonant-induced current activates a wireless implanted LED

A. (Left) Voltage supply and custom controller box.
(Right) Faraday cage containing transmitter coil and mouse cage.

B. Schematic showing principle of magnetic induction and arrangement of receiver.

C. Receiver size and circuit. The receiver consists of a copper coil, LED and capacitor.

gel. Embryos were rinsed with warm saline solution and returned to the abdomen, after which time the muscle and skin were sutured.

Whole-cell recordings

Membrane potential was recorded in current clamp at 10 kHz and filtered at 3 kHz (Multiclamp 700b; Molecular Devices) in vivo as described previously (Leighton et al., 2020). For current clamp recordings electrodes (4.5–6 MΩ) were filled with intracellular solution (105 mM K gluconate, 10 mM HEPES, 30 mM KCl, 10 mM phosphocreatine, 4 mM MgATP, and 0.3 mM GTP; Golshani et al., 2009).

RESULTS

Wirelessly activating LED implants through resonance induction

Our experimental set-up is shown in Figure 1A. Pups are housed with their mothers in their nests inside a normal homecage. This is kept inside a larger Faraday cage (190x240 mm) with an embedded induction coil to generate the magnetic field for current induction (Supplementary Figure 1A). A standard lab voltage supply powers this coil. A custom box containing a microcontroller (Arduino Uno), sine-wave generator and an amplifier allow the experimenter to turn on the induction loop and adjust the magnetic field strength inside the cage. Driving the system using an open-source microcontroller allows the user to easily adjust the duration and pattern of stimulation. The field is resonant at 6.78 MHz.

The Faraday cage is equipped with an interlock switch, such that the voltage on the transmitting coil is automatically stopped when the door from the cage is open for animal care (Supplementary Fig 1B). To prevent dirt collecting and reducing this distance, the edges can be coated in epoxy or silicon. The transmitting coil is encapsulated in a waterproof polyethylene housing, and all potentially high voltages are strictly inside this housing.

Target pups are implanted with a receiver coil coupled to an LED, which receives a current when the induction loop is active (Fig 1B). The circuit board of the receiver weighs 80 mg (Fig 1C). It contains only a small capacitor (9.1 nF), a copper coil, and a small (1.6 x 1.1 x 0.3 mm) blue LED (Würth Elektronik), printed on malleable

flex board. Heating the implant and shaping it around a cylindrical mould allows it to conform to the shape of the pup's back. We coated the flex board in resin to protect the implanted components and smooth out any rough edges of the flex board. Depending on the experimental goal, various wavelengths or types of LED could be used on this implant.

Verifying neuronal activation

During a burst of spontaneous activity, many neurons are active simultaneously, firing a few action potentials in a row before falling silent again (Colonnese et al., 2010; Rochefort et al., 2009). As spontaneous activity most likely relies on burst-dependent-synaptic plasticity to wire up the developing brain (Butts and Rokhsar,

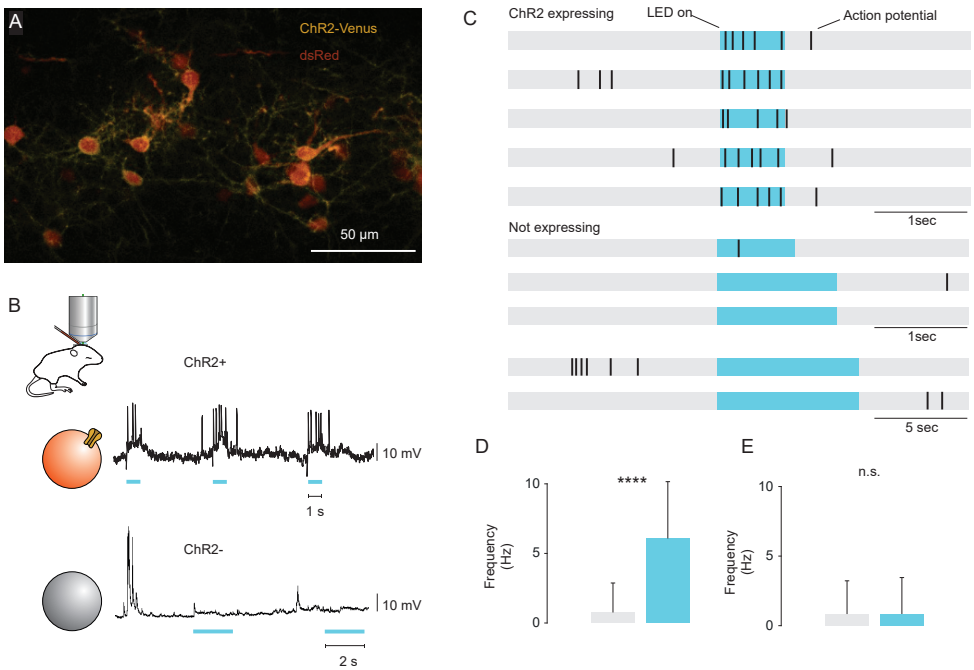

Figure 2, Burst-like activations can be induced using ChR2

A. Cells expressing dsRed in cytoplasm and Venus-tagged ChR2 in membranes.
B. Example cell recordings in vivo in cells with (above) and without (below) ChR2.
C. Action potentials fired during optogenetic stimulation. Recorded in whole-cell configuration in cells with (above) and without (below) ChR2.
D. Frequency of action potential firing before and during light stimulation in cells expressing ChR2 (paired t-test, n = 83 activations, $p < 0.0001$).
E. Frequency of action potential firing before and during light stimulation in cells not expressing ChR2 (paired t-test, n = 54 activations, n.s.).

2001; Butts et al., 2007), we aimed to mimic burst patterns of spontaneous activity during the second postnatal week.

We took advantage of the thin skull of neonatal rodents and provide the light stimulation through the skull rather than performing a craniotomy. To test that the light intensity of the LED was sufficient to activate cells even through the skull, we performed ***in vivo*** whole-cell recordings. We expressed the light-sensitive channel ChR2 in pyramidal cells in visual cortex layer 2/3 (L2/3), by performing ***in utero*** electroporation at E16. The red fluorescent protein dsRed was co-expressed for easy recognition of cells (Fig 2A). We used two-photon-targeted whole-cell recordings of pyramidal cells ***in vivo*** to record spiking responses to illumination by the LED. Cells expressing ChR2 responded reliably to the light stimulus (Fig 2B-D).

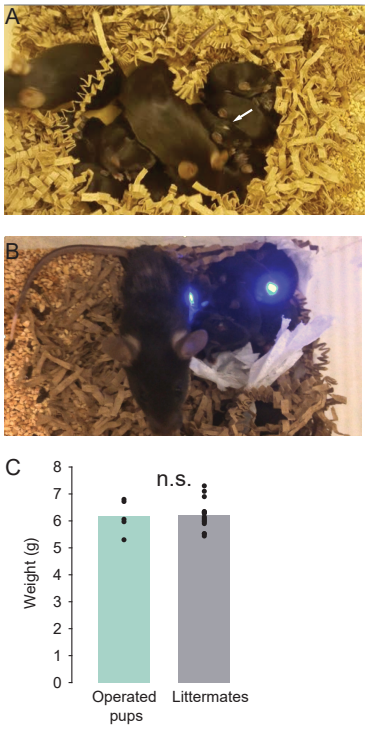

Figure 3, Implanted pups are accepted back into the nest

A. Pups were accepted back into the nest after surgery. Arrowhead: dental cement cap.
B. LEDs remained functional 3 days after implant surgery and return to the nest.
C. Comparison of pup weights two days after surgery, n = 5 implanted, n = 16 unplanted, Wilcoxon rank sum test, n.s.

With 1 second duration of stimulation at 5mW we obtained burst patterns similar to natural spontaneous activity (Fig 1C). Cells that did not express ChR2 did not increase spiking frequency in response to LED activation (Fig 2E).

Optimizing implant protocol for pup re-acceptance

The LED receiver must be implanted in a manner that does not prevent the mother from accepting operated pups back into the nest. Mother mice can reject or kill pups that appear weak or harmed, so a smooth surgery is essential. We found that the protocol below resulted in pups being accepted by the mother: 48 hours after surgery at P11, the implanted pups were in the nest and being fed (Fig 3A). The implant was still in place and functioning (Fig 3B) and their weights were not different from their non-implanted littermates (Fig 3C).

Equipment

Heating pad
Rat-tooth forceps
Surgical scissors
Wide forceps
UV lamp
LED lamp (will detect the fluorophore expressed in the animal)
Blunt needle
Dental cement
Skin glue
Super glue
Pup-sized isoflurane cone
Local analgesic

Protocol

1. Remove the pup from the nest using gloves.
2. Weigh to establish baseline body weight.
3. Induce isoflurane anaesthesia at 3% for 3 minutes in an induction box.
4. Remove and place pup in custom, pup-size nose holder.
5. Inject Metacam into flank (0.025 ml)
6. Reduce isoflurane to 2%
7. Using scissors, make a straight opening in the back for the receiver.
8. Cut a very small opening on the side of the head that expresses the construct.
9. Use a wide needle with the blade tip removed to tunnel the LED under the

skin, from the back to the head.

10. Using a fluorescence detection lamp, verify the exact location of expression in the cortex.
11. Shape the receiver wires with forceps so that the LED will naturally fall down on the skull.
12. Insert the coil and verify that the receiver lies flush with the body of the animal.
13. Apply superglue to LED and glue to skull.
14. Cover with layer of dental cement and cure it with light. Do not attempt to close the opening on the head as this increases the chance of the mother removing the implant. Instead, use dental cement to cover all exposed skull.
15. Close the opening on the back with small dots of skin glue.
16. Turn off isoflurane and allow pup to wake up. Ensure that the pup is fully warm before returning to the nest.

DISCUSSION

Here, we describe an approach for wireless activation that allows young pups to remain in the nest with their mother while receiving specifically timed optogenetic stimulation. There is a range of different possible methods for wireless optogenetic stimulation, reviewed in Qazi et al., 2018. Head-mounted devices, at around 2-3 g, cannot be supported by the pups at this age. Use of, for instance, an aimed laser is impractical when housing the pups in the homecage with the mother (Wang et al., 2020). Instead, we used a resonance induction method similar to Shin et al., (2017) and extended the application of wireless optogenetics to pups during the second postnatal week. Pups recovered well, having been taken back into the nests and cared for by the dams.

Safety of both investigators and experimental animals is an important concern in building setups with high voltages and magnetic fields. The field is resonant at 6.78 MHz, an ISM (Industrial, Scientific and Medical) frequency chosen to prevent interference of the magnetic field with other equipment. The chosen frequency (6.78 MHz) is much lower than the, for instance, 2.4 GHz that induces heating in a microwave oven. At 6.78 MHz there is no notable absorption of energy by the water or bedding in the cage. To further prevent possible interference, we placed the cage in a Faraday cage. Putting it in a Faraday cage slightly alters the resonance frequency, but this can be tuned easily with the choice of capacitors. Expected peak power level in practical use is around 10 W, equalling a maximum magnetic field of 0.6 mA/micrometer at the elevation level of the mice. The current induced in the mouse brain is limited by the impedance of tissue inside the brain. We compared this value to typical transcranial magnetic stimulation (TMS) threshold levels, around 1.5 T. The optogenetic transmit coil operates (at 10 W accepted power) at a level of 0.75 mT, 2000 times less than TMS threshold.

While using this technique, it is important to consider the consequence of evoking additional activity for the whole network, as it is possible that evoked activity suppresses intrinsic activity, rather than simply occurring side-by-side. Acute experiments using, for instance, calcium imaging, could confirm whether wirelessly induced spontaneous activity occurs in a truly additive manner, or whether the developing network adapts to the manipulation.

The ability to manipulate spontaneous activity accurately, reliably and chronically in the neonatal mouse, without excessive disruption of its behaviour, opens up a wide range of fresh research opportunities. This is also relevant to neurodevelopmental disease models; mice with the Fragile X (FraX) mutation have more synchronised spontaneous activity than wild-type animals (Cheyne et al., 2019; Goncalves et al., 2013). By allowing specifically timed activation of neurons, the information encoded in the characteristics of spontaneous activity can be tested using this wireless system.

Compared to other long-term manipulations, one of the major benefits of this technique is that it is flexible. The microcontroller allows the user to adjust the pattern of activity induced using millisecond precision, and the power supply can be adjusted to increase or decrease magnetic field strength. This is particularly relevant in pups as spontaneous activity patterns change quickly during development (Ackman et al., 2012; Colonnese et al., 2010; Rochefort et al., 2009; Siegel et al., 2012), requiring tailored stimulation paradigms to match a pup's age. This is in contrast to, for instance, expressing a chemogenetic construct such as DREADD, which can either excite or inhibit cells but without precise timing. Here, we used the 'classic' opsin ChR2, but recent years have seen the development of many new types of opsin (Deisseroth and Hegemann, 2017; Schoenenberger et al., 2011). Their different sensitivities and kinetics could be used to adapt this technique depending on the desired manipulation.

Acknowledgements

We thank Christiaan Levelt for critically reading the manuscript and Monique van Mourik for technical assistance. This work was supported by grants of the Netherlands Organization for Scientific Research (NWO, ALW Open Program grants, no. 819.02.017, 822.02.006 and ALWOP.216; ALW Vici, no. 865.12.001), the "Stichting Vrienden van het Herseninstituut"

REFERENCES

Ackman, J.B., Burbridge, T.J., and Crair, M.C. (2012). Retinal waves coordinate patterned activity throughout the developing visual system. Nature *490*, 219–225.

Butts, D.A., and Rokhsar, D.S. (2001). The information content of spontaneous retinal waves. J. Neurosci. *21*, 961–973.

Butts, D.A., Kanold, P.O., and Shatz, C.J. (2007). A Burst-Based "Hebbian" Learning Rule at Retinogeniculate Synapses Links Retinal Waves to Activity-Dependent Refinement. PLoS Biol *5*, e61.

Cheyne, J.E., Zabouri, N., Baddeley, D., and Lohmann, C. (2019). Spontaneous activity patterns are altered in the developing visual cortex of the Fmr1 knockout mouse. Front. Neural Circuits *13*.

Colonnese, M.T., Kaminska, A., Minlebaev, M., Milh, M., Bloem, B., Lescure, S., Moriette, G., Chiron, C., Ben-Ari, Y., and Khazipov, R. (2010). A Conserved Switch in Sensory Processing Prepares Developing Neocortex for Vision. Neuron *67*, 480–498.

Deisseroth, K., and Hegemann, P. (2017). The form and function of channelrhodopsin. Science *357*.

Golshani, P., Goncalves, J.T., Khoshkhoo, S., Mostany, R., Smirnakis, S., and Portera-Cailliau, C. (2009). Internally Mediated Developmental Desynchronization of Neocortical Network Activity. J. Neurosci. *29*, 10890–10899.

Goncalves, J.T., Anstey, J.E., Golshani, P., and Portera-Cailliau, C. (2013). Circuit level defects in the developing neocortex of Fragile X mice. Nat Neurosci *16*, 903–909.

Greenham, L. (1977). Sexing mouse pups. Lab. Anim. *11*, 181–184.

Harvey, A.R., Ehlert, E., Wit, J., Drummond, E.S., Pollett, M.A., Ruitenberg, M., Plant, G.W., Verhaagen, J., and Levelt, C.N. (2009). Use of GFP to Analyze Morphology, Connectivity, and Function of Cells in the Central Nervous System. In Viral Applications of Green Fluorescent Protein, B.W. Hicks, ed. (Totowa, NJ: Humana Press), pp. 63–95.

Kirkby, L.A., Sack, G.S., Firl, A., and Feller, M.B. (2013). A Role for Correlated Spontaneous Activity in the Assembly of Neural Circuits. Neuron *80*, 1129–1144.

Leighton, A.H., and Lohmann, C. (2016). The Wiring of Developing Sensory Circuits-From Patterned Spontaneous Activity to Synaptic Plasticity Mechanisms. Front. Neural Circuits *10*, 71.

Leighton, A.H., Houwen, G.J., Cheyne, J.E., Maldonado, P.P., Winter, F.D., and Lohmann, C. (2020). Control of spontaneous activity patterns by inhibitory signaling in the developing visual cortex. BioRxiv 2020.02.21.959262.

Luhmann, H.J., Sinning, A., Yang, J.-W., Reyes-Puerta, V., Stüttgen, M.C., Kirischuk, S., and Kilb, W. (2016). Spontaneous Neuronal Activity in Developing Neocortical Networks: From Single Cells to Large-Scale Interactions. Front. Neural Circuits *10*.

Orso, R., Creutzberg, K.C., Wearick-Silva, L.E., Wendt Viola, T., Tractenberg, S.G., Benetti, F., and Grassi-Oliveira, R. (2019). How Early Life Stress Impact Maternal Care: A Systematic Review of Rodent Studies. Front. Behav. Neurosci. *13*.

Qazi, R., Kim, C.Y., Byun, S.-H., and Jeong, J.-W. (2018). Microscale Inorganic LED Based Wireless Neural Systems for Chronic in vivo Optogenetics. Front. Neurosci. *12*.

Rochefort, N.L., Garaschuk, O., Milos, R.I., Narushima, M., Marandi, N., Pichler, B., Kovalchuk, Y., and Konnerth, A. (2009). Sparsification of neuronal activity in the visual cortex at eye-opening. Proc. Natl. Acad. Sci. *106*, 15049–15054.

Schoenenberger, P., Scharer, Y.P., and Oertner, T.G. (2011). Channelrhodopsin as a tool to investigate synaptic transmission and plasticity. Exp.Physiol *96*, 34–39.

Shin, G., Gomez, A.M., Al-Hasani, R., Jeong, Y.R., Kim, J., Xie, Z., Banks, A., Lee, S.M., Han, S.Y., Yoo, C.J., et al. (2017). Flexible Near-Field Wireless Optoelectronics as Subdermal Implants for Broad Applications in Optogenetics. Neuron *93*, 509-521.e3.

Siegel, F., Heimel, J.A., Peters, J., and Lohmann, C. (2012). Peripheral and central inputs shape network dynamics in the developing visual cortex in vivo. Curr. Biol. *22*, 253–258.

Simon, D.K., and O'Leary, D.D. (1992). Development of topographic order in the mammalian retinocollicular projection. J. Neurosci. *12*, 1212–1232.

Tractenberg, S.G., Levandowski, M.L., de Azeredo, L.A., Orso, R., Roithmann, L.G., Hoffmann, E.S., Brenhouse, H., and Grassi-Oliveira, R. (2016). An overview of maternal separation effects on behavioural outcomes in mice: Evidence from a four-stage methodological systematic review. Neurosci. Biobehav. Rev. *68*, 489–503.

Urban, D.J., and Roth, B.L. (2015). DREADDs (designer receptors exclusively activated by designer drugs): chemogenetic tools with therapeutic utility. Annu. Rev. Pharmacol. Toxicol. *55*, 399–417.

Wang, Y., Xie, K., Yue, H., Chen, X., Luo, X., Liao, Q., Liu, M., Wang, F., and Shi, P. (2020). Flexible and fully implantable upconversion device for wireless optogenetic stimulation of the spinal cord in behaving animals. Nanoscale *12*, 2406–2414.

SUPPLEMENTARY FIGURES

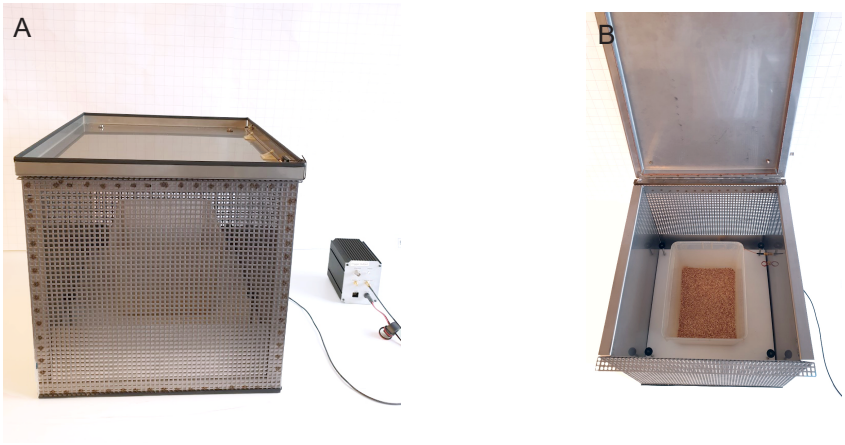

Supplementary Figure 1.

A. Faraday cage containing animal home cage (left) beside controller box with microcontroller, sine-wave generator and amplifier (right).
B. When the cage is opened, the interlock switch turns off the voltage on the induction loop.

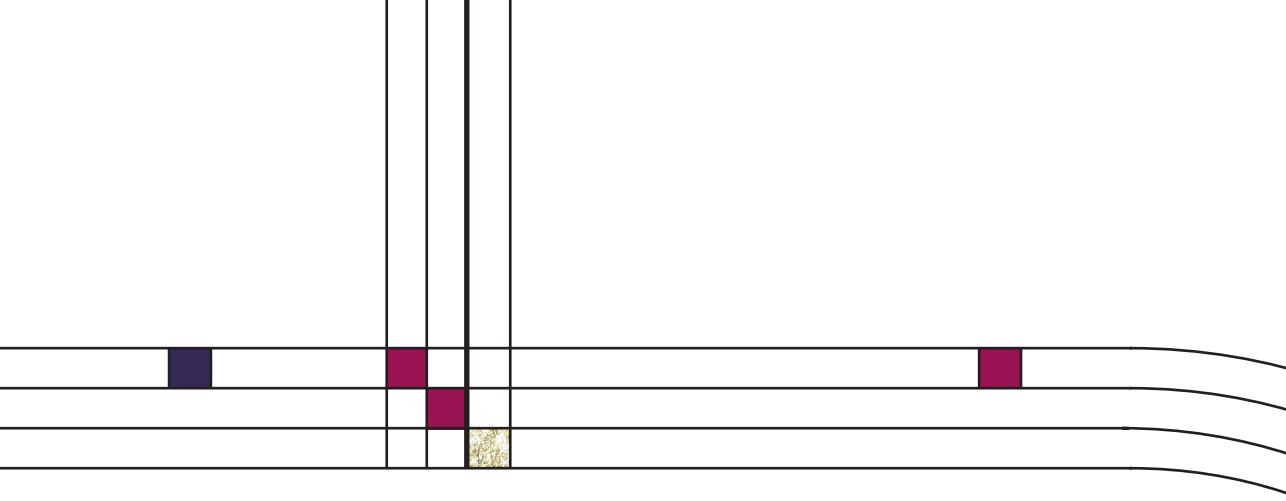

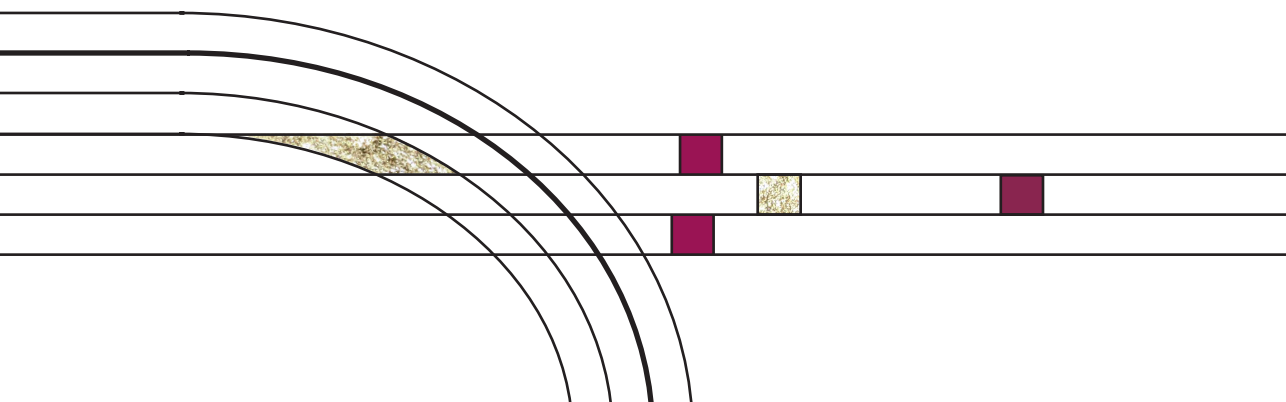

CHAPTER 6

Discussion

Partly adapted from Leighton and Lohmann, 2016

Introduction

Non-evoked activity has been described throughout developing sensory systems, in visual (Torborg and Feller, 2005), auditory (Clause et al., 2014), somatosensory (Allene et al., 2008) and olfactory (Ron Yu and Gogos, 2004) circuits. It also appears across species, in ferrets (Chapman, 2000) and rodents as well as humans (Colonnese et al., 2010). The exact properties of the activity patterns can vary widely in terms of amplitude, duration, spread or cell participation, and the various guises of spontaneous activity has been the topic of several excellent reviews (Ackman and Crair, 2014; Allene and Cossart, 2010; Blankenship and Feller, 2009; Kerschensteiner, 2014; Kirkby et al., 2013). Technological advances have allowed imaging of spontaneous activity in the live animal, confirming that several types of spontaneous activity patterns exist during development in sensory regions ***in vivo***.

In this thesis, I show that normal patterning of spontaneous activity requires a careful balance of excitatory and inhibitory signalling. Furthermore, specific interneuron subtypes can control certain features, even at this early age. These

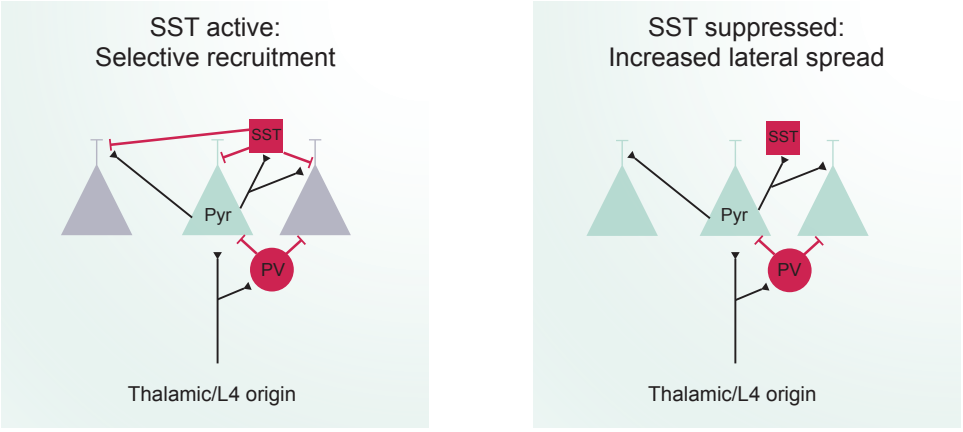

Figure 1, Inhibitory cells during spontaneous activity
Possible network model in which simultaneous feedforward activation of pyramidal and parvalbumin (PV) cells restricts the number of action potentials fired by a cell. Lateral spread of events is prevented by SST targeting dendrites. Upon suppression of SST cells, lateral inhibition is removed and a wider range of neurons are activated during each event. Green: firing neuron, grey: silent neuron. Black lines: firing excitatory axons. Red lines: firing inhibitory axons

features are also sensitive to cholinergic signalling, opening up new questions about the influence of the internal state of the neonatal animal on its activity patterns, and the resulting wiring of the young network. By zooming in to the individual dendrite, we can even see refinement at work at relatively short timescales. At the synaptic level, spontaneous activity uses co-activity to remove out-of-sync or far away sites and promote the emergence of domains. Finally, to test the causality of these relationships in the future, we have developed tools that allow specific manipulation of activity patterns.

Inhibitory signalling during the second postnatal week

In recent years, new evidence has changed our view on the effect of GABA on the postsynaptic cell during early development (Zilberter, 2016). Previously, work using predominantly slice electrophysiology led to the GABA switch hypothesis. The high intracellular chloride concentration of young cells causes an efflux of negatively charged chloride when GABAergic channels are opened, depolarizing the cells. As the composition of channels changes (specifically, NKCC1 reduces and KCC2 increases) during development, the intracellular chloride concentration decreases and GABA becomes hyperpolarizing from around P8 (He et al., 2014; Valeeva et al., 2016). Recent results have shown that these findings do not mean that interneurons are necessarily excitatory during early development. Valeeva et al., (2016) confirmed ***in vitro*** findings using optogenetic stimulation of GABA-ergic interneurons, which lead to an increase in glutamatergic excitatory postsynaptic currents only in young animals. However, the same experiment performed ***in vivo*** lead to a decrease in glutamatergic responses. Additionally, though puffing GABA onto young neurons did depolarize cells, it did not lead to action potential firing (Kirmse et al., 2015) and application of the $GABA_AR$ antagonist gabazine greatly increased activity rates, similar to the picrotoxin experiment in Chapter 2. It therefore seems that there is a developmental moment where GABA switches from depolarizing to hyperpolarising, but that the functional consequences of this are perhaps less dramatic than previously thought. The primary role of GABA may be to cause shunting inhibition, where the main role of interneuron activity is to reduce membrane impedance through the opening of chloride channels. This decreased impedance and the subsequent large increase in current required to induce membrane potential changes, 'clamps' the cell at a negative potential,

decreasing the likelihood of action potential firing. It is not yet known what causes this difference between ***in vitro*** and ***in vivo*** findings (Valeeva et al., 2016).

In Chapter 2, we show that even before eye-opening, inhibitory signalling shaped the properties of spontaneous activity, which in turn will refine the developing network. In the adult brain, inhibitory interneuron subtypes perform specific roles (Fig 1). The suppression of SST-expressing interneurons was performed only a few days after interneurons had finished migration into the cortical plate (Del Rio et al., 1992; Miyoshi and Fishell, 2011). Discovering whether other subtypes such as VIP or PV expressing interneurons play specific roles in development could help us better understand the functional circuit that produces spontaneous activity. Possibly, inhibitory control is already modular, such that a particular cell type controls specific pattern features which underlie refinement of the emerging cortical networks.

Long-term reductions in spontaneous activity, perhaps using the same DREADD construct as in Chapter 2 and long-term injections of CNO, could perhaps clarify the functional consequences of these described activity patterns. If SST cells are suppressed during the second postnatal week, leading to larger waves, does this prevent refinement upon eye-opening? Chronic CNO injections combined with retinotopic mapping could demonstrate the functional relevance of the finding that SST cells control lateral activity spread. It would be particularly interesting to tie in the synaptic organization findings in Chapter 4, using these altered spontaneous activity waves. For instance, do domains develop normally when more cells are recruited to an event? One could imagine that more synchronous activity could be problematic for synaptic organization, given higher overall co-activity. Alternatively, the low release probability at the developing synapse may introduce enough noise that the increase in recruitment can be overcome. These experiments would help us understand the sensitivity of the developing brain to the features of spontaneous activity. Given that we found that suppressing SST cells increased network correlations, it is surprising that we did not detect many changes of spontaneous activity patterning upon mecamylamine application. In the adult, acetylcholine release transiently increases the connection strength between pyramidal- and SST cells (Urban-Ciecko and Barth, 2016) via nicotinic receptors. In turn, strengthened somatostatin inhibition reduces network synchrony (Chen et al., 2015). We had hypothesised

that we may find a similar relationship between cholinergic signalling, inhibitory interneurons and network correlation in these developing mice. Verifying whether nicotinergic signalling truly does not modulate spontaneous activity patterns will be the first step in understanding these results before investigating whether this interaction is different during development than in the adult brain.

Making up 40% of inhibitory cells, parvalbumin-expressing interneurons are the most common type of inhibitory interneuron in L2/3 (Rudy et al., 2011). Most parvalbumin-expressing cells are fast-spiking, and target the soma or proximal dendrite, providing strong inhibition (van Versendaal and Levelt, 2016). Understanding their contribution to spontaneous activity patterning is made trickier by the late expression of the protein parvalbumin itself- throughout the central nervous system, parvalbumin expression has a sudden onset around P13. The use of a synaptotagmin-2-cre mouse line could allow activity modification of these cells (Sommeijer and Levelt, 2012). This vesicle protein is expressed earlier than parvalbumin itself, and can be detected before eye-opening. Particularly, this mouse line would allow us to test the hypothesis posited in Chapter 2, that the desynchronization of spontaneous activity may occur due to the strengthening of parvalbumin synapses.

Neurodevelopmental disorders are associated with synaptic and inhibitory deficiencies

Though this thesis focuses on development in wild-type animals, these data can open up new questions regarding our understanding of certain neurodevelopmental disorders. Fragile X syndrome is a genetic disorder in which more than 200 repeats of a CGG motif in the FMR1 gene prevents normal expression. It is the most common inherited form of intellectual disability and patients often present with autism spectrum disorder (Hagerman et al., 2017). The switch of GABA from a depolarizing to hyperpolarizing neurotransmitter happens later in slices FMR1 knockout mice than in WT controls (He et al., 2014). However, given the previously mentioned difficulty of extrapolating these ***in vitro*** results to ***in vivo***, what does this mean for brain development in these knockouts? Cheyne et al. (2019) found increased participation in ***in vivo*** spontaneous activity in these knockout animals. Linking inhibition, spontaneous activity patterns and the consequences for

developmental wiring may help us understand how the FMR1 mutation leads to such a severe phenotype.

Differences in spine morphology and density have been reported in Fragile X syndrome. Patients have a higher density of spines on distal dendrites, and these spines have immature morphology (reviewed in Bagni and Zukin, 2019; Martínez-Cerdeño, 2017). In Chapter 4, we show that developing synapses are carefully organized during the second postnatal week, in an activity-dependent manner. We do not yet know whether FMR1 knockout animals also produce domains of high-activity synapses. If these synaptic domains do in fact promote spinogenesis, absent or abnormal domains may underlie the immature profile of synapses in the FMR1 mouse. Exploring synaptic organization and subsequent maturation in these phenotypes is a huge project, but a promising avenue for understanding the disorder.

L- and H-events at the level of the synapse

Classically, Hebbian learning, the postulate that neurons that fire together, wire together (Hebb, 1949) has been thought to underlie the developmental shaping of higher areas by peripherally generated spontaneous activity. The repeated firing of presynaptic neurons together with the cells they project to strengthens both those feedforward connections and lateral connections between postsynaptic cells being simultaneously depolarized. Conversely, when a postsynaptic cell fires an action potential without presynaptic glutamate release, the strength of the connection decreases, so that an existing strong connection can indirectly decrease the strength of other inputs by causing asynchronous action potentials.

There is empirical evidence for Hebbian learning as an important plasticity mechanism during sensory development (Žiburkus et al., 2009). A recent study directly measured synaptic strengthening and weakening, implicated an important role for LTD in refinement. Lee et al., 2014 examined the patterning of the LGN at the level of the individual synapse using a mouse model with altered AMPA receptors. This mouse lacks the major histocompatibility complex (MHC) class 1 immune proteins H2-Kb and H2-Db (KbDb −/−). This does not affect their retinal waves, but impairs eye-specific segregation in the thalamus. In healthy animals, the convergence from the retina to the LGN is developmentally reduced until only

1-3 retinal ganglion cells project to each postsynaptic cell. The KbDb-/- mouse does not show the synapse elimination necessary to achieve this convergence. LTP could be induced normally through pairing LGN cell depolarization with a presynaptic 10Hz activity train, which is within the frequency range of, for instance, spindle bursts (Khazipov et al., 2004). When pre- and postsynaptic stimulations were offset in time, which would normally cause LTD, the synapses did not weaken. This imbalance towards LTP was due to the high calcium permeability of the AMPA receptors in the KbDb knockout- when their permeability was reduced, LTD could be induced. Restoring H2-Db only to neurons rescued the phenotype, indicating that the protein specifically plays a role in neurons rather than in a systemic immune response.

Interestingly, in this experiment, the overall amount of excitation received by each postsynaptic cell was the same- the higher number of terminating fibres was compensated for by each fibre having a weaker synaptic strength, even though cells were capable of LTP. In fact, many manipulations of activity result in unrefined projections- these have larger termination areas, made up of more individual fibres than in wild type. When these projections are tested, the overall innervation strength is similar, as each individual axon has a weaker effect on the postsynaptic cells (Clause et al., 2014; Hirtz et al., 2012; Lee et al., 2014). This suggests that besides classic Hebbian learning, there may be homeostatic plasticity mechanisms in place to maintain overall projection strength.

Different plasticity mechanisms exist and may act side-by-side. Using a wide range of different techniques, we see a split into two types of activity: L- and H-events. One possible reason for having two types of events during development would be if they performed different functions. Siegel et al., (2012) posited that L-events could cause strengthening of correctly targeted synapses, promoting the refinement of retinotopic maps. H-events could perform synaptic homeostasis, similar to a proposed role of slow-wave sleep in the synaptic homeostasis hypothesis (SHY) (Tononi and Cirelli, 2006, 2012). Wosniack et al., (2021) modelled this interaction between L- and H-events and found that robust refinement required adaptive H-event amplitudes, where strong H-events proceeded strong L-events. This prediction was borne out in the ***in vivo*** data and led to topographic refinement as well as sparsification of spontaneous activity over time.

How could H-events perform homeostasis? In adult cortex during sleep or anaesthesia, neurons have 'up' and 'down' states, reflected in membrane potentials either far or close to firing threshold, and up states are usually accompanied by spiking. González-Rueda et al., (2018) used urethane-induced slow-waves to observe synaptic plasticity during up and down states. During down states, when membrane potential is low and spiking is rare, synapses between L4 and L2/3 followed typical spike-timing-dependent-plasticity (STDP) rules- stimulation of L4 afferents followed by L2/3 spiking led to increased synaptic strength, whereas the reverse temporal order resulted in synaptic depression. However, during up-states, LTD was not observed in either protocol. When stimulation preceded postsynaptic firing, synapses were not strengthened but remained stable. Unlike the SHY hypothesis mentioned above, this rule is not a global scaling rule affecting all synapses in the network, but only those that are active. In simulated wake and sleep, this specificity led to a weight-dependent downscaling of synaptic strength (where stronger synapses changed less), increasing overall signal-to-noise ratio. In an ultrastructural study (de Vivo et al., 2017), the scaling effects of sleep could be seen by measuring axon-spine interface (ASI) after sleep or wake. A size-dependent scaling rule was found that reflected this weight-dependent scaling- larger ASIs changed less. One group of synapses did not scale at all- the largest 20% of synapses. These could correspond to the high activity sites we see in our synaptic populations. If a similar mechanism is at work during H-events, they may allow the network to maintain learned differences in synaptic weight rather than scaling down differences in synaptic strength. Visualizing or inducing

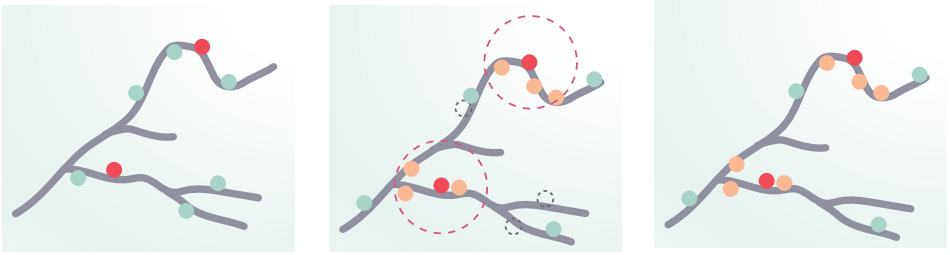

Figure 2, The development of highly active synaptic domains during the second postnatal week

Left panel: synapses are arranged on the dendrite, Either a specific or random subset (20%) have higher activity levels than the rest. Middle panel: synapses within 12 µm of these high-activity sites are stabilised or even increase their activity levels, whereas those further away reduce activity and eventually even disappear. Though synapses are added randomly, this pattern leads to the emergence of highly active domains (right panel).

pre-synaptic activity is essential for testing this idea, in order to judge whether a synapse failed to participate in an event. As the modulation of activity in a state-dependent manner emerges only during the second postnatal week (Colonnese, 2014), perhaps H-events are necessary whilst sleep has not yet developed the characteristics required to improve signal-to-noise ratio.

Functional implications of activity-based synaptic domains

When recording from young dendrites in the visual cortex, we saw a large number of infrequently active synaptic sites as well as a subset of highly-active synaptic sites. Synaptic density increased dramatically during the course of the second postnatal week, in line with previous findings (Blue and Parnavelas, 1983; Defelipe, 1997). During a single 30-minute recording in very young animals, we saw that synaptic sites that are more than 12 µm away from a highly active site tend to decrease their activity. In contrast, those close by a high-activity site are stabilized or increase their activity. By the end of the second postnatal week, synapses have become organized into 'domains' so that highly-active sites have higher average activity surrounding them (Fig 2).

Due to their spatial restriction and high co-activity, it is possible that domains are setting up initiation sites for active local mechanisms such as dendritic spikes. This would allow supra-linear amplification of these inputs when activated simultaneously (Sjostrom et al., 2008), increasing their relative influence on cell output. However, which synapses are given such important positions even before the eyes open?

Given that domains form around high-activity sites, understanding the origin of this subset of synapses may be a promising next step. One possibility is that high-activity synapses form between cells that receive similar inputs. Sharing feedforward inputs is likely to lead to high co-activity, which may have protected or strengthened synapses (Ko et al., 2013), and co-activity-based-stabilisation would further encourage synapses from cells with similar activation patterns to stabilize at these locations. In this scenario, domains would act as strong connections between cells that represent similar parts of the visual field. During the first postnatal week, clonally related cells (from the same progenitor) are connected

via gap-junctions, sharing electrical and chemical signals (Yu et al., 2009). Later, these cells will preferentially form chemical synapses with each other, and are likely to be tuned to similar orientations (Li et al., 2012; Ohtsuki et al., 2012; Yu et al., 2009), intuitively linking spontaneous activity to orientation specificity. If this gap-junction connection is blocked, the preferential chemical synapses between sister cells is prevented (Yu et al., 2012). When Hagihara et al., (2015) greatly reduced spontaneous activity frequency by expressing the potassium channel Kir2.1, orientation tuning developed normally. However, it is not known whether the shared orientation preference of clonally related cells was maintained in this manipulation. Using methods to identify clonally related cells (García-Moreno et al., 2014; Li et al., 2012) could help us understand the origin of these high-activity sites and domain formation.

One of the major challenges during development is setting up and maintaining multiple maps simultaneously, each representing various properties that are crucial to vision. The adult visual cortex has a retinotopic map, as well as left-and right eye segregation and columnar organization of orientation specificity (Ohki and Reid, 2007; Kaschube, 2014). The retinotopy of V1 must also be aligned to that of higher order areas. Perhaps the lower density areas outside of the domains we report are available for other representations or task-related synapses that occur after eye-opening.

Synapses were split in two different morphologies- shaft synapses, which formed directly on the dendrite, and spine synapses, which were characterized by their distinct protruding morphology. Both synapse types occurred in roughly equal proportions during the second postnatal week. Shaft synapses are common in the young brain (Reilly et al., 2011), in contrast to the adult where most excitatory synapses are formed on protruding spines (Berry and Nedivi, 2017). How the system moves from predominantly shaft-based to spine-based signalling without losing synaptic organisation is unclear. The original hypothesis, that shaft synapses become spine synapses through supplementary morphology (Miller and Peters, 1981), has not to our knowledge been supported by direct observation. Furthermore, morphologically identified spines do not necessarily have functional synapses (Cane et al., 2014) as measured by their lack the essential synaptic protein psd-95. Instead of developing from shaft synapses, spine synapses may appear

close to shaft synapses (Reilly et al., 2011), perhaps feeding off of synaptogenic signals caused by local high activity. In the domains we describe, low activity sites adapt their activity depending on whether or not they are in a domain. This could encourage spinogenesis in these regions and maintain the organisation set out by shaft synapses.

To truly understand their function, it would be necessary to visualize what happens to domains after eye-opening. The organization of synapses along the adult dendrite is a controversial topic, and whether functional clustering is found depends on the parameter measured. Neither orientation tuning nor preferred frequency was found to cluster synapses in the adult mouse (Chen et al., 2011; Iacaruso et al., 2017), but synapses with similar receptive fields do tend to be closer together (Iacaruso et al., 2017). It may be that functional clustering comes into its own in a more task-related manner, acting as a coincidence detector rather than a straightforward feature sensor (Poirazi and Mel, 2001). When mice learned a new motor task, 1/3 of synapses appeared next to another novel spine (Fu et al., 2012), indicating that new domains may be formed throughout life. A longitudinal study following the fate and sensory tuning of domains after eye-opening would help us link this developmental finding to adult function. Given how fundamental the retinotopic map is to vision, these high activity sites and surrounding domains may protect retinotopic organization while the brain undergoes the extensive plasticity typical of the critical period after eye-opening.

In view of the spatial precision of excitatory synapses, inhibitory synapses may also be organised in space. In a theoretical study, Gidon and Segev (2012) predict that the most effective way to suppress synaptic 'hotspots' (analogous to our domains) may be for inhibitory synapses to be located distally and off-path (further from the soma than the hotspot, rather than between the hotspot and the soma). Particularly given that we put forward an important role for inhibition during the second postnatal week, visualizing inhibitory synaptic activity (for instance with tags for the inhibitory synapse protein gephyrin and chloride indicators, though synaptic-level precision ***in vivo*** is as of yet technically challenging) in relation to domains could help us understand whether domains are gated by inhibition and how this is best achieved.

How hard-wired is spontaneous activity?

By observing spontaneous events at synaptic, cellular and population level, I have aimed to ask questions about the network which produces the activity, and how it is in turn shaped by the features of that activity. Spontaneous activity is not just an emergent feature of the young nervous system, but a powerful means to set up connections that form the basis of the developing brain. Rather than thinking of spontaneous activity as almost hard-wired, with the true potential for organisation and plasticity only occurring once the eyes open, this thesis suggests that spontaneous activity is more receptive to change than previously thought. If changes in inhibition or the attentive state of the animal can change the features of this activity, small changes in experience during this time could have life-long effects. The work in this thesis presents a contribution to our understanding of the importance of neuromodulation, inhibitory signalling and synaptic organization when building a brain.

REFERENCES

Bagni, C., and Zukin, R.S. (2019). A Synaptic Perspective of Fragile X Syndrome and Autism Spectrum Disorders. Neuron *101*, 1070–1088.

Berry, K.P., and Nedivi, E. (2017). Spine dynamics: Are they all the same? Neuron *96*, 43–55.

Blue, M.E., and Parnavelas, J.G. (1983). The formation and maturation of synapses in the visual cortex of the rat. II. Quantitative analysis. J. Neurocytol. *12*, 697–712.

Cane, M., Maco, B., Knott, G., and Holtmaat, A. (2014). The Relationship between PSD-95 Clustering and Spine Stability In Vivo. J. Neurosci. *34*, 2075–2086.

Chen, N., Sugihara, H., and Sur, M. (2015). An acetylcholine-activated microcircuit drives temporal dynamics of cortical activity. Nature Neuroscience *18*, 892–902.

Chen, X., Leischner, U., Rochefort, N.L., Nelken, I., and Konnerth, A. (2011). Functional mapping of single spines in cortical neurons in vivo. Nature *475*, 501–505.

Cheyne, J.E., Zabouri, N., Baddeley, D., and Lohmann, C. (2019). Spontaneous activity patterns are altered in the developing visual cortex of the Fmr1 knockout mouse. Front. Neural Circuits *13*.

Colonnese, M.T. (2014). Rapid Developmental Emergence of Stable Depolarization during Wakefulness by Inhibitory Balancing of Cortical Network Excitability. J. Neurosci. *34*, 5477–5485.

Defelipe, J. (1997). Types of neurons, synaptic connections and chemical characteristics of

cells immunoreactive for calbindin- D28K, parvalbumin and calretinin in the neocortex. J Chem.Neuroanat. *14*, 1–19.

Del Rio, J.A., Soriano, E., and Ferrer, I. (1992). Development of GABA-immunoreactivity in the neocortex of the mouse. J. Comp. Neurol. *326*, 501–526.

Fu, M., Yu, X., Lu, J., and Zuo, Y. (2012). Repetitive motor learning induces coordinated formation of clustered dendritic spines in vivo. Nature *483*, 92–95.

García-Moreno, F., Vasistha, N.A., Begbie, J., and Molnár, Z. (2014). CLoNe is a new method to target single progenitors and study their progeny in mouse and chick. Development *141*, 1589–1598.

Gidon, A., and Segev, I. (2012). Principles governing the operation of synaptic inhibition in dendrites. Neuron *75*, 330–341.

González-Rueda, A., Pedrosa, V., Feord, R.C., Clopath, C., and Paulsen, O. (2018). Activity-Dependent Downscaling of Subthreshold Synaptic Inputs during Slow-Wave-Sleep-like Activity In Vivo. Neuron *97*, 1244–1252.

Hagerman, R.J., Berry-Kravis, E., Hazlett, H.C., Bailey Jr, D.B., Moine, H., Kooy, R.F., Tassone, F., Gantois, I., Sonenberg, N., Mandel, J.L., et al. (2017). Fragile X syndrome. Nature Reviews Disease Primers *3*, 17065.

Hagihara, K.M., Murakami, T., Yoshida, T., Tagawa, Y., and Ohki, K. (2015). Neuronal activity is not required for the initial formation and maturation of visual selectivity. Nature Neuroscience *18*, 1780–1788.

He, Q., Nomura, T., Xu, J., and Contractor, A. (2014). The Developmental Switch in GABA Polarity Is Delayed in Fragile X Mice. J. Neurosci. *34*, 446–450.

Iacaruso, M.F., Gasler, I.T., and Hofer, S.B. (2017). Synaptic organization of visual space in primary visual cortex. Nature *547*, 449–452.

Kirmse, K., Kummer, M., Kovalchuk, Y., Witte, O.W., Garaschuk, O., and Holthoff, K. (2015). GABA depolarizes immature neurons and inhibits network activity in the neonatal neocortex in vivo. Nat Commun *6*, 7750.

Ko, H., Cossell, L., Baragli, C., Antolik, J., Clopath, C., Hofer, S.B., and Mrsic-Flogel, T.D. (2013). The emergence of functional microcircuits in visual cortex. Nature *496*, 96–100.

Leighton, A.H., and Lohmann, C. (2016). The Wiring of Developing Sensory Circuits-From Patterned Spontaneous Activity to Synaptic Plasticity Mechanisms. Front Neural Circuits *10*, 71.

Li, Y., Lu, H., Cheng, P. lin, Ge, S., Xu, H., Shi, S.H., and Dan, Y. (2012). Clonally related visual cortical neurons show similar stimulus feature selectivity. Nature *486*, 118–121.

Martínez-Cerdeño, V. (2017). Dendrite and spine modifications in autism and related neurodevelopmental disorders in patients and animal models. Developmental

Neurobiology *77*, 393–404.

Miller, M., and Peters, A. (1981). Maturation of rat visual cortex. II. A combined Golgi-electron microscope study of pyramidal neurons. J.Comp Neurol. *203*, 555–573.

Miyoshi, G., and Fishell, G. (2011). GABAergic Interneuron Lineages Selectively Sort into Specific Cortical Layers during Early Postnatal Development. Cereb Cortex *21*, 845–852.

Ohtsuki, G., Nishiyama, M., Yoshida, T., Murakami, T., Histed, M., Lois, C., and Ohki, K. (2012). Similarity of Visual Selectivity among Clonally Related Neurons in Visual Cortex. Neuron *75*, 65–72.

Poirazi, P., and Mel, B.W. (2001). Impact of active dendrites and structural plasticity on the memory capacity of neural tissue. Neuron *29*, 779–796.

Reilly, J.E., Hanson, H.H., and Phillips, G.R. (2011). Persistence of excitatory shaft synapses adjacent to newly emerged dendritic protrusions. Mol.Cell Neurosci.

Rudy, B., Fishell, G., Lee, S., and Hjerling-Leffler, J. (2011). Three Groups of Interneurons Account for Nearly 100% of Neocortical GABAergic Neurons. Dev Neurobiol *71*, 45–61.

Sjostrom, P.J., Rancz, E.A., Roth, A., and Hausser, M. (2008). Dendritic excitability and synaptic plasticity. Physiol Rev. *88*, 769–840.

Sommeijer, J.P., and Levelt, C.N. (2012). Synaptotagmin-2 is a reliable marker for parvalbumin positive inhibitory boutons in the mouse visual cortex. PLoS ONE. *7*, e35323.

Urban-Ciecko, J., and Barth, A.L. (2016). Somatostatin-expressing neurons in cortical networks. Nat Rev Neurosci *17*, 401–409.

Valeeva, G., Tressard, T., Mukhtarov, M., Baude, A., and Khazipov, R. (2016). An Optogenetic Approach for Investigation of Excitatory and Inhibitory Network GABA Actions in Mice Expressing Channelrhodopsin-2 in GABAergic Neurons. J. Neurosci. *36*, 5961–5973.

van Versendaal, D., and Levelt, C.N. (2016). Inhibitory interneurons in visual cortical plasticity. Cell. Mol. Life Sci. *73*, 3677–3691.

de Vivo, L., Bellesi, M., Marshall, W., Bushong, E.A., Ellisman, M.H., Tononi, G., and Cirelli, C. (2017). Ultrastructural Evidence for Synaptic Scaling Across the Wake/sleep Cycle. Science *355*, 507–510.

Wosniack, M.E., Kirchner, J.H., Chao, L.-Y., Zabouri, N., Lohmann, C., and Gjorgjieva, J. (2021). Adaptation of spontaneous activity in the developing visual cortex. ELife *10*, e61619.

Yu, Y.C., Bultje, R.S., Wang, X., and Shi, S.H. (2009). Specific synapses develop preferentially among sister excitatory neurons in the neocortex. Nature.

Yu, Y.C., He, S., Chen, S., Fu, Y., Brown, K.N., Yao, X.H., Ma, J., Gao, K.P., Sosinsky, G.E., Huang, K., et al. (2012). Preferential electrical coupling regulates neocortical lineage-dependent microcircuit assembly. Nature *486*, 113–117.

Zilberter, M. (2016). Reality of Inhibitory GABA in Neonatal Brain: Time to Rewrite the Textbooks? J. Neurosci. *36*, 10242–10244.

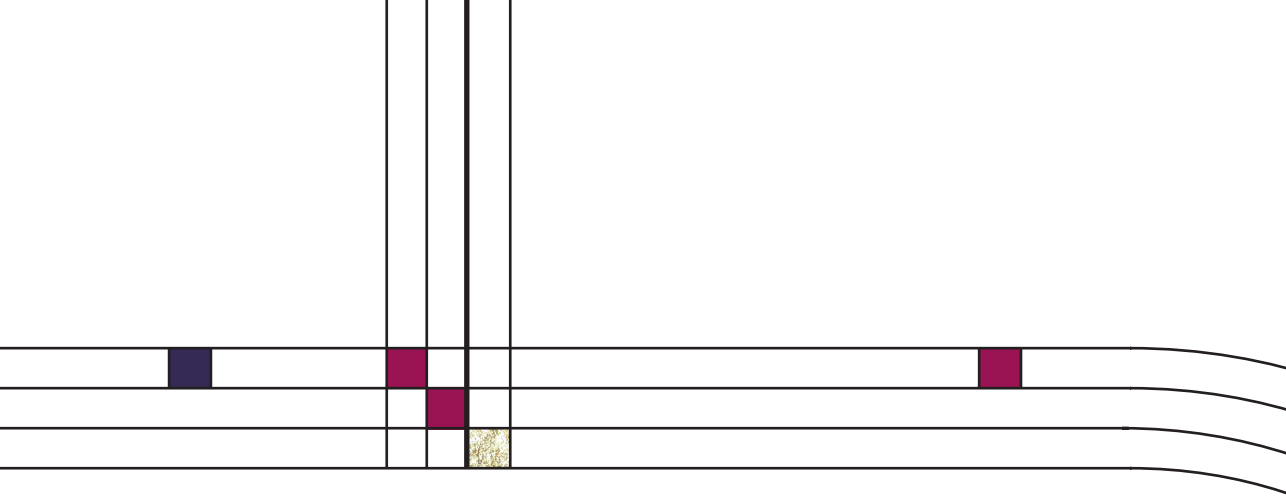

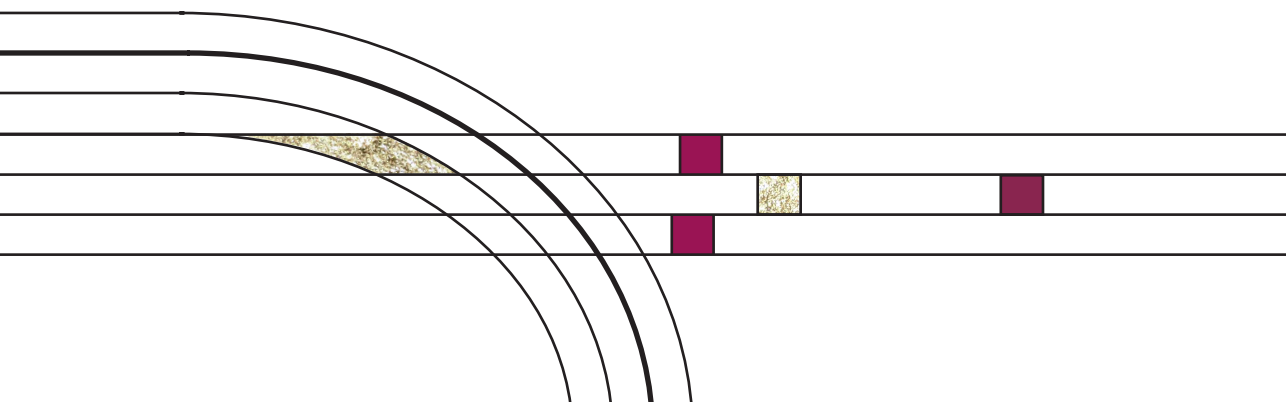

Appendix

SUMMARY

The connections between neurons allow information to be transported throughout the nervous system, whether this information comes from the senses or from stored memories, and whether it leads to decision making or muscle activation. Inaccurate or imprecise wiring between neurons can misroute important information, or cause over- or under-excitation of the nervous system.

Connections are initially created during early development, and become fine-tuned as 'practice' spontaneous activity strengthens well-placed synapses and prunes aberrant connections. Spontaneous activity is generated by the developing brain itself, and can therefore encode structural information; for instance, neighbouring cells in the retina are more likely to be active at the same time than two cells that are physically further apart. This information can be passed on to other regions of the nervous system, both shaping and being shaped by the developing brain.

A connection between two cells is not an all-or-nothing bridge; synapses can be strong or weak, and multiple synapses can work together to produce a net larger effect on a cell and increase the likelihood of their activity being passed along. By recording high resolution images of individual neurons, we can actually see connections being formed and regulated in a living animal. Those synapses that do not activate together with their neighbours are often weakened and removed. In this thesis, I show that connections are preferentially maintained if they are close to other, active connections, creating high activity stretches along the dendrite.

I further show that the patterning of spontaneous activity relies on a specific type of inhibitory interneuron. Without the activity of these somatostatin-expressing interneurons, spontaneous activations can recruit more cells and activate a larger proportion of the retinotopic map. Both excitatory and inhibitory activity are required to shape spontaneous activity patterns and restrict activations to a small area of the brain.

As adults, we are often acutely aware of our state- whether we are stressed, attentive, or relaxed is something that we can physically feel and that is reflected in our neural activity. By showing that cholinergic signalling can alter the properties

of spontaneous activity, we suggest that state is important even in very young animals.

Finally, to causally assert the relationship between spontaneous activity and the developing brain, we developed a wireless tool that allows specific manipulation of activity patterns with minimal interference with natural animal behaviour.

NEDERLANDSTALIGE SAMENVATTING

De verbindingen tussen neuronen zorgen voor het transport van informatie door het zenuwstelsel- informatie afkomstig van de zintuigen of van opgeslagen herinneringen kan daardoor leiden tot besluitvorming of spieractivering. Onnauwkeurige of onvoldoende verbindinen tussen neuronen kan ervoor zorgen dat belangrijke informatie op de verkeerde plek terecht komt en kan over- of onderprikkeling van het zenuwstelsel veroorzaken.

Verbindingen worden in de eerste instantie gevormd tijdens de vroege ontwikkeling, en worden verfijnd door 'spontane activiteit'. Deze activaties versterken goed geplaatste synapsen en snoeit afwijkende verbindingen weg. Spontane activiteit wordt door de ontwikkelende hersenen zelf gegenereerd en kan daarom structurele informatie encoderen. Bjvoorbeeld, de kans is groter dat cellen die regelmatig samen actief zijn, ook fysiek naast elkaar gepositioneerd zijn in de retina. Deze structurele informatie kan via de spontane activiteit worden doorgegeven aan andere delen van het zenuwstelsel, waardoor de ontwikkelende hersenen gevormd worden.

Verbindingen tussen cellen kunnen sterk of zwak zijn, en meerdere synapsen kunnen samenwerken om met zijn allen een groter effect op een cel te hebben, waardoor de kans toeneemt dat hun activiteit wordt doorgegeven. Via hoge resolutie beelden van individuele neuronen kunnen we daadwerkelijk zien hoe verbindingen worden gevormd en gereguleerd in een levend dier. We zien dan dat de synapsen die niet meespelen met hun buren worden verzwakt en verwijderd. In dit proefschrift laat ik zien dat verbindingen bij voorkeur in stand worden gehouden als ze dicht bij andere, actieve verbindingen liggen, waardoor er langs de dendriet stukken met een hoge activiteit ontstaan.

Ik laat daarnaast zien dat de precieze eigenschappen van spontane activiteit afhankelijk zijn van een specifiek type 'remmend' interneuron. Zonder de activiteit van deze interneuronen kunnen spontane activaties zich verder verspreiden, waardoor meer cellen en een groter deel van de retinotopische kaart worden geactiveerd. Zowel excitatoire als inhibitoire activiteit zijn nodig om spontane activiteitspatronen vorm te geven en activatie te beperken tot een klein gebied van de hersenen.

Als volwassenen zijn we ons vaak erg bewust of we ons ontspannen of juist gestressed voelen. Onze physiologische staat wordt ook weerspiegeld in onze neurale activiteit. Door aan te tonen dat cholinerge signalering de eigenschappen van spontane activiteit kan veranderen, laten wij zien dat staat, aandacht en stress wellicht zelfs bij zeer jonge dieren belangrijk is voor de vorming van de hersenen.

Tenslotte ontwikkelden wij een methode om de relatie tussen spontane activiteit en de zich ontwikkelende hersenen causaal te testen. Deze methode werkt door een LED lampje in de hersenen draadloos aan te sturen, waardoor specifieke manipulatie van activiteitspatronen mogelijk wordt gemaakt terwijl de muis natuurlijk diergedrag kan blijven vertonen.

BIOGRAPHY

Alexandra Helen Leighton (London, 1989) was educated in London, Amsterdam, and Edinburgh. She studied Pyschobiologie at the University of Amsterdam (BSc, awarded ***cum laude*** in 2011). At the UvA, Leighton was an active member of the Congo Conference committee, organizing a yearly conference on topics ranging from 'Crime and Punishment- a case of biology' to 'Sex - an evolutionary success story'. During her BSc internship, she worked with Simon van Gaal in the laboratory of Victor Lamme, using EEG to research whether human subjects are able to unconsciously integrate the meaning of multiple words.

In 2012 she undertook a one-year internship at the laboratory of Professor Maria Fitzgerald at University College London, studying the development of itch and scratch sensation, and was awarded her MSc in Brain and Cognitive Sciences (***cum laude***) in 2013.

During her PhD at the Netherlands Institute for Neuroscience, Leighton was staff representative and head of the PhD committee, where she was committed to evaluating and improving employee safety. She developed a keen interest in how the scientific community can improve research outcomes through greater attention to the well-being of employees and more effective use of resources. In 2019, this interest led her to join Open Ephys, a not-for-profit that develops, produces and disseminates open-source electronics and software for Neuroscience. She currently works as support, training, and outreach manager at Open Ephys Production Site, in Lisbon, Portugal, and is engaged in setting up a network of experts to support scientists as they use open-source tools. Leighton developed and continues to curate the Open Ephys online platform for fundamental neuroscience learning and is the course director for the Cajal Advanced Training Programme Course on Extracellular Electrophysiology Acquisition.

Alongside science, Alex Leighton enjoys painting, and has had her artworks featured in Scientific American and installed at the Champalimaud Foundation in Lisbon.

ACKNOWLEDGEMENTS

I'll have to deplete the thesaurus of synonyms for 'amazing' to do justice to the many people who have helped and encouraged me over the years. I'll also do my best to reference obscure inside jokes that nobody else cares about.

A lot of my time at the NIN was spent on my own in a dark microscope room, but I can't help but notice that most of my favourite memories involve other humans. Humans such as **Juliette Cheyne**, whose contagious laugh and genuine love for science lit up the first years of my PhD. Thank you for teaching me all the things and for bravely standing up for us. I still crack up thinking of Juliette, **Dragos Niculescu, Gertjan Houwen** and **Johan Winnubst** playing our elaborate lab-Olympics, thank you all for being unique, hilarious and encouraging. Dragos, I wish I *had* stolen your cookie, so that I could admit to it here. Thank you **chiki,** I mean **Paloma Maldonado** for your sincerity and ability to see the best in people, and for teaching me to swear in Spanish. When I saw how thoroughly **Vicky Busch** considered every topic, I realised I'd have to up my science-game, thank you for making me think things through. **Monique van Mourik** – you are just so smart and so *sensible*, thank you for laughing at me only half as much as you could have. Thank you to the students who brought new energy to the lab; **Anouk Heuvelmans** for your meticulous organisation and sense of humour, **Björn Holtze** for your determination and excellent Sinterklaas poem, and **Mike van Zwieten** for letting us call you Rob.

My promotors **Christiaan Levelt** and **Pieter Roelfsema**, thank you for stepping in and making it possible for me to cross the finish line. It can't have been easy to navigate this particular trajectory, but it means a lot to me that you found a way.

Dorien, zonder jou was dit nooit gelukt. Bedankt voor je inzet, visie en steun. Ook enorm bedankt aan alle dierverzorgers op het insituut, met name **Rainier**, **Gerrit-Jan**, **Gavin** en **Sammy**, voor jullie vakkundigheid en geduld met mijn eindeloze vragen en last-minute verzoeken. Thanks to all those of the Partysquad/Borrel.. well whatever it was called- **Emma Ruimschotel**, **Tessa Lodder**, **Areg Barsegyan** and **Sharon de Vries**, the real sfeermakers of my time at the NIN. Thanks **Hugo** for coming up with new British stereotypes every time I saw you in the hall.

Special thanks to **Matt Self** for telling me 'Nobody else needs to find it funny, as long as you do' which has served me well in many situations, not least while writing this section. Thanks and cheers to everyone else who made the Friday afternoon borrels fun, except **Robin**, because he introduced me to a lethal white wine and sprite combination that I do not wish to further discuss.

I need to thank **Marcus Howlett** for being not only a thoughtful colleague, but also a true friend and party animal. **Mustafa Hamada** for your brutal sense of humour (my granny knitted that sweater) and encouragement. **Carla da Silva Matos** for your warmth and tenacity, and both **Roxana Kooijmans** and **Aleksandra Badura** for advice and fierce support. Thank you, **Tara** and **Jessica** for listening when I needed it most, and being either cheerleaders or town criers, whatever the situation demanded. I'd also like to thank **Alexander Heimel** for teaching me that the only way to get people to attend an event is to provide free food, and for asking annoyingly good questions even during the most boring of meetings.

Over the years, many people helped make Amsterdam an amazing place to live. Thanks to **Thomas de Jong**, **Niel de Jong** and our cat **Emma**-**Beyoncé**, Djakartaterras became my most fun home and the only place I would happily wake up at 4 am to Milky Chance. Thank you to anyone who came to our parties, especially Partytenters **Lisa, Lenny,** and **Sophie** and my friends-in-law de **Bikkels van de Brouwerij**. Many more thanks to those who stayed to clean up afterwards (basically only **Sam Vlessing**).

Douze Points go to **Lianne Klaver** and **Madison Carr**, I am so glad that we made it through our assorted breakdowns, PhD chaos, and (worst of all) planned spontaneity, to grow into a supportive group where no topic is off-limits. I'm not sure how I would have made it through without the cheapest Pizzabakkers-wine with **Rhianne Loonstra** and, later on, better Portuguese wine together with **Tiago. Jeroen**, wat hebben we toch gelachen om die pan.

Ik kan niet ontkennen dat deze PhD een behoorlijke strijd is geweest, en niet op de manieren die ik van tevoren aan had zien komen. Dankzij de wijsheid van **Pien** en **Heleen** en de inzichten en steun van alle meiden van het dinsdag-groepje heb ik er ook veel van kunnen leren. Ik wil ook **Claartje van Sijl** bedanken voor goed advies en inspiratie toen ik het gevoel had er alleen voor te staan.

This PhD even followed me to Portugal, so I'd like to thank everyone there who helped make Lisbon my new home: Bubble-buddy **Sara Bent**, cocktail conversationalists **Abi Obasanya** and **Kate Barnett,** rooftop-bbq-afficionados **Megha**, **Baylor**, **Georg** & **Solène**, the teams at OEPS and Open Ephys, and, of course, **Dany** and **Tiga**. Thank you 'Women in tech' **Julia Huntenburg** and **Clemence Ligneul-** even when it gets tiring having to remind people that we exist, seeing you both balance intelligence and determination with care and humour always gives me fresh energy.

In the UK, it is customary to express love and appreciation only through sarcasm. I hope that my family can bear with me, as they have during this whole PhD, while I fly in the face of this tradition for just a few sentences. To my parents, **Gill & John Leighton**. I am free to try difficult things because I have a safe and very funny home to return to. Thank you for teaching me to value tenacity, originality, and accents. **Freddie**, you're the person I think of when I need to channel patience and integrity, thank you for always setting such a good example and for being the funniest person I know. Finally, to my **grandparents**, who taught me to find something good in every day, to treasure what I have, and to laugh at myself.

Emma Taselaar, Hoofd Enthousiasme en top-tenniscoach. Doordat je overal zo diep over nadenkt, biedt een gesprek met jou altijd nieuwe inzichten en hoop. Ik heb het idee dat je steeds op cruciale momenten belt of invliegt en als een zonnetje voor licht en inspiratie zorgt.

Cátia Silva, you weird little lentil. Despite being the only person to repeatedly tell me: '***we are not friends'***, I am very glad that you finally conceded. I've learned a lot from watching you ask the important questions and relentlessly dig the best out of others. May your fields always be full for those who deserve it, and as barren as Holendrecht for those who do not. Thank you for being so generous, brave and resourceful. In general.

BEEP BEEP, is that **Kim Mertens** in a tessie? Ik vind het lastig om een vriendschap met zoveel verschillende facetten samen te vatten, al helemaal omdat dit boekje volgens de VU geen immoreel content mag bevatten. Jij bent mijn partybuddy, coach, cheerleader en wifey for lifey, en ik ben zo trots op hoe onze vriendschap met ons meegroeit en ontwikkelt. Ik ben eindeloos dankbaar dat ik jouw kracht, humor en buikspieren altijd aan mijn kant heb staan.

Dan **Guido** nog. Vaak zeggen mensen dat ze de liefde gevonden hebben, maar wij hebben het juist zorgvuldig samen opgebouwd. Met jou is het leven altijd een feestje, ook als het tegenzit. Je kunt me constant verbazen door zo blij, energiek en lief te zijn; je hebt duidelijk veel te veel van een of andere neurotransmitter. Ik hoop dat ik er nooit helemaal aan gewend raak.